UNIVERSITY OF CALGARY

Channel Estimation of Frequency Selective Channels for MIMO-OFDM

by

Kathryn Kar Ying Lo

A THESIS
SUBMITTED TO THE FACULTY OF GRADUATE STUDIES
IN PARTIAL FULFILMENT OF THE REQUIREMENTS FOR THE
DEGREE OF MASTER OF SCIENCE
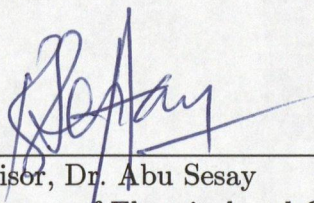
DEPARTMENT OF ELECTRICAL AND COMPUTER ENGINEERING
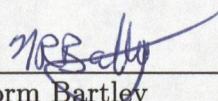
CALGARY, ALBERTA

September, 2005

UNIVERSITY OF CALGARY

FACULTY OF GRADUATE STUDIES

The undersigned certify that they have read, and recommend to the Faculty of Graduate Studies for acceptance, a thesis entitled "Channel Estimation of Frequency Selective Channels for MIMO-OFDM" submitted by Kathryn Kar Ying Lo in partial fulfilment of the requirements of the degree of Master of Science.

_____

Supervisor, Dr. Abu Sesay
Department of Electrical and Computer Engineering

_____

Mr. Norm Bartley
Department of Electrical and Computer Engineering

_____

Dr. Yang Gao
Department of Geomatics Engineering

Sept-14/05
_____
Date

Abstract

Multiple-input-multiple-output (MIMO) antenna architecture has the ability to increase capacity and reliability of a wireless communication system. Orthogonal frequency division multiplexing (OFDM) is well-known for efficient high speed transmission and robustness to frequency selective channels. Hence, the integration of the two technologies has the potential to meet the ever growing demands of future communication systems. A major challenge of implementing MIMO-OFDM is the complicated receiver design. This thesis focuses on the simplification of the channel estimation component of the receiver structure. Low-complexity estimation techniques using QR decomposition are proposed for estimating time-invariant frequency selective channels. In addition, the QR decomposition methods are recursively implemented to estimate time-varying channels. The results show that the application of QR decomposition greatly reduces the complexity of channel estimation.

Acknowledgements

This thesis could not have been completed without the help and support of many people. First and foremost, I would like to express my sincere gratitude to my advisor, Professor Abu Sesay, for his guidance, support, and encouragement throughout the course of this work. He has given me excellent guidance, yet allowed me ample freedom in my research. It has truly been an honour to work under his supervision.

I would like to thank all my colleagues at TRLabs for creating such a helpful and pleasant work environment. Special thanks to Siva Muruganathan for his insightful suggestions in the development of this work and his unique sense of humour. I want to thank Hendry Agus for his help in resolving many technical difficulties and his company on some late nights at work. Many thanks to Reza Pasand, John Shaskin, and Xiaohua Zeng for their friendship, encouragement, and all the unforgettable memories we have shared in the past two years.

My deepest appreciation goes to my family for their continual love and support throughout my life. I sincerely thank my parents for all their sacrifices to give me the opportunity to pursue my education. I am forever indebt to my loving Aunt Lily and Uncle Jim for all that they have provided me. I am grateful to my brother, Kin, for his yummy cooking and daily rides. Many thanks to my dear friends: Anne, Eva, and Sunrose for their cheerful perspectives and encouragement. At last, I am most grateful to Steven for his endless love, patience, support and understanding.

iv

Dedications

To my beloved

Mom and Dad,

Aunt Lily and Uncle Jim,

and

Steven

Table of Contents

List of Tables

List of Figures

List of Abbreviations and Acronyms

Symbol	Definition
4G	fourth-generation
AWGN	additive white Gaussian noise
BER	bit error rate
BLAST	Bell Laboratories layered space-time
BMMSE	Bayesian minimum mean square error
BWA	broadcast wireless access
CDMA	code division multiple access
CFR	channel frequency response
CIR	channel impulse response
CP	cyclic prefix
CSI	channel state information
DAB	digital audio broadcasting
DGR	decoupled Givens rotation
DSP	digital signal processors
DVB	digital video broadcasting
EM	expectation maximization
EVD	eigenvalue decomposition
FFT	fast Fourier transform
FLOP	floating point operation
GR	Givens rotation
GSM	global system for mobile communications
H-QRD	Householder QR decomposition
IC	integrated circuit
ICI	interchannel interference
IFFT	inverse fast Fourier transform
IQRD	inverse QR decomposition
ISI	intersymbol interference
LMS	least mean square
LS	least square

LU	lower upper
MAN	metropolitan area network
MIMO	multiple input multiple output
ML	maximum likelihood
MMSE	minimum mean square error
MSE	mean square error
MVUE	minimum variance unbiased estimator
OFDM	orthogonal frequency division multiplexing
PDF	probability density function
QAM	quadrature amplitude modulation
QRD	QR decomposition
RLS	recursive least squares
rms	root-mean square
SNR	output signal to noise ratio
SOS	second order statistics
SVD	singular value decomposition
V-BLAST	vertical Bell Laboratory layered space time
WLAN	wireless local area networks

CHAPTER ONE

INTRODUCTION

1.1 Overview

Wireless communication has exhibited explosive growth in the past two decades and has become an essential part of everyday communication. The growing acceptance and dependence on wireless communication has driven the need for higher data rates and stricter reliability requirements. To support emerging multimedia applications researchers must look for better ways of exploiting the limited radio spectrum while maintaining the quality of service required by the users. Recent developments suggest that the use of multiple transmit and receive antennas can significantly enhance the performance and reliability of a wireless communication system. Multiple input multiple output (MIMO) systems take advantage of spatial diversity obtained through the spatially separated antennas in a dense multipath scattering environment [1]. Theoretical studies indicate that the capacity of MIMO systems grows linearly with the number of transmit antennas used. Many recent works have focused on exploiting the added spatial dimension to increase capacity [2]-[5]. In particular, the revolutionary vertical Bell Laboratory Layered Space Time (V-BLAST) architecture proposed by Foschini achieved the theoretical capacity limits of the MIMO architecture [6]. The multiple antennas configuration exploits the multipath effect to accomplish the additional spatial diversity. However, the multipath effect also causes the negative effect of frequency selectivity of the channel. Orthogonal frequency division multiplexing (OFDM) is a promising multi-carrier modulation scheme

that shows high spectral efficiency and robustness to frequency selective channels. In OFDM, a frequency-selective channel is divided into a number of parallel frequency-flat subchannels, thereby reducing the receiver signal processing of the system. OFDM has been adopted in many wireless standards such as digital audio broadcasting (DAB) [7], digital video broadcasting (DVB) [8], HIPERLAN/2 [9], IEEE 802.11a wireless local area networks (WLAN) [10], IEEE 802.16a metropolitan area network (MAN) [11], and a potential candidate for fourth-generation (4G) mobile wireless systems. The combination of OFDM and MIMO is a promising technique to achieve high bandwidth efficiencies and system performance. In fact, MIMO-OFDM is being considered for the upcoming IEEE 802.11n standard, a developing standard for high data rate WLANs [1].

1.2 Motivations

MIMO-OFDM has the potential to meet the increasing high speed and reliability demands of the future. In order for this technology to truly succeed in commercial deployment there are still several technical obstacles that must be tackled. A major impediment in MIMO-OFDM is the complicated receiver signal processing. The simultaneous emission of the signals from the multiple transmit antennas increases the mutual interference imposed on the signals, therefore, much more complex detection schemes are required to extract the transmitted signals. For example, the complexity of a maximum likelihood detector increases exponentially with the number of transmit antennas. Spatial equalizers and space-time coding has been proposed to simplify the detection for MIMO-OFDM systems [12]-[14]. Note, coherent detection requires knowledge of the channel; therefore, accurate channel estimation is crucial in realizing the full potential of

MIMO-OFDM. Channel estimation for OFDM has been well researched in literature. The extension of the results to MIMO-OFDM channel estimation is substantially more complicated. In a MIMO system, multiple channels have to be estimated simultaneously. The increased number of channel unknowns significantly increases the computational complexity of the channel estimation algorithm. Previous works have investigated the problem of channel estimation in MIMO-OFDM [15]-[18]. The most common approach is training-based estimation, where a known pilot sequence is transmitted and used at the receiver to determine the channel. The least square (LS) approach and the minimum mean square error (MMSE) approach are the usual methods for training-based estimation. The LS and MMSE solutions are relative simple compared to other estimation techniques such as blind estimation. However, both solutions still require complex matrix inversions, which are undesirable in real time implementation. In [18], specific training sequences design and pilot placement patterns are used to obtain the channel frequency response (CFR) of the channel in attempt to reduce the estimation complexity. Note that the number of unknowns of the CFR is usually significantly greater than the number of unknowns in the channel impulse response (CIR). In [19], it is proven that computational complexity can be reduced by estimating the CIR as opposed to the CFR. The proposed solution reduces the number of unknowns to be solved, but the solution still requires a matrix inversion. The main objective of our research is to explore methods for reducing the complexity of the channel estimation for MIMO-OFDM. We propose the use of QR decomposition to solve for the channel unknowns, which eliminates the matrix inversion operation. The

QR decomposition is low in complexity, stable and can be efficiently implemented in hardware.

1.3 Thesis Contributions

The main contributions of this thesis are described below.

- A QR decomposition method is introduced to reduce the complexity of LS estimation of a time invariant channel for a MIMO-OFDM. Complexity comparisons indicate that the QR decomposition method reduces the complexity substantially. Similarly, a novel QR decomposition method is developed for MMSE channel estimation. The MMSE solution is modified into the LS form so that QR decomposition can be efficiently applied. The results show a significant reduction in complexity as compared to the standard MMSE solution.

- A decoupled QR decomposition which requires no square root and fewer division operations is implemented to further reduce that complexity of the channel estimation.

- Investigation of the recursive implementation of the QR decomposition LS and MMSE for time-varying channels. The results show that the adaptive methods have better performance than the block based methods with the use of fewer pilot tones. In addition, simulations demonstrate that the QR decomposition methods converge faster that the recursive least squares (RLS) methods. The low complexity inverse-QR method is also applied to further reduce complexity.

1.4 Thesis Outline

In Chapter 2, background information on wireless communication channels is provided to aid the understanding of the problem of channel estimation. Also, an introduction of OFDM and MIMO system is given and the important characteristics of both technologies are emphasized. Finally, a complete system model of an MIMO-OFDM system is presented.

In Chapter 3, a literature survey of previous works on channel estimation for MIMO-OFDM is presented. Basic estimation theory of classical and Bayesian estimation is discussed. Representative methods of both classes are highlighted and in particular, the derivation of the LS and MMSE estimators are presented. The LS and MMSE solutions are adapted to the OFDM and MIMO-OFDM channel estimation. A performance analysis is performed to compare the LS and MMSE method for estimating the CIR of MIMO-OFDM systems.

In Chapter 4, first a review of QR decomposition and the different methods of determining the QR decomposition are provided. The details of using the Householder method, Givens rotation methods, and the decoupled Givens rotation method to solve for LS channel estimates are described. A performance and complexity analysis is performed to demonstrate the complexity reductions of the proposed implementations. Moreover, the MMSE solution is modified into the LS form in order to implement the QR decomposition mentioned. Similarly, the QR decomposition MMSE solution is compared with the standard MMSE solution.

In Chapter 5, adaptive channel estimation techniques are studied for time varying environments. The previous proposed QR decomposition method is

recursively implemented to track the changes of the channel. The adaptive algorithms are compared with block-based channel estimations.

In Chapter 6, a conclusion of the work presented in this thesis is given and some possible future works are suggested to extend this research.

CHAPTER TWO

BACKGROUND

In this chapter, basic wireless propagation theory is provided with emphasis on the impact of the small-scale fading effects on the wireless channel. In Section 2.2, an introduction of MIMO systems is given, and the various gains of MIMO systems are highlighted. Section 2.3 discusses the basics of OFDM modulation. Finally, in Section 2.4 a system model of a MIMO-OFDM is described.

2.1 Wireless Propagation Characteristics

The wireless propagation environment places fundamental limitations on the performance of the wireless communication system because the transmitted signal travels through different paths and interact with objects in the environment. These interactions include reflection, refraction, diffraction, and scattering which cause attenuation and variations in the received signal power and phase of the transmitted signal. In addition, the relative movement between the transmitter and receiver generates a Doppler shift which also impact the fading characteristics of the signal [20].

The effects of the wireless environment can be categorized as path loss or attenuation, large-scale (long-term) fading, and small-scale (short-term) fading [21]. The path loss effect refers to the decrease in signal power as the distance of the receiver increases with respect to the transmitter. The term fading describes the fluctuations in the envelope of the transmitted signal as it travels from the

transmitter to the receiver. Although channel fading is unpredictable, stochastic models have been developed to accurately predict the fading characteristics. Channel models are useful for designing communication systems. Large-scale fading, as the name implies, is the observations of the signal envelope over a large distance, i.e. several kilometres. In large-scale fading the signal varies slowly and has a lognormal distribution over distance as shown in Figure 2.1(a). Small-scale fading is observed within shorter distances or over a short period of time. In small-scale fading, rapid fluctuations of the signal envelope are observed. Small-scale fading can be described by the Rayleigh distribution, which is depicted in Figure 2.1(b). When a strong line-of-sight path exists, the Rician distribution is used to describe the small-scale fading [20].
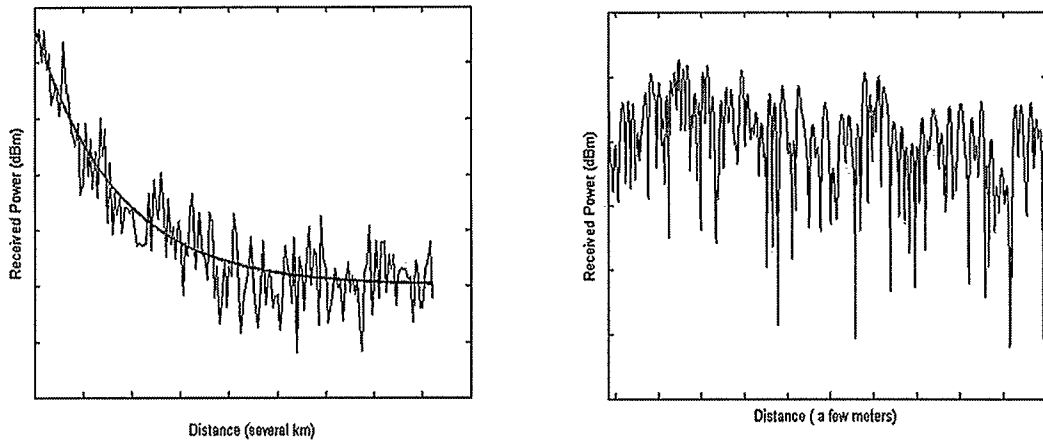
Figure 2.1: (a) Attenuation and lognormal fading effect on a signal over several kilometres. (b) Small-fading effects over a shorter distance of several meters.

In order to model a wireless communication system we first need to understand the wireless propagation characteristics so that a correct channel model can be developed. Generally, path loss and large-scale fading are frequency independent and more relevant for cell-site planning [21]. Combating small-scale fading is more pertinent in the design of reliable and efficient communication system. The three most important effects of small-scale fading is rapid fluctuations in signal strength over short time interval, random frequency modulation caused by Doppler shifts on different multipath signals, and time dispersion due to the arrival delays of the multipath signals [20]. In the following section, the two major causes, multipath and Doppler shift, of these effects will be described.

2.1.1 Multipath Effect

The multipath effect is a phenomenon that causes multiple versions of the transmitted signal to arrive at the receiver at different time delays. Reflecting objects and scatterers in the transmission environment generate multiple versions of the transmitted signal as shown in Figure 2.2. Each of the paths will have different characteristics, such as amplitude, phase, arrive time, and angle of arrival. The multiple signals may constructively or destructively add up at the receiver, thus creating the rapid fluctuations in the received signal envelope. When the signals add up constructively it will increase the signal power at the receiver, but destructive summation will cause fades in the received signal, which corresponds to the sudden drops in received power shown in Figure 2.1(b).
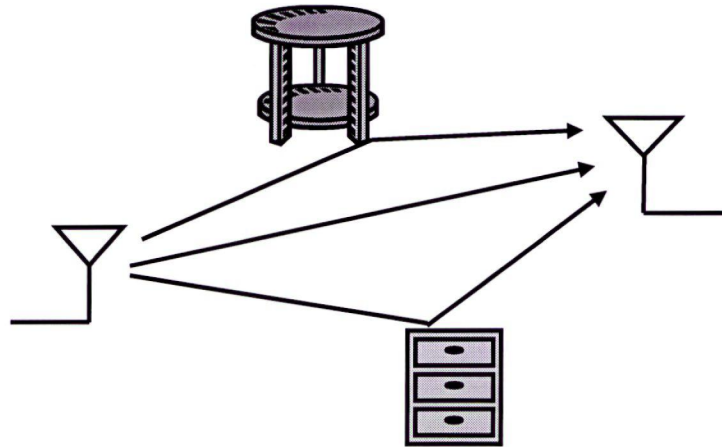
Figure 2.2: The multipath effect

Multipath does not only cause fluctuations in the received power, but it also affects the shape of the pulse as it is transmitted through the channel [21]. The arrival of the multiple versions will broaden the transmitted signal. As illustrated in Figure 2.3, the transmitted signal arriving at different times will overlap with each other and lead to a broadening of the envelope of the pulse.

(a)   (b)
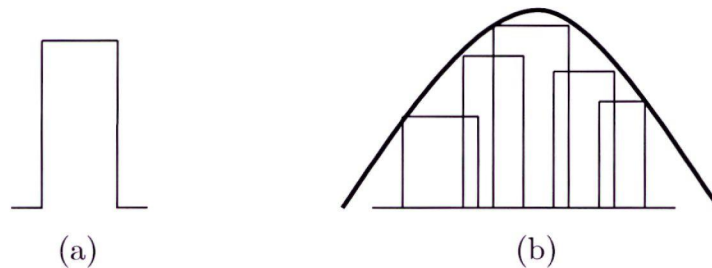
Figure 2.3: (a) A transmitted pulse. (b) Multiple copies of the transmitted signal arriving at different times causing a widened envelope of the pulse [21].

The signal power and arrival times of the multipath signals are used to characterize the channel. The typical impulse response of a channel is as shown in Figure 2.4, which is also known as the power delay profile of the channel. Assuming a narrow impulse is transmitted, each of the spikes in Figure 2.4 represents one of the multipath components. The parameters used to describe the power delay profile are the mean excess delay, root-mean square (rms) delay spread, and excess delay spread (X dB). The mean excess delay is defined as

$$\bar{\tau} = \frac{\sum_k p_k \tau_k}{\sum_k p_k}, \qquad (2.1)$$

where p_k is the power of the kth path and τ_k is the arrival time of the kth path. The rms delay spread is defined as

$$\sigma_d = \sqrt{\overline{\tau^2} - (\bar{\tau})^2}, \qquad (2.2)$$

where

$$\overline{\tau^2} = \frac{\sum_k p_k \tau_k^2}{\sum_k p_k} \qquad (2.3)$$

is the mean square delay. Finally the excess delay spread (X dB) refers to the time between the highest power signal and the arrival of a signal that is X dB below the maximum [20].
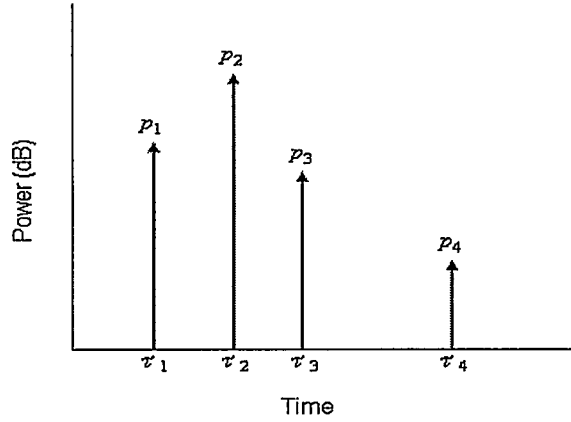
Figure 2.4: An impulse response of a wireless channel [21]

In the frequency domain, the channel can be described in terms of the coherence bandwidth. The coherence bandwidth, B_C, is a measure of the range of frequencies within which the amplitude is highly correlated. The coherence bandwidth is inversely proportional to the rms delay spread, and the specific relationship depends on the particular channel impulse response. The delay spread parameters and the coherence bandwidth determine whether the signal experience flat fading or frequency selective fading.

Flat fading occurs when the bandwidth of the signal, B_S, is much smaller than the B_C. Correspondingly, in the time domain the symbol period, T_S, is significantly larger than the rms delay spread. In flat fading, the spectral characteristics of the transmitted signal are maintained at the receiver. However, in the time domain, the transmitted signal will vary in amplitude over time due to the channel gains. The Rayleigh distribution is commonly used to describe the amplitude distribution [20]. Flat fading can cause deep fades, which will require increasing the signal power at the transmitter to compensate the power lost due to the deep fades.

A transmitted signal with a bandwidth greater than the coherence bandwidth of the channel will experience frequency selective fading. This causes different frequency components of the transmitted signal to experience different gains, hence the term frequency selective. From the time domain perspective, the symbol period is shorter than the rms delay spread. The channel will spread the signal beyond the symbol period and induce intersymbol interference (ISI) onto the next transmitted symbol. Frequency selective fading is harder to model than flat fading since each multipath component must be modeled [20].

2.1.2 Doppler Effect

Another effect that causes small-scale fading of a transmitted signal is the Doppler Effect. The motion of the receiver with respect to the transmitter results in a Doppler shift in the frequency, which changes the channel. Looking at Figure 2.5, where a mobile is moving at velocity, v, the Doppler shift is defined as

$$f_d = \frac{v}{c}\cos(\theta), \qquad (2.4)$$

where c is the velocity of the electromagnetic wave propagation in free space and θ is the angle as depicted in Figure 2.5. Taking into account the Doppler shift, the instantaneous frequency, f_{in}, will be

$$f_{in} = f_c \pm f_d, \qquad (2.5)$$

where f_c is the carrier frequency. Depending on the direction the receiver is moving with respect to the transmitter, the Doppler shift may be positive or negative. From Equation (2.4) it is clear that the value of the Doppler shift depends on the velocity of the receiver. Moreover, the significance of the Doppler shift depends on the carrier frequency of the signal. The coherence time, T_c, is

inversely proportional to the Doppler shift, which is the time interval in which the channel impulses are highly correlated. Evidently, the Doppler shift will affect how fast the channel is changing. The rate of change of the channel is classified as slow fading or fast fading.

The transmitted signal experiences slow fading when the symbol period is much smaller than the coherence time of the channel. In the frequency domain, this implies that the signal bandwidth is much greater than the Doppler shift. This means that the Doppler spread is negligible at the receiver.

Fast fading occurs when the symbol period is greater than the coherence time of the channel. The changing of the channel within one symbol period will distort the transmitted signal. In the frequency domain, the signal bandwidth is smaller than the Doppler shift [20].
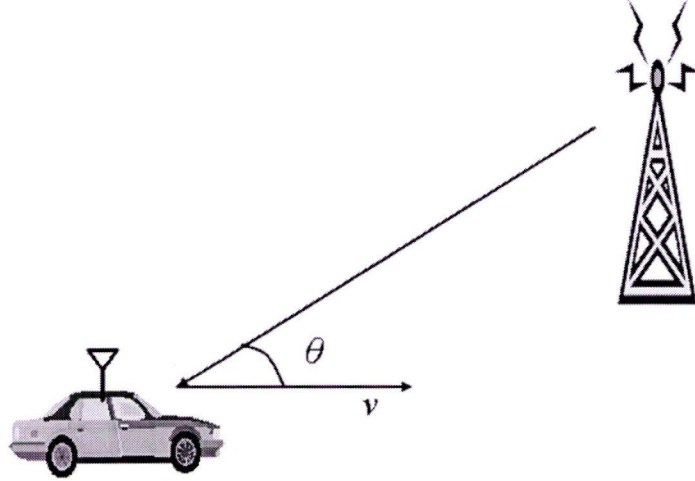
Figure 2.5: A receiver moving at velocity v, thus causing a Doppler shift.

As discussed above, small-scale fading can be described in two different ways due to two different phenomena. First, small-scale fading can be flat or frequency selective due to the multipath behaviours of the environment. This refers to the behaviour of the channel in the frequency domain. Secondly, it can be described as slow or fast fading due the Doppler shift caused by the motion of the receiver. Slow and fasting fading describes the rate the channel changes in the time domain.

2.2 Introduction to MIMO

A MIMO communication system uses multiple antennas at the transmitter and receiver to achieve various advantages. Traditionally, antenna arrays have been used at the transmitter and receiver to achieve array gain, which increases the output SNR of the system. In the mid-1990s, adaptive antennas and smart antennas were introduced to describe antennas arrays that are made adaptive in a manner that it changes its transmission and reception characteristics when the radio environment changes. Array antennas have been implemented in GSM networks [22], fixed broadband wireless access (BWA) networks [23], and third generation (3G) CDMA networks [24]. More recently, a new way of using the multiple antennas has been discovered to achieve diversity and multiplexing gain by exploiting the once negative effect of multipath. Under suitable conditions, i.e. a scatter rich environment, the channel paths between the different transmit and receive antennas can be treated as independent channels due to the multipath effects caused by the scatterers. Initial works in this research area ([6],[2]), suggests that MIMO effectively takes advantage of the random fading and multipath delay spread to increase the transfer rates of the system. The

exploitation of this additional 'spatial' degree of freedom can increase the throughput and improve the performance of the system [25]. In summary, the main advantages of MIMO systems can be categorized as array gain, diversity gain, and spatial multiplexing gain.

2.2.1 Array Gain

Array gain is achieved by coherently combining the signals from the multiple antennas to increase the average output signal to noise ratio (SNR), which will improve the range and coverage of the system. Figure 2.6 illustrates a simple case of a system consisting of one transmit antenna and a set of receive antenna array. Assume the distance between the transmitter and receiver is significantly larger than the antenna separation of the array at the receiver, then the received signal at each antenna will differ in phase due to the relative delay caused by the antenna separation. To maximize the received signal energy, an optimal receiver will use beamforming techniques to adjust for the different delays of the multiple antennas so that the received signals can be constructively combined [25]. This will yield a M_r-fold power gain, where M_r is the number of receive antennas. In a MIMO case where antenna arrays are used at the transmitter and receiver, then a $M_t M_r$-fold power gain is achievable, where M_t is the number of transmit antennas. Beamforming requires knowledge of the channel state information (CSI) at the transmitter and receiver to appropriately compensate for the delays. Typically, the channel can be estimated at the receiver; however, the CSI is harder to obtain at the transmitter.
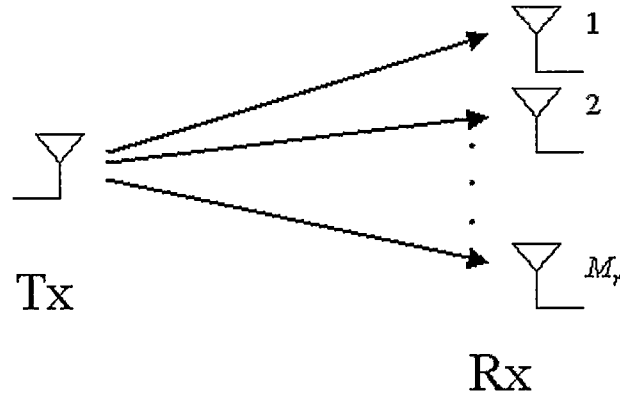
Figure 2.6: Single transmit and multiple receive antenna system

2.2.2 Diversity Gain

Diversity is a technique used to mitigate fading in wireless links by transmitting a signal over multiple independently fading paths. The main idea behind diversity is that by transmitting multiple copies of the signal increases the probability that at least one copy is received correctly at the receiver. Diversity can be obtained through time, frequency, or space. Time diversity assumes that a signal will experience independent fading at different times due to changes in the channel. To achieve time diversity a signal is coded and interleaved so that multiple copies of the signal are transmitted at intervals greater than the channel coherence time. The benefit of time diversity is that it does not require additional hardware. However, it requires memory storage of the repeated signals for processing [21]. Frequency diversity is achieved when the carrier frequencies are sufficiently separated such that each carrier frequency will experience independent fading. In frequency diversity, the same signal is transmitted on various independent carrier frequencies. Multiple receivers are used to detect the multiple signals at different carrier frequencies, and the one with the highest

signal energy will be selected. Alternatively, a multi-antenna system can exploit the independent multipath channels to achieve spatial diversity. The benefit of spatial diversity is that no additional receiver hardware is required as in frequency diversity, or memory storage as in time diversity. The diversity order is the total number of independent fading signal paths between the transmitter and receiver, which depends on the spatial separation of the antennas and the scatterness of the environment. The maximum spatial diversity gain of a MIMO system is $M_t M_r$. Joint diversity schemes such as space-time and space-frequency coding at the transmitter and receiver has been developed to increase the diversity order of the system. In 1998, independent pioneer work by Alamouti in [26] and Tarokh et al. in [27] developed a breakthrough space-time transmitter diversity system that provides diversity gain without sacrificing the bandwidth.

2.2.3 Spatial Multiplexing Gain

Multiplexing gain is achieved through transmitting different signals on independent channels in a MIMO system. The multiplexing gain order is the number of parallel independent spatial data pipes in the same frequency band between the transmitter and receiver. As shown in Figure 2.7, a signal is split into two parts and transmitted on two separate antennas. At each receive antenna it will detect a signal from a specific transmit antenna and the signals from other antennas will be seen as interference. Combining techniques are required at the receiver to eliminate the interference and to multiplex the signal back together. As demonstrated, capacity gain is achieved by reducing the transmission time without using additional bandwidth. In [6], Foschini proposed the groundbreaking BLAST (Bell Laboratories Layered Space-Time) architecture

which utilizes the multiple transmit and receive antennas to achieve multiplexing gains. It was shown under scatter-rich environments the achievable gain is linear with the number of independent channels. Since then, many other works have further investigated the performance and capacity limits of BLAST in various environments and system requirements.
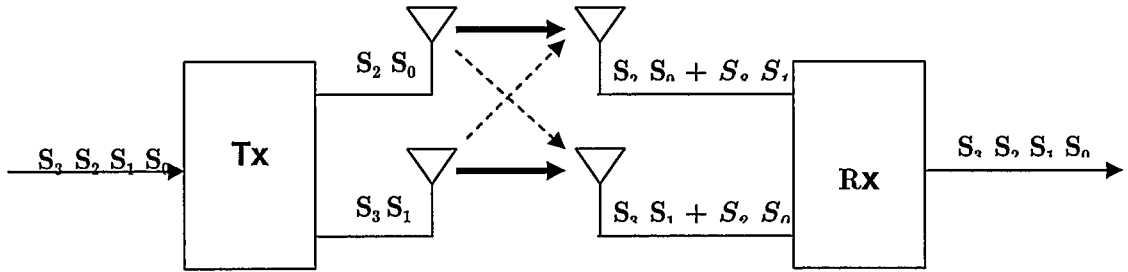
Figure 2.7: Multiplexing gain 2x2 MIMO system

In summary, the use of MIMO has many benefits. However, it is not possible to achieve all the above benefits of MIMO techniques in one system as some of them are mutually conflicting goals. In general, a MIMO system improves

- Spectral efficiency: multiplexing gain

- Link reliability: diversity gain

- Coverage: Diversity gain and array gain

- Capacity: multiplexing gain

2.3 Introduction to OFDM

In recent years, OFDM has gained considerable attention as it shows to be a promising technique for high data rate transmission. In OFDM, a broadband signal is split into multiple parallel narrowband signals, and then modulated onto orthogonal subcarriers for transmission. One of the most attractive features of OFDM is its robustness against frequency selective channels. The OFDM operation converts a frequency selective channel into multiple parallel flat fading channels, which greatly simplifies the channel estimation and equalization tasks of the receiver. When a wideband signal passes through a frequency selective channel as shown in Figure 2.8(a), a significant portion of the signal is lost due to the deep fades in the channel. However, when the wideband signal is OFDM modulated, the frequency spectrum will be a composition of overlapping narrowband signals as shown in Figure 2.8(b). Now, when the OFDM modulated signal passes through the frequency selective channel only the narrowband signals at the location of the fades will be affected. In addition, it can be observed that each of the narrowband signals experiences flat fading; therefore, the channel response can be obtained simply by dividing the output signal by the input signal. Moreover, OFDM is bandwidth efficient since the subchannels can overlap yet still be separated due to the use of orthogonal subcarriers. With the current advancements in digital signal processor (DSP) and integrated circuit (IC) technology OFDM can be efficient implemented by using the inverse fast Fourier transform (IFFT) and fast Fourier transform (FFT) for modulation and demodulation, respectively.
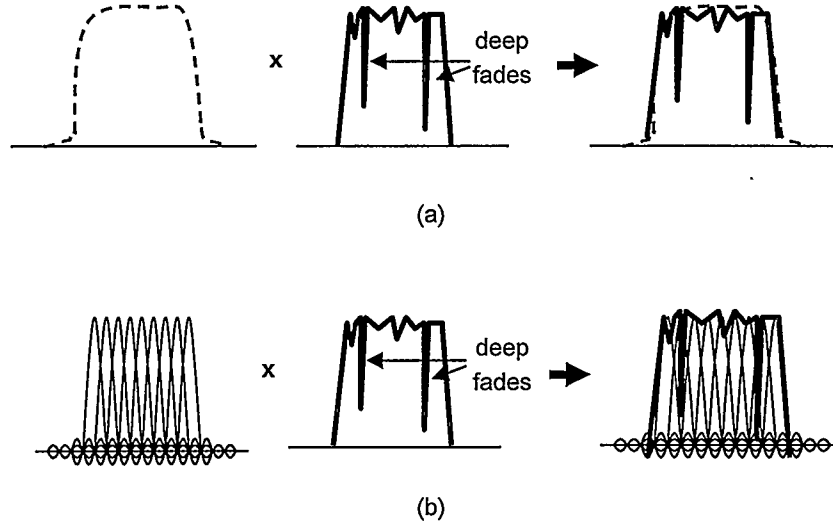
Figure 2.8: (a) A wideband signal multiplied with a frequency selective channel. (b) A OFDM signal multiplied with a frequency selective channel.

A schematic diagram of the complete structure of an OFDM system is shown in Figure 2.9. The blocks on the top row correspond to components in the transmitter and the bottom row to the receiver. The input data stream is modulated using regular modulation techniques such as phase shift keying (PSK) or quadrature amplitude modulation (QAM). The modulated signal $X(n)$ ($n = 0$, $1, ... N$, where N is the number of subcarriers) is converted into parallel signals and passed to the IFFT block. The IFFT operation modulates the parallel signals onto orthogonal subcarriers as a group. The narrowband signals outputted are $x(k)$ ($k = 0, 1, ... N$), where

$$x(k) = \frac{1}{\sqrt{N}} \sum_{n=0}^{N-1} X(n) e^{j2\pi kn/N}, \qquad 0 \leq k \leq N-1 \qquad (2.6)$$

When an OFDM signal passes through the channel it will experience ISI and interchannel interference (ICI). The ISI arises from channel delay spread and ICI

is caused by the loss of orthogonality of the subcarriers due to the frequency response of the channel. In order to eliminate the effects of ISI and ICI a cyclic prefix (CP) of length N_{cp} , where N_{cp} is greater than the channel order, is appended to the beginning of the signal. The total length of the signal becomes $N+N_{cp}$. In the cyclic prefix extension, the end portion of the signal will be copied and appended to the beginning of the signal. Repeating the last elements at the beginning converts the linear convolution of the channel into circular convolution thereby preserving the orthogonality of the subcarriers [28]. At the receiver the inverse operations are performed to recover the transmitted bits.
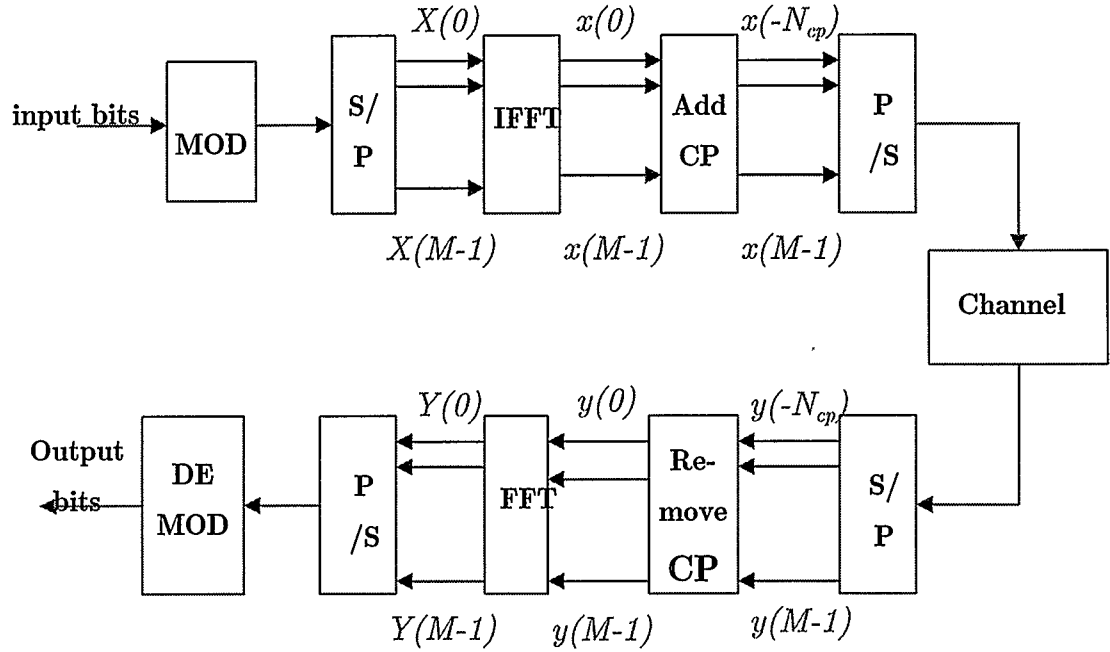
Figure 2.9: Schematic diagram of OFDM system

2.4 MIMO-OFDM System Model

OFDM is a promising physical layer technology for high data rate wireless communication due to its effectiveness in frequency selective fading, high spectral efficiency, and low computational complexity. MIMO systems have the ability to improve spectral efficiency, link reliability, coverage or capacity depending on how the system is implemented. Clearly, OFDM integrated with MIMO transceivers will further enhance the performance and throughput of a system.

A typical MIMO-OFDM system is depicted in Figure 2.10. The system consists of M_t transmit antennas and M_r receive antennas. At time t, a block of binary input data stream is modulated, and then passed through the MIMO encoder to produce M_t data streams for transmission over the multiple antennas. The data can be space-time coded for diversity gain, or de-mulitplexed for spatial multiplexing gain. Each of the M_t data streams is grouped into blocks of N symbols, and then OFDM modulated for transmission across the MIMO channels. The received signal at each antenna will be a summation of all the signals from the multiple paths plus the noise. The noise process is additive white Gaussian noise (AWGN) with zero mean and variance σ_n^2. It is assumed that the signal and noise are independent of each other, which is a common assumption made in literature.
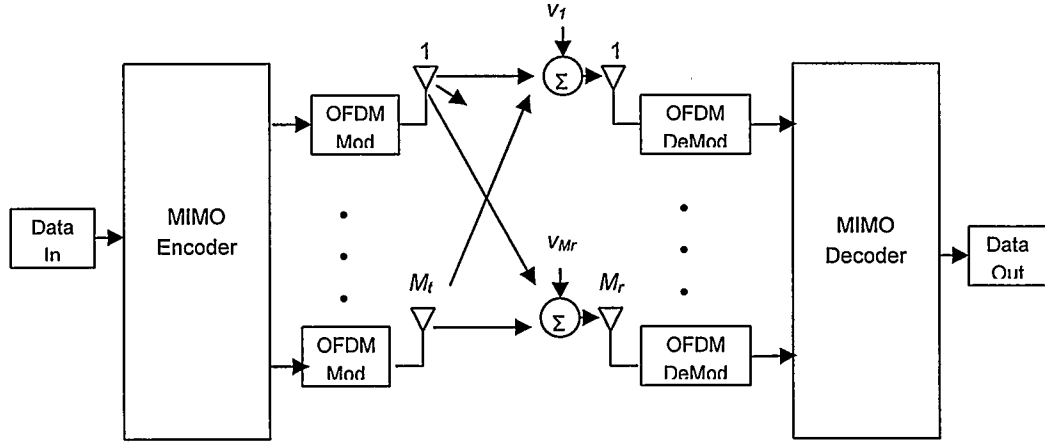
Figure 2.10: MIMO-OFDM system

2.4.1 Channel Model

The channel considered in this thesis is a frequency selective Rayleigh fading channel. The radio channel can be modeled as a linear filter with a time varying impulse response [20]. Characterizing the channel as an impulse response will provide all the necessary information required for simulation and analysis of signal transmission through the channel. The impulse response for a fading multipath channel is modeled as

$$h(\tau,t) = \sum_{i=1}^{L} a_i(t)\, \delta(\tau - \tau_i(t)), \qquad (2.7)$$

where $a_i(t)$ is the complex amplitude, $\tau_i(t)$ is the delay of the ith path and L is the length of the channel. The amplitude and the number of paths are dependent on the dispersiveness of the wireless channel. The frequency response at time t is

$$H(t,f) = \int h(\tau,t) e^{-j2\pi f t} d\tau. \qquad (2.8)$$

In an OFDM system, the channel frequency response can be expressed as

$$H[n,k] = \sum_{l=0}^{L-1} h[n,l] e^{-j2\pi kl/K},$$

(2.9)

where K is the number of tones of the OFDM block.

In general, wireless communication channels are time-varying either due to the motion of the transmitter or receiver, or the change in the wireless environment. However, in indoor environments under lower mobility scenarios the channel variations are slow and can be ignored for the duration of a packet. Then Equation (2.9) can be rewritten as

$$H[k] = \sum_{l=0}^{L-1} h[l] e^{-j2\pi kl/K}.$$

(2.10)

2.4.2 Mathematical Model of System

Consider the MIMO-OFDM system, diagrammed in Figure 2.10, consisting of M_t transmit and M_r receive antennas operating in a Rayleigh frequency selective fading environment. The tap-delay channel model of the multiple channels is shown in Figure 2.11. Let $\mathbf{S}_t^{(i)}$ be the frequency domain input block of N complex-valued symbol prior to OFDM processing at time t at the ith transmit antenna, where $\mathbf{S}_t^{(i)} = \left[S_t^{(i)}(0), S_t^{(i)}(1), \cdots, S_t^{(i)}(N-1) \right]^H$, $i = 1, 2, \ldots M_t$ and $s_t^{(i)}$ is the time domain representation after the IFFT operation with N_{cp} CP symbols inserted, where $\mathbf{s}_t^{(i)} = \left[s_t^{(i)}(0), s_t^{(i)}(1), \cdots, s_t^{(i)}(N+N_{cp}-1) \right]^H$, $i = 1, 2, \ldots M_t$.
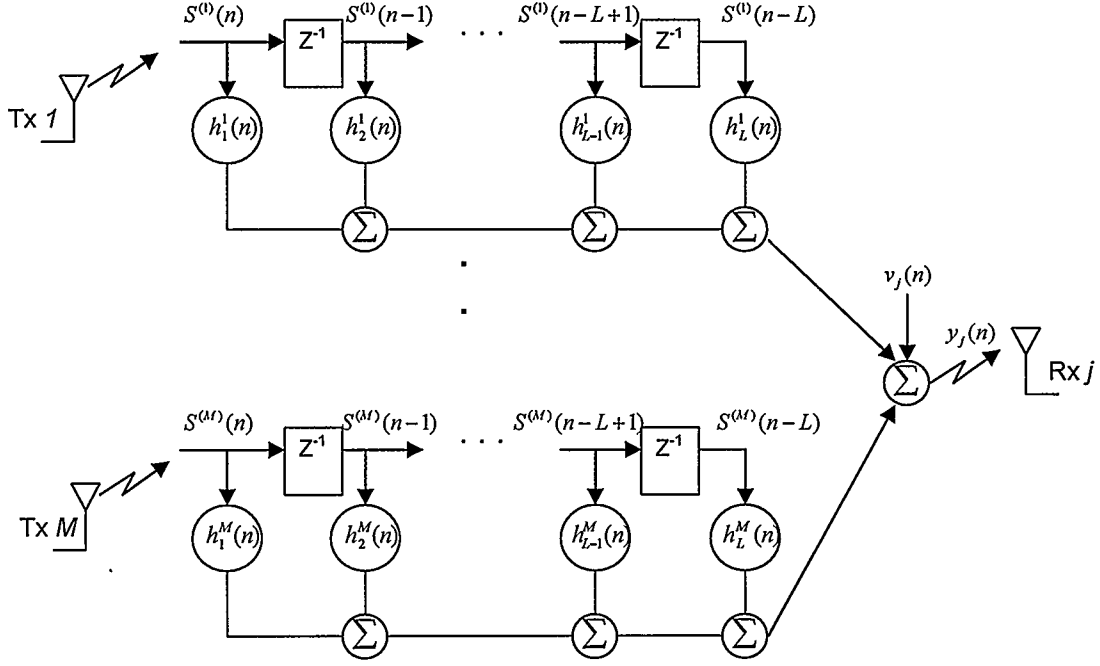
Figure 2.11: Tap delay line model of MIMO channel

2.4.2.1 Received Signal Prior to OFDM Demodulation

The time domain received signal at the jth antenna before OFDM demodulation depicted in Figure 2.11 can be represented as

$$y_t^{(j)}(n) = \sum_{i=1}^{M_t} \sum_{l=0}^{L_{ji}-1} h^{(j,i)}(l)\, s_t^{(i)}(n-l) + v_t^{(j)}(n), \qquad n=0,1,\ldots,(N+N_{cp})-1 \qquad (2.11)$$

where $h^{(j,i)}(l)$ $(l = 0,1,\ldots,L_{ji})$ is the channel response between the ith transmitter and the jth receiver, and L_{ji} is the channel order and $v_t^{(j)}(n)$ is the AWGN. In vector form the received signals for all M_r receive antennas can be written as

$$\mathbf{y}_t(n) = \sum_{i=1}^{M_t} \sum_{l=0}^{L-1} \mathbf{h}^{(i)}(l) s_t^{(i)}(n-l) + \mathbf{v}_t^{(j)}(n), \qquad n=0,1,\ldots,(N+N_{cp})-1 \qquad (2.12)$$

where, $\mathbf{y}_t(n) = \left[y_t^{(1)}(n), y_t^{(2)}(n), \cdots, y_t^{(M_r)}(n) \right]^H$, $\mathbf{h}^{(i)}(l) = \left[h^{(1,i)}(l), h^{(2,i)}(l), \cdots, h^{(M_r,i)}(l) \right]^H$,

and $\mathbf{v}_t(n) = \left[v_t^{(1)}(n), v_t^{(2)}(n), \cdots, v_t^{(M_r)}(n) \right]^H$, all with dimensions $(M_r \times 1)$. By changing the summation order of Equation (2.12) the received vector can be re-written as

$$\mathbf{y}_t(n) = \sum_{l=0}^{L-1} \mathbf{h}(l) \mathbf{s}_t(n-l) + \mathbf{v}_t(n), \qquad n = 0,1,...(N+N_{cp})-1 \qquad (2.13)$$

where $\mathbf{h}(l) = \left[\mathbf{h}^{(1,i)}(l), \mathbf{h}^{(2,i)}(l), \cdots, \mathbf{h}^{(M_r,i)}(l) \right]$ is a matrix of size $(M_r \times M_t)$ and

$\mathbf{s}_t(n-l) = \left[s^{(1)}(n-l), s^{(2)}(n-l), \cdots, s^{(M_t)}(n-l) \right]^H$ is $(M_t \times 1)$ vector. Finally, in matrix form Equation (2.13) can be expressed as

$$\mathbf{y}_t = \mathbf{G}\mathbf{s}_t + \mathbf{v}_t, \qquad t = 0,1,2,... \qquad (2.14)$$

where $\mathbf{y}_t = \left[\mathbf{y}_t(0), \mathbf{y}_t(1), \cdots, \mathbf{y}_t(N+N_{cp}-1) \right]^H$ is a vector of size $(M_t(N+P) \times 1)$,

$$\mathbf{G} = \begin{bmatrix} \mathbf{h}(0) & & & & & \\ \mathbf{h}(1) & \mathbf{h}(0) & & & & \\ . & \mathbf{h}(1) & . & & & \\ . & . & . & & & \\ . & . & . & . & & \\ \mathbf{h}(L-1) & . & & . & . & \\ & \mathbf{h}(L-1) & & & . & . \\ & & . & & . & \mathbf{h}(0) \\ & & . & & & \mathbf{h}(1) \\ & & & . & & . \\ & & & . & & . \\ & & & & . & . \\ & & & & & \mathbf{h}(L-1) \end{bmatrix}$$

is a block toeplitz matrix with dimensions of $(M_t(N+N_{cp}) \times M_r N)$,

$\mathbf{s}_t = \left[\mathbf{s}_t(0), \mathbf{s}_t(1), \cdots, \mathbf{s}_t(N-1) \right]^H$ is a $(M_r N \times 1)$ vector and

$\mathbf{v}_t = \left[\mathbf{v}_t(0), \mathbf{v}_t(1), \cdots, \mathbf{v}_t(N+N_{cp}-1) \right]^H$ is a $(M_t(N+N_{cp}) \times 1)$ vector.

2.4.2.2 Received Signal after OFDM Demodulation

After $\mathbf{y}_t$ is OFDM demodulated by the FFT transformation and the CP is removed, the signal at receive antenna j^{th} in the frequency domain representation is

$$Y_k^{(j)} = \sum_{i=1}^{M_t} H_k^{(j,i)} S_k^{(i)} + V_k^{(j)}, \qquad k = 0,1,\ldots N-1 \tag{2.15}$$

where, $H_k^{(j,i)}$ is the frequency response at the kth subcarrier, $S_k^{(i)}$ is the transmitted signal in the frequency domain, and $V_k^{(j)}$ is the noise in the frequency domain. The frequency response of the channel $H_k^{(j,i)}$ is obtained as described in Equation (2.9). The $V_k^{(j)}$ is defined as

$$V_k^{(j)} = \frac{1}{\sqrt{N}} \sum_{n=0}^{N-1} v^{(j)}(n) e^{-j2\pi kn/K}. \tag{2.16}$$

The vector form equation for all N subcarriers can be expressed as

$$\mathbf{Y}^{(j)} = \sum_{i=1}^{M_t} \mathbf{X}^{(j,i)} \mathbf{H}^{(j,i)} + \mathbf{V}^{(j)}, \tag{2.17}$$

where $\mathbf{Y}^{(j)} = \left[Y_0^{(j)}, Y_1^{(j)}, \cdots, Y_{N-1}^{(j)} \right]^H$ is a vector of size $(N \times 1)$,

$\mathbf{X}^{(j,i)} = diag\left\{ S_0^{(j,i)}, S_1^{(j,i)}, \cdots, S_{N-1}^{(j,i)} \right\}$ is a diagonal matrix with dimensions $(N \times N)$,

$\mathbf{V}^{(j)} = \left[V_0^{(j)}, V_1^{(j)}, \cdots, V_{N-1}^{(j)} \right]^H$ and $\mathbf{H}^{(j,i)} = \left[H_0^{(j,i)}, H_1^{(j,i)}, \cdots, H_{N-1}^{(j,i)} \right]^H$ is $(N \times 1)$ vector. The received signal for all the receive antennas can be expressed in the following form

$$\mathscr{Y} = \mathscr{X}\mathscr{H} + \mathscr{V} \tag{2.18}$$

where $\mathscr{Y} = \left[\mathbf{Y}^{(1)}, \mathbf{Y}^{(2)}, \cdots, \mathbf{Y}^{(M_r)} \right]$, $\mathscr{X} = \left[\mathbf{X}^{(1)}, \mathbf{X}^{(2)}, \cdots, \mathbf{X}^{(M_t)} \right]$, $\mathscr{V} = \left[\mathbf{V}^{(1)}, \mathbf{V}^{(2)}, \cdots, \mathbf{V}^{(M_r)} \right]$, and

$$\mathcal{H} = \begin{bmatrix} \mathbf{H}^{(1,1)} & \mathbf{H}^{(1,2)} & \cdots & \mathbf{H}^{(1,M_r)} \\ \mathbf{H}^{(2,1)} & \mathbf{H}^{(2,2)} & & \vdots \\ \vdots & & \ddots & \vdots \\ \mathbf{H}^{(M_t,1)} & \cdots & \cdots & \mathbf{H}^{(M_t,M_r)} \end{bmatrix}.$$

2.5 Summary

In this chapter, we discussed the effects imposed on the wireless channel due to small-scale fading. The multipath effect and Doppler shift causes the channel to be flat, frequency selective, slow, or fast fading. A scatter-rich environment generates multiple copies of the transmitted signal and causes them to be received at different times at the receiver. The multipath delays cause the signal to experience frequency selectivity as explained in Section 2.2. In Section 2.3, we discussed that this negative effect of multipath signals can be exploited to improve the capacity and reliability of the system. We discovered in Section 2.4 that OFDM techniques are very robust in combating frequency selective channels. Therefore, combining MIMO and OFDM is beneficial to future communication system. We thoroughly described and mathematically modeled a MIMO-OFDM system in Section 2.5.

CHAPTER THREE

CHANNEL ESTIMATION

In this chapter, a general overview on estimation theory is provided and the problem of channel estimation in a communication system is investigated. In Section 3.2, the training-based least squares (LS) estimator and Bayesian minimum mean square error (BMMSE) estimator are derived. Finally, simulation results of LS and BMMSE estimation for a MIMO-OFDM system is shown in Section 3.3.

At the receiver, the ultimate goal is to recover the signal that was originally transmitted. A variety of equalization and signal detection techniques have been developed for MIMO systems depending on whether it is a diversity or spatial multiplexing system. Regardless of the type of MIMO system, most of the equalization/detection schemes require knowledge of the channel information in order to recover the signal. Hence, developing an efficient method of approximating the transmission channel between the transmitter and receiver is an essential component of the receiver design. There are some studies on joint channel estimation and detection and blind detection where the channel estimates are not required [29] and [30]. Generally, these schemes are higher in complexity or lead to performance loss. In this thesis, we will only focus on the channel estimation component of the receiver design.

3.1 General Channel Estimation Overview

Channel estimation can be categorized into two classes, training-based or blind channel estimation, each with its benefits and disadvantages. In training-based estimation a pilot sequence known to the receiver is embedded into the signal block and transmitted over the channel. At the receiver, the channel is estimated using the received signal and the known training sequence. Some advantages of training based estimation are high accuracy, relative lower complexity, and many existing standards such as GSM and IEEE 802.11a have allocated time slots for training sequence transmission. A drawback of training-based estimation is reduced bandwidth efficiency due to the wasteful transmission of training sequence. Blind estimation on the other hand does not require a training sequence; instead it estimates the channel based solely on the received signal. Through the exploitation of the statistical properties of the received signal and channel structure an estimate of the channel is generated. A widely studied blind estimation technique is the subspace method using second order statistics (SOS). In the subspace method, the autocorrelation matrix of the received signal is decomposed into the signal and noise subspace. Due to the orthogonality of the noise and signal subspace, the channel estimates can be calculated based on the noise subspace [31]. There are several issues to be noted when using this blind technique. Firstly, the subspace method requires knowledge of the channel order. Some subspace methods can fail if the channel is over estimated. More importantly, the decomposition of the autocorrelation function via eigenvalue decomposition (EVD) or singular value decomposition (SVD) is highly complex. In real-time systems, these blind estimation techniques cannot be practically implemented due to their intense computational complexity. In addition, blind

methods rely on time averaging over a constant period, thus requiring the channel to be slow varying over a large packet of symbols. This makes blind algorithm not suitable for fast varying channels. In general, blind channel estimation techniques are restrictive since it relies on some data or channel assumptions, and it is high in computational complexity. Due to these impracticalities of blind estimation, we focus our research on the more practical technique of training-based channel estimation.

3.2 Estimation Theory

This section will provide some basic background knowledge on estimation theory. In estimation theory there are two general types of estimation approaches: 1) classical estimation, and 2) Bayesian estimation. In the classical approach, the vector to be estimated is viewed as a deterministic but unknown vector and the estimate is determined based on the probability density function (PDF). In Bayesian estimation the unknown vector is regarded as a random vector and prior information such as the mean, variance, and apriori PDF are used to determine the estimate. The following section briefly summarizes the derivation of the two types of estimators. For more detailed derivations refer to [32].

3.2.1 Classical Estimation

In classical estimation, the optimal estimator is one that is unbiased with minimum variance. In general as mentioned in [32], the minimum variance unbiased estimator (MVUE) does not always exist. A popular suboptimal

estimator is the maximum likelihood (ML) estimate which approaches optimality for large data sets. In the ML approach, the estimation problem is posed as the maximization of the likelihood function parameterized by the unknown CIR vector. However, a closed-form solution for this problem might not always exist. In [15], an expectation maximization (EM) algorithm is proposed to solve this incomplete problem. The EM algorithm breaks the ML problem into a sequence of quadratic optimizations that can be iteratively solved to give an estimate that approaches the ML estimate. The performance of the EM algorithm largely depends on the initial estimate. The EM algorithm was used for channel estimation for a MIMO-OFDM system in [33]. The drawback of the ML estimator is that the PDF of the unknown vector must have a maximum or else the estimate might not converge. Also, this method only approaches optimality when a large set of data is available.

3.2.1.1 Least Squares Estimation

In practice, the least squares (LS) estimator is more commonly used due to its ease of implementation and acceptable performance. The criteria for a good estimator are that it is unbiased and has minimum variance. The LS estimator uses variance as a measure of performance by choosing an estimate that minimizes the error between the estimate and the true value. We will briefly present the derivation of the LS estimator using the following general linear data model:

$$\mathbf{Y} = \mathbf{H}\boldsymbol{\theta} + \mathbf{W} \tag{3.1}$$

where $\mathbf{H}$ is a known N x P matrix, $\boldsymbol{\theta}$ is P x 1 vector, and $\mathbf{W}$ is a N x 1 vector. The objective is to determine an estimate $\boldsymbol{\theta}$ vector. The LS approach tries to solve the estimation problem by minimizing the following cost function:

$$J(\boldsymbol{\theta}) = (\mathbf{Y} - \mathbf{H\theta})^H (\mathbf{Y} - \mathbf{H\theta}). \tag{3.2}$$

The gradient of the above equation is

$$\frac{\partial J(\boldsymbol{\theta})}{\partial \boldsymbol{\theta}} = -2\mathbf{H}^H \boldsymbol{\theta} + 2(\mathbf{H})^H \mathbf{H\theta}. \tag{3.3}$$

Equating the gradient to zero will yield the LS estimate

$$\hat{\boldsymbol{\theta}} = (\mathbf{H}^H \mathbf{H})^{-1} (\mathbf{H})^H \mathbf{Y}. \tag{3.4}$$

3.2.1.2 Least Squares Estimation MSE Bound

Given the estimate, $\hat{\boldsymbol{\theta}}$, the mean square error (MSE) of the estimate is defined as

$$MSE_{\hat{\boldsymbol{\theta}}} = \frac{1}{P} E \left\{ \left\| \hat{\boldsymbol{\theta}} - \boldsymbol{\theta} \right\|^2 \right\}. \tag{3.5}$$

Substitute the LS estimate from Equation (3.4) into Equation (3.5). Then, the MSE of the LS estimator becomes

$$
\begin{aligned}
MSE_{LS} &= \frac{1}{P} E \left\{ \left\| (\mathbf{H}^H \mathbf{H})^{-1} (\mathbf{H})^H \mathbf{Y} - \boldsymbol{\theta} \right\|^2 \right\} \\
&= \frac{1}{P} Trace \left\{ E \left\{ (\mathbf{H}^H \mathbf{H})^{-1} (\mathbf{H})^H \mathbf{W})(\mathbf{H}^H \mathbf{H})^{-1} (\mathbf{H})^H \mathbf{W})^H \right\} \right\} \\
&= \frac{1}{P} Trace \left\{ ((\mathbf{H}^H \mathbf{H})^{-1} \mathbf{H}^H E \left\{ \mathbf{W} \mathbf{W}^H \right\} \mathbf{H} (\mathbf{H}^H \mathbf{H})^{-1} \right\} \\
&= \frac{\sigma_W^2}{P} Trace \left\{ (\mathbf{H}^H \mathbf{H})^{-1} \right\}.
\end{aligned}
\tag{3.6}
$$

3.2.2 Bayesian Estimation

When some prior knowledge about the unknown vector of the system is available it can be incorporated into the estimator to enhance the performance. If the prior knowledge is accurate, a Bayesian estimator will outperform the optimal classical estimator. This comes at the price of added computational complexity and dependence on additional information of the unknown vector.

3.2.2.1 Minimum Mean Square Error Estimation

The MMSE estimator is a popular Bayesian approach that uses the prior knowledge of the PDF of the unknown vector. The MMSE estimator is developed using the same linear model as in Equation (3.1). The Bayesian MSE is defined as

$$Bmse(\hat{\theta}) = E[(\theta - \hat{\theta})^2].$$
(3.7)

In Bayesian estimation, θ is a random variable, therefore the expectation operation is with respect to the joint PDF $p(\mathbf{Y},\theta)$. So the estimator can be rewritten as

$$Bmse(\hat{\theta}) = \int \int (\theta - \hat{\theta})^2 p(\mathbf{Y},\theta) \, d\mathbf{Y} \, d\theta.$$
(3.8)

Using the Bayes' theorem

$$p(\mathbf{Y},\theta) = p(\theta \mid \mathbf{Y}) p(\mathbf{Y})$$
(3.9)

the estimate becomes

$$Bmse(\hat{\theta}) = \int \left[\int (\theta - \hat{\theta})^2 p(\theta \mid \mathbf{Y}) d\theta \right] p(\mathbf{Y}) d\mathbf{Y}.$$
(3.10)

Taking the gradient of Equation (3.10) and equating it to zero will give the Bayesian MMSE estimate of

$$\hat{\theta} = \int \theta \, p(\theta \mid Y) d\theta \qquad (3.11)$$

or

$$\hat{\theta} = E(\theta \mid Y), \qquad (3.12)$$

which is simply the mean of the posterior PDF $p(\theta \mid Y)$. If the unknown vector and the noise vector are Gaussian with zero mean and uncorrelated, then the posterior PDF $p(\theta \mid Y)$ is also Gaussian with mean defined as

$$
\begin{aligned}
E(\theta \mid Y) &= E(Y) + \mathbf{C}_0 \mathbf{H}^H (\mathbf{H} \mathbf{C}_0 \mathbf{H}^H + \mathbf{C}_W)^{-1} (Y - E(Y)) \\
&= \mathbf{C}_0 \mathbf{H}^H (\mathbf{H} \mathbf{C}_0 \mathbf{H}^H + \mathbf{C}_W)^{-1} Y.
\end{aligned}
\qquad (3.13)
$$

which is the solution of MMSE estimation of θ.

3.2.2.2 Minimum Mean Square Estimation MSE Bound

In MMSE estimation the error is defined as

$$
\begin{aligned}
\varepsilon &= \theta - \hat{\theta} \\
&= \theta - E(\theta \mid Y).
\end{aligned}
\qquad (3.14)
$$

The error covariance matrix is defined as

$$
\begin{aligned}
\mathbf{C}_\varepsilon &= E_{Y,\theta}(\varepsilon \varepsilon^H) \\
&= E_{Y,\theta}\left\{ (\theta - E(\theta \mid Y))(\theta - E(\theta \mid Y))^H \right\} \\
&= E_Y E_{\theta \mid Y}\left\{ (\theta - E(\theta \mid Y))(\theta - E(\theta \mid Y))^H \right\} \\
&= E_Y(\mathbf{C}_{\theta \mid Y}),
\end{aligned}
\qquad (3.15)
$$

where $\mathbf{C}_{\theta \mid Y}$, the covariance matrix of the posterior PDF $p(\theta \mid Y)$, is

$$C_{0|Y} = C_{00} - C_{0Y}C_{YY}^{-1}C_{Y0}. \tag{3.16}$$

Since the $C_{0|Y}$ does not depend on Y, then

$$C_\varepsilon = C_{h|Y}. \tag{3.17}$$

Note that, $C_{00} = C_0$, $C_{0Y} = C_0 H^H$, $C_{YY} = H C_0 H^H + C_W$, and $C_{Y0} = H C_0$ so,

$$C_\varepsilon = C_0 - C_0 H^H (H C_0 H^H + C_W)^{-1} H C_0 \tag{3.18}$$

or

$$C_\varepsilon = \left(C_0^{-1} + H^H C_W^{-1} H\right)^{-1}. \tag{3.19}$$

The diagonal elements $[C_\varepsilon]_{(i,i)}$, where $i = 0, 1, \ldots, P$, are defined as

$$[C_\varepsilon]_{(i,i)} = \int\int (\theta_i - E(\theta_i \,|\, Y))^2 \, p(Y, \theta_i) \, dY \, d\theta_i, \tag{3.20}$$

which are the minimum MSE for θ_i.

3.2.3 Remarks of LS and MMSE Estimation

1. In LS estimation, according to Equation (3.4), the known matrix H must be full rank to ensure the invertibility of $(H^H H)$. On the contrary, in MMSE estimation, H does not need to be full rank to ensure the invertibility of $(H C_0 H^H + C_W)$ in Equation (3.11).

2. If there is no prior knowledge about the channel, $C_h^{-1} = 0$, then the MMSE estimator reduces to the same form as a classical estimator.

3. The MMSE estimator has better performance than LS estimation at the cost of higher complexity. But in the MMSE approach apriori knowledge of the unknown vector is required. The calculation of the unknown covariance

matrix and the inverse operation significantly increases the computational complexity.

The LS and MMSE estimator represent estimators from separate classes with different underlying assumptions; therefore, they can not be compared equivalently. There is not a straightforward answer as to which is a better estimation technique. The MMSE estimator requires additional prior knowledge about the unknown vector and additive noise. With such information the performance will exceed that of the best classical estimator. The LS makes no assumption of the unknown vector and provide adequate result at a lower computational cost.

3.3 Channel Estimation

In Section 3.2, the LS and MMSE estimator for general linear data models was presented. Now, we will discuss the application of the LS and MMSE estimation to channel estimation in MIMO-OFDM systems. First, a literature review of previous work on channel estimation for MIMO-OFDM is provided. Then the channel estimation problem structure for OFDM will be developed, and finally it will be extended to a MIMO-OFDM system.

In training-based channel estimation the pilot symbols can be placed in block-typed structures or comb-typed structures. As shown in Figure 3.1(a), for block-type arrangement the entire OFDM symbol is dedicated to carry pilot symbols on all the subcarriers. The estimate obtained with the training symbol will be used to detect the data symbols within the OFDM packet. This arrangement is most suitable for static or slow varying channels. However, in a time varying channel the comb-type structure as depicted in Figure 3.1(b) is
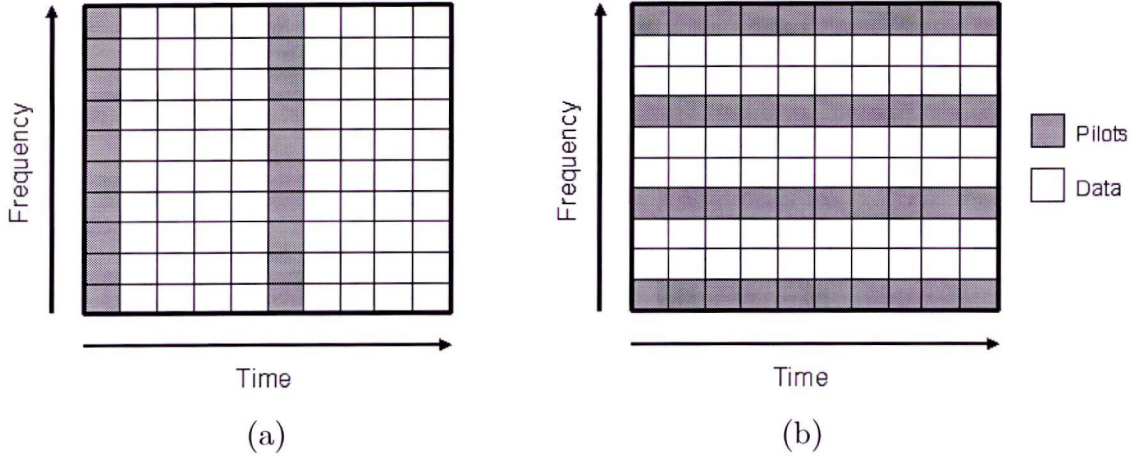
Figure 3.1: (a) Block-type pilot arrangement. (b) Comb-type pilot arrangement.

more suitable. In the comb-type arrangement, pilot symbols are sparsely spread on selected subcarriers and repeated over multiple symbols. Channel estimation is performed at each symbol and interpolation is required to infer the channel frequency values of the non-pilot subcarriers. In [34], a study of various interpolation techniques was performed for OFDM systems. The choice of pilot arrangement depends on the channel environment.

3.3.1 Literature Review

Channel estimation for OFDM received significant amount of attention since the mid 1990's. Van de Beek et al. were one of the first to look at the basic solutions of LS and MMSE estimation for OFDM in [35]. In this work, van de Beek used the property that the channel is a finite-length impulse response to develop a system model so that the LS and MMSE estimator can be applied. He showed the CIR can be estimated in the frequency domain by structuring the CFR as a linear transformation of the CIR through the IFFT operation. This

type of estimators became know as transform-domain estimators. To further reduce the complexity, van de Beek proposed a rank reduced method which only considers the channel multipaths with significant energy. Transform-domain channel estimation was further researched by Edfors et al. in [36]. He studied the performance of the low-complexity LS and MMSE estimators of van de Beek and showed that at high SNR there is an irreducible MSE floor. In [37], Edfors proposed the use of SVD to achieve an optimal low-rank channel estimator. However, implementation of the SVD operation is high in complexity.

The works mentioned so far only take into consideration the frequency-domain correlations of the frequency response of the channel. In [38], Yi et al. derived a MMSE channel estimator which made full use of the time and frequency domain correlations of the CFR of time-varying dispersive channels. He showed his robust channel estimator can significantly improve the performance of OFDM systems in rapid dispersive fading channels. However, this estimator requires at least one entire OFDM system for initial training and continual feedback of the detected signal to track the channel changes. In [16], Yi extended this work to obtain a channel estimator for MIMO-OFDM systems. This method is highly complex because of the inversion of a large matrix due to the increase in number of channels. To resolve this, Yi proposed complexity reduction by means of training sequence design and signal processing simplifications in [39]. In [17], Minn et al. also proposed a reduced complexity channel estimator by exploiting the correlation of the adjacent subchannel responses. The size of the matrix inversion was reduced by half, but the performance of the system showed a slight BER degradation. However, all these solutions still required the complicated inverse operation which is not well-suited for real-time implementation.

Thus far, the methods discussed are based of block-type arrangement of the pilot symbols. In [40], Yi studies the comb-type arrangement for channel estimation and proposed an MMSE interpolator for obtaining the non-pilot subcarriers. He was able to show that the performance of interpolation-based method was better than the decision-directed method in his previous work found in [38]. In [41], Jones et al. proposes that L pilot symbols are sufficient for estimating the channel frequency response with a channel impulse response of L multipath components. Different and exclusive equi-spaced pilots were assigned to each transmitter branch for MIMO-OFDM systems. Similar work was proposed by Jeon et al. in [42]. In Jeon's method, the pilot symbols of each transmitter are chosen such that they are orthogonal.

In summary, there has been a handful of research in the area of channel estimation for MIMO-OFDM. Earlier works were only applicable to OFDM systems, but in recent years, the works have been extended to MIMO-OFDM due to the promising potentials of combining MIMO-OFDM. In much of the works reviewed, performance of the channel estimation scheme is the primary concern. Channel estimation in MIMO-OFDM is a complicated problem because there are more unknowns to be determined. Usually the solution involves an inversion of a large matrix. The problem of complexity has to be addressed because ultimately the algorithm needs to be implemented in hardware. In some recent works, the complexity problem has been addressed. In [17], complexity reduction was achieved by reducing the matrix by half through the exploitation of the correlation between the subcarriers. Another technique proposed in [39] uses specially design training sequence to avoid the complex matrix inversion. However, the need for specific training sequence reduces the robustness of the

algorithm. The work presented in Chapter 4 focuses on the development of a low complexity channel estimation technique that eliminates matrix inversion without setting limitations on the design of the training sequence.

3.3.2 OFDM Channel Estimation

One of the main attractions of OFDM for frequency selective channels is its ability to simplify the channel estimation process. It was shown in Figure 2.8(b) that in the frequency domain the transmitted signal on each subcarrier is multiplied by a small portion of the channel frequency response, where each subcarrier only experiences flat fading. Referring to the schematic diagram of an OFDM system found in Figure 2.9, the channel estimation can be performed after the FFT block in the frequency domain. The received signal can be modeled with the following equation:

$$\mathbf{Y} = \mathbf{X}\mathbf{H} + \mathbf{V}, \tag{3.21}$$

where $\mathbf{Y}$ is the received signal vector, $\mathbf{X}$ is a diagonal matrix of the transmitted signal, $\mathbf{H}$ is the channel frequency response vector, and $\mathbf{V}$ is the noise vector in the frequency domain. The received signal in Equation (3.21) has the same structure as the general linear data model described by Equation (3.1). Using the results of the LS and MMSE estimator developed in Section 3.2, the LS estimator for an OFDM system is described as:

$$\hat{\mathbf{H}}_{LS} = \left(\mathbf{X}^H \mathbf{X}\right)^{-1} \mathbf{X}^H \mathbf{Y}. \tag{3.22}$$

Since $\mathbf{X}$ is a diagonal matrix, the estimate is reduced to

$$\hat{\mathbf{H}}_{LS} = \mathbf{X}^{-1} \mathbf{Y}. \tag{3.23}$$

This indicates that the LS estimate of the frequency response channel is simply the division of the received signal by the transmitted signal.

The MMSE estimator for OFDM is defined by

$$\hat{\mathbf{H}}_{MMSE} = \mathbf{C}_{\mathrm{H}}\mathbf{X}^{H}(\mathbf{X}\mathbf{C}_{\mathrm{H}}\mathbf{X}^{H} + \mathbf{C}_{\mathrm{V}})^{-1}\mathbf{Y}, \qquad (3.24)$$

where $\mathbf{C}_{\mathrm{H}}$ and $\mathbf{C}_{\mathrm{V}}$ is the covariance of the channel frequency response and noise, respectively.

3.3.3 MIMO-OFDM Channel Estimation

The problem of channel estimation for OFDM has been well researched; however, the results are not directly applicable to MIMO-OFDM systems. In MIMO systems, the number of channels increases by $M_t M_r$-folds, where M_t and M_r is the number of transmit and receive antenna, respectively. This significantly increases the number of unknowns to be solved. Conventional estimation techniques for single input single output (SISO) systems have to be modified to be applicable in MIMO systems.

Using the MIMO-OFDM system model described in Chapter 2, we will develop the channel estimator for MIMO-OFDM. We will assume a 2-by-2 MIIMO system to illustrate the added complexity of MIMO-OFDM channel estimation. The received signal at the jth antenna for the kth subcarrier in expanded form is defined as:

$$Y_k^{(j)}[n] = H_k^{(j,1)}S_k^{(1)}[n] + H_k^{(j,2)}S_k^{(2)}[n] + V_k^{(j)}, \qquad k = 0,1,...,N-1. \qquad (3.25)$$

The above equation is under determined. There are two unknown elements ($H_k^{(j,1)}$ and $H_k^{(j,2)}$) from different channels, however the unknowns cannot be solved with

just one equation. In a 2-by-2 system, two samples of the received signal, $Y_k^{(j)}[n]$ and $Y_k^{(j)}[n+1]$, are required to estimate $H_k^{(j,1)}$ and $H_k^{(j,2)}$. If we examine one OFDM block of N subcarriers, the received signal at the jth antenna is represented by the following equation

$$\begin{bmatrix} Y_1^j(n) \\ Y_2^j(n) \\ \vdots \\ Y_N^j(n) \end{bmatrix} = \begin{bmatrix} S_1^1(n) & 0 & \cdots & 0 & \cdots & S_1^{M_t}(n) & 0 & \cdots & 0 \\ 0 & S_2^1(n) & & \vdots & \cdots & 0 & S_2^{M_t}(n) & & \vdots \\ \vdots & & \ddots & 0 & \cdots & \vdots & & \ddots & 0 \\ 0 & \cdots & 0 & S_N^1(n) & \cdots & 0 & \cdots & 0 & S_N^{M_t}(n) \end{bmatrix} \begin{bmatrix} H_1^{(1,j)} \\ H_2^{(1,j)} \\ \vdots \\ H_N^{(1,j)} \\ \vdots \\ H_1^{(M_t,j)} \\ H_2^{(M_t,j)} \\ \vdots \\ H_N^{(M_t,j)} \end{bmatrix} + \begin{bmatrix} V_1^j(n) \\ V_2^j(n) \\ \vdots \\ V_N^j(n) \end{bmatrix} \tag{3.26}$$

$$\mathbf{Y}^{(j)} = \mathscr{X} \mathbf{H}^{(j)} + \mathbf{V}^{(j)}$$

Note, the $\mathbf{H}^{(j)}$ vector contains NM_t unknown elements but there are only N equations available in a block. In general, for M_t transmit antennas we need to collect a minimum of M_t blocks to solve for the channel unknowns. The complexity of the estimation problem increases significantly since the matrix size is increased by M_t-folds. This problem can be reduced by looking at an alternate representation of the received signal, called the transform-domain estimator that was first proposed by van de Beek in [35] for OFDM systems. Basically, we know that the CFR is a Fourier transform of the CIR, which is a linear transformation through the IFFT operation. In other words, the CFR can be expressed in terms of the CIR through the Fourier transformation. Hence, the received signal model in Equation (3.26) can be expressed in terms of the CIR. The benefit of this representation is that usually the length of the CIR is much less then the number

of subcarriers of the system. In order to model the received signal in terms of the CIR we first need to express the CFR as a function of the CIR. In Equation (2.9), the Fourier transform of a single CIR is defined. The equation can be rewritten in vector form as

$$\mathbf{H}^{(j,i)} = \mathbf{F}\mathbf{h}^{(j,i)},$$

(3.27)

where $\mathbf{F} =$

$$\begin{bmatrix} 1 & 1 & 1 & \cdots & 1 \\ 1 & e^{-\frac{j2\pi(1)(1)}{N}} & e^{-\frac{j2\pi(1)(2)}{N}} & & e^{-\frac{j2\pi(1)(L-1)}{N}} \\ 1 & e^{-\frac{j2\pi(2)(1)}{N}} & e^{-\frac{j2\pi(2)(2)}{N}} & & \cdot \\ \cdot & & \cdot & & \cdot & \cdot \\ \cdot & & & \cdot & & \cdot \\ \cdot & & & & \cdot & \cdot \\ 1 & e^{-\frac{j2\pi(N-1)(1)}{N}} & & \cdots & e^{-\frac{j2\pi(N-1)(L-1)}{N}} \end{bmatrix}$$

is the called the Fourier transform matrix of size $(N \times L)$, and $\mathbf{h}^{(j,i)} = \left[h^{(j,i)}(0), h^{(j,i)}(1), \cdots, h^{(j,i)}(L-1) \right]^{H}$ is the $(L \times 1)$ channel impulse vector. To extend the Fourier transformation to multiple channels we need to define the following:

$$\Phi = \begin{bmatrix} \mathbf{F} & \mathbf{0} & \cdots & \mathbf{0} \\ \mathbf{0} & \mathbf{F} & & \vdots \\ \vdots & & \ddots & \mathbf{0} \\ \mathbf{0} & \cdots & \mathbf{0} & \mathbf{F} \end{bmatrix}$$ is a block diagonal matrix of M_t $\mathbf{F}$'s, and

$\mathbf{h}^{(j)} = \left[\mathbf{h}^{(j,1)}, \mathbf{h}^{(j,2)}, \cdots, \mathbf{h}^{(j,M_t)} \right]^{H}$ is a $(M_t L \times 1)$ vector. Then the alternate received signal of the jth antenna in terms of the CIR can be expressed as

$$\begin{aligned} \mathbf{Y}^{(j)} &= \mathcal{X}\Phi\mathbf{h}^{(j)} + \mathbf{V}^{(j)} \\ &= \mathbf{W}\mathbf{h}^{(j)} + \mathbf{V}^{(j)} \end{aligned}$$

(3.28)

In this representation, the number of elements in $\mathbf{h}^{(j)}$ to be resolved are $M_t L$. If we assume that the number of subcarriers, N, in an OFDM block is greater than $M_t L$, then only one OFDM is required to solve for $\mathbf{h}^{(j)}$.

Using the received signal model in Equation (3.28) the LS estimate is expressed as:

$$\hat{\mathbf{h}}^{(j)} = (\mathbf{W}^H \mathbf{W})^{-1} \mathbf{W}^H \mathbf{Y}^{(j)} \tag{3.29}$$

The $(\mathbf{W}^H \mathbf{W})^{-1}$ term has the dimensions of $(M_t L \times M_t L)$ which is still full rank if $M_t L \leq N$. Using the same model, the MMSE estimate becomes

$$\hat{\mathbf{h}}^{(j)} = \mathbf{C}_\mathbf{h} \mathbf{W}^H (\mathbf{W} \mathbf{C}_\mathbf{h} \mathbf{W}^H + \mathbf{C}_\mathbf{V})^{-1} \mathbf{Y}^{(j)}. \tag{3.30}$$

Assume the noise is AWGN ($\mathbf{C}_\mathbf{V} = \sigma_\mathbf{V}^2 \mathbf{I}$) and using the matrix inversion theorem the MMSE channel estimate can be alternatively written as

$$\hat{\mathbf{h}}^{(j)} = (\sigma_\mathbf{V}^2 \mathbf{C}_\mathbf{h}^{-1} + \mathbf{W}^H \mathbf{W})^{-1} \mathbf{W}^H \mathbf{Y}^{(j)}. \tag{3.31}$$

3.4 Simulation Results

A simulation of an MIMO-OFDM system was developed to compare the performance of the LS and MMSE estimator under different circumstances.

3.4.1 System Parameters

    i. Number of transmitter, $M_t = 2$

    ii. Number of receiver, $M_r = 2$

    iii. 16-QAM modulation

    iv. Number of subcarriers, $N = 64$

v. Cyclic Prefix, $N_{cp} = N/4$

vi. OFDM block size, $N + N_{cp}$

vii. Sampling time, $T_s = 1/80$ MHz

viii. RMS delay spread, $T_{rms} = 25$ ns

ix. The exponential decaying Rayleigh fading channel model proposed by Naftali Chayat for the IEEE 802.11-98/156r2 standard is used [45]. The channel has L paths where the amplitude of each path varies independently according to the Rayleigh distribution with an exponential power delay profile, and can be represented as

$$h_l = \mathcal{N}(0, 1/2\sigma_l^2) + j\, \mathcal{N}(0, 1/2\sigma_l^2), \quad l = 0, 1, \ldots, L\text{-}1 \qquad (3.32)$$

where $\sigma_l^2 = (1 - e^{-\frac{T_s}{T_{rms}}}) e^{-\frac{lT_s}{T_{rms}}}$ and $\mathcal{N}(0, 1/2\sigma_l^2)$ is a zero mean Gaussian random variable with variance $1/2\sigma_l^2$. The $\left(1 - e^{-\frac{T_s}{T_{rms}}}\right)$ is chosen such that the channel gain is unity $\left(\text{i.e. } \sum_{l=0}^{L-1} \sigma_l^2 = 1\right)$, where L, the length of the channel is approximated by

$$L = \frac{10 T_{rms}}{T_S}. \qquad (3.33)$$

In addition, the channel assumed to be quasi-static, meaning that the channel remains relatively constant for the duration of the OFDM packet.

3.4.2 Performance Analysis

A training symbol is placed at the beginning of the OFDM block. The channel estimate obtained from the training symbol will be used to detect the

remaining data symbols within the block. The training symbol is composed of random Gaussian numbers constrained by the total power used to transmit a single OFDM signal. According to system parameters, the channel is gain is unity, so the SNR is defined as

$$SNR = \frac{E_s}{\sigma_v^2},$$

(3.34)

where E_s is the symbol power. The performance of the two estimation techniques is measured in terms of the MSE of the channel estimates and the bit error rate (BER) of a zero-forcing detector based of the channel estimates.

Figure 3.2 shows the MSE curve of the simulated results of the LS and MMSE estimators and the theoretical bounds of both estimators as derived in Section 3.2.1.2 and 3.2.2.2, respectively. It confirms that MMSE estimator has a better performance, and that at high SNR (i.e. 30 dB) the MMSE estimator has equivalent performance as the LS estimator. This can be explained by looking at the MMSE estimation in Equation (3.31). When the SNR is high, the noise power (σ_v^2) is low, it will reduce the effect of $\mathbf{C}_h^{-1}$. Therefore, when the noise power approaches zero, the MMSE estimator will approach the LS estimator. Also, from Figure 3.2, we observe that there is a performance gap between the simulated estimators and the theoretical bounds. The can be explain by looking at the MSE bounds defined by Equation (3.6) and (3.20), which indicates that the minimum MSE depends on the training sequence transmitted. Since in our simulated case a random training sequence was used, it will not achieve the minimum MSE. From this observation we can see that optimal training sequence can be selected to minimize the error of the channel estimates. In [18], a thorough analysis is presented on the selection of optimal training design for MIMO-OFDM
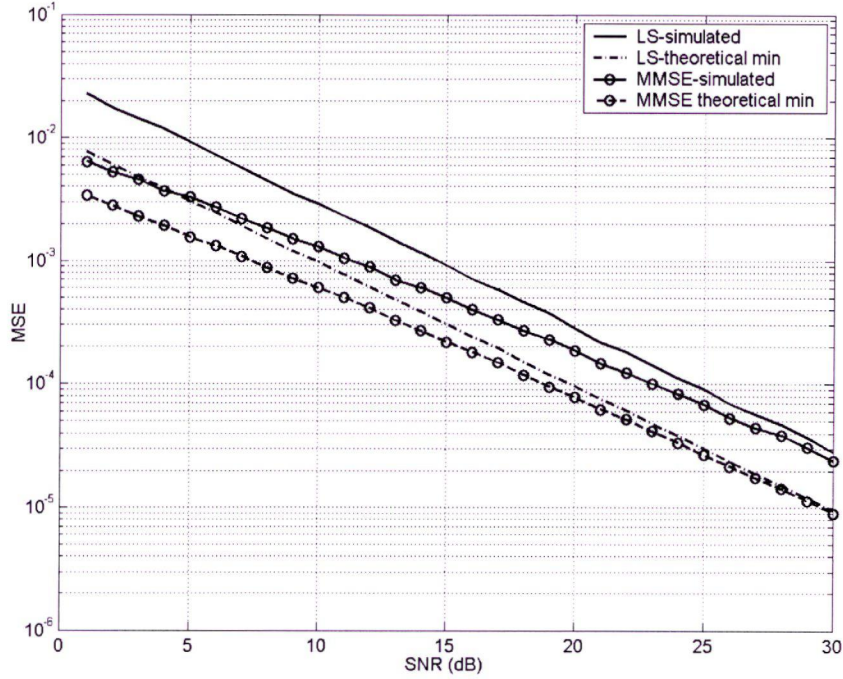
Figure 3.2: MSE curve for simulated LS estimation and minimum theoretical MSE

systems. However, as mentioned before, a fixed training sequence design limits the robustness of the system. For this thesis, we will not restrict our channel estimation analysis to assume some fixed training sequence design.

Figure 3.3 shows the performance of the LS and MMSE estimator in terms of BER in comparison to perfect channel knowledge. Due to the estimation errors of the LS and MMSE estimators, it will have a higher BER than when the exact channel is known. The results of the BER curve in Figure 3.3 agree with the results observed for the MSE curve in Figure 3.2, where the MMSE has better performance than the LS method.
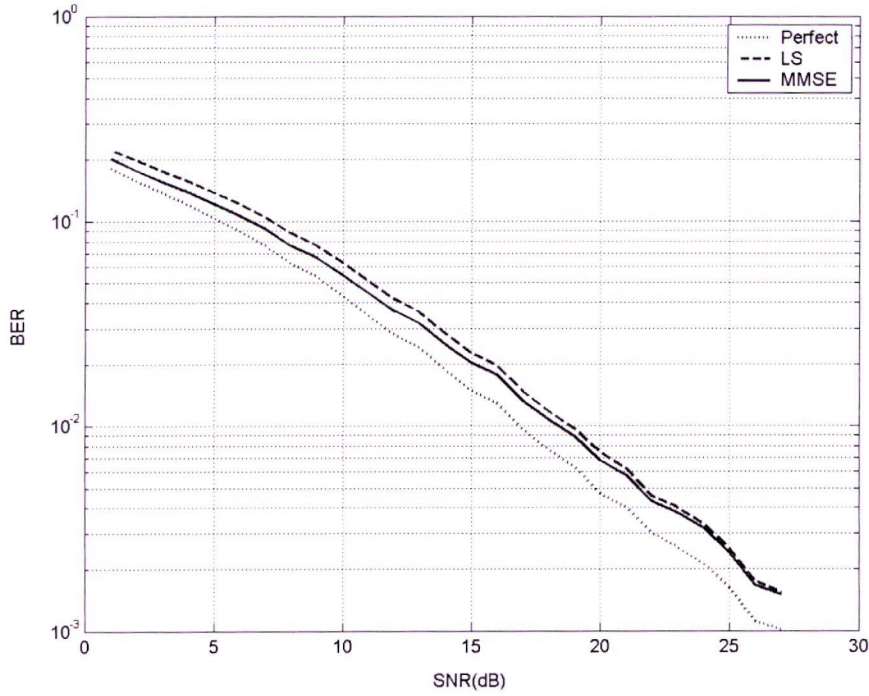
Figure 3.3: BER curve for LS and MMSE Estimator and Perfect CIR

The performance of the estimators for various channel lengths was investigated. The length of the channel is determined by the T_{rms}, according to Equation (3.33) the greater the T_{rms} the longer the channel length. Figure 3.4 show the results of the LS estimator for channel lengths of 21, 15, 11, 9, 6, and 2. The accuracy of the estimates increased as the number of channel lengths decreased. Mathematically, a larger L implies that there are more unknown to be solved for a given set of equations, hence the accuracy will decrease. The results for the MMSE estimator are shown in Figure 3.5. For the MMSE estimator, the performance degradation due to increase in channel length varies for different SNR values. At low SNR, the channel length does not seem to affect the MSE value. However, for higher SNR the trend is similar to that of the LS estimator,
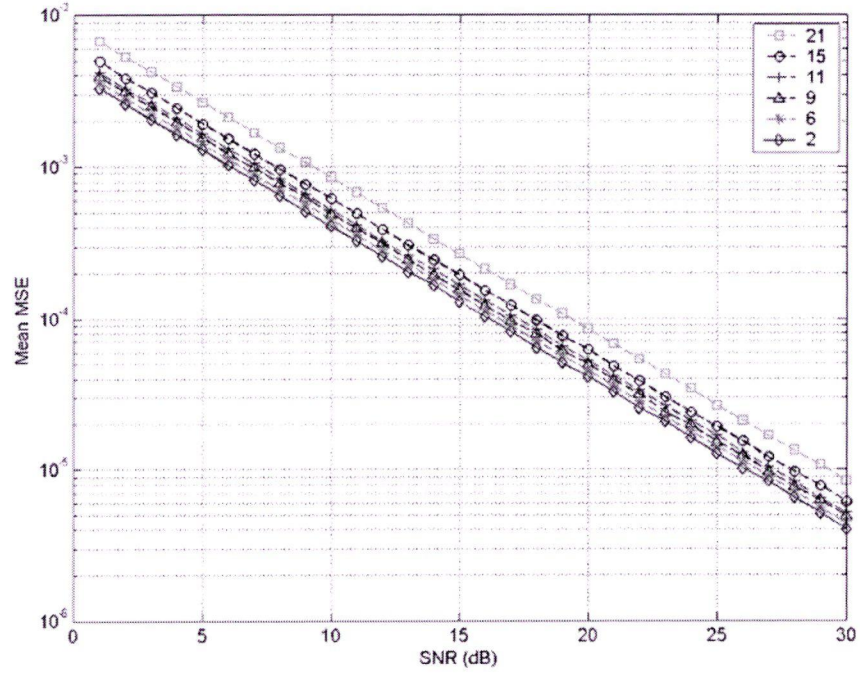
Figure 3.4: MSE curve for LS estimator for various channel lengths

which is expected because the MMSE estimator approaches the LS estimator at high SNRs. Again, according to Equation (3.31) when the noise power is high, the impact of the $\mathbf{C}_h^{-1}$ is emphasized. This implies that the performance of the MMSE estimator at low SNRs largely depend on the $\mathbf{C}_h^{-1}$.
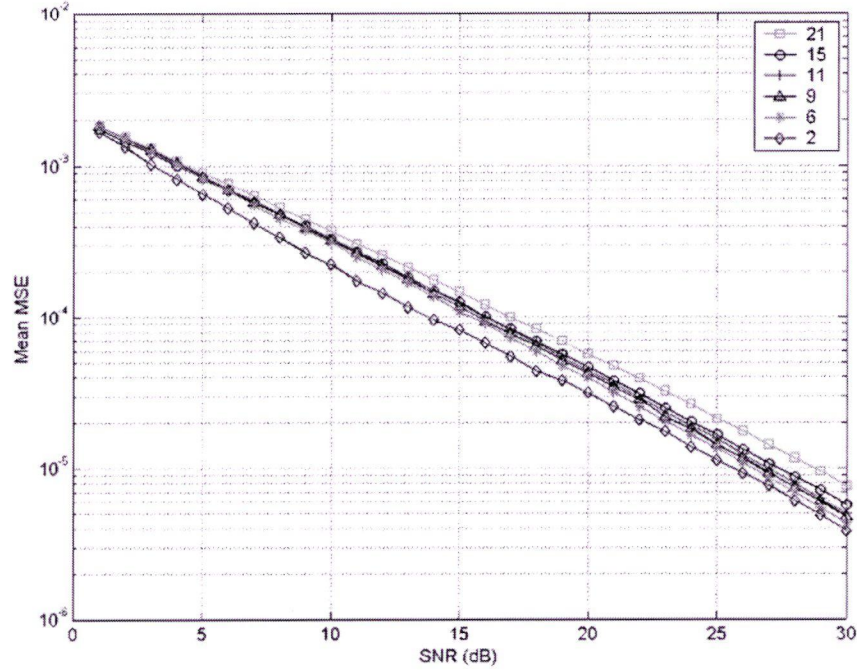
Figure 3.5: MSE curve for LS estimator for various channel lengths

From the simulation results obtained in this section, several conclusions can be drawn regarding the performance of the LS and MMSE estimator. First, at low SNRs the MMSE outperforms the LS and it is more robust to the channel length. However, at high SNR, the MMSE is equivalent to LS. When taking complexity into account, the MMSE estimation is not a good choice under high SNR scenarios.

3.5 Summary

In this chapter, we discussed the options for channel estimation and concluded that training-based estimation is preferable to blind estimation due to its relative low complexity. Two representative training-based estimation

techniques, LS and MMSE, were presented for MIMO-OFDM channel estimation. Our analysis confirmed that in terms of performance the MMSE estimator is better than the LS estimator. However, the complexity of the MMSE is significantly higher than LS. Moreover, the MMSE requires some prior knowledge of the channel, which may not be available in real-time applications. Taking all this into consideration, the MMSE may not always be the best choice.

CHAPTER FOUR

QR DECOMPOSITION CHANNEL ESTIMATION

In the Chapter 3, the general solutions for LS and MMSE channel estimation were developed. The LS and MMSE solution involved matrix inversions, which are high in computational complexity. In this chapter we propose a low-complexity LS and MMSE channel estimator using QR decomposition. First, the application of QR decomposition for LS estimation will be described in Section 4.1. In Section 4.2 low complexity techniques are proposed for MMSE estimation

4.1 QR Decomposition for LS Channel Estimation

Direct computation of the LS solution involves a matrix inversion, which is high complexity and undesirable for hardware implementation. Matrix decomposition-based least square schemes such as Cholesky, lower upper (LU), SVD, and QR decomposition (QRD) avoid explicit inversions and are more robust and well suited for hardware implementation. The details of these schemes can be found in [46]. The QR decomposition is preferable because of the clever implementation of the scheme in a highly parallel systolic array architecture by Gentleman and Kung [47]. In addition, QRD guarantees numerical stability by minimizing errors caused by machine roundoffs [46].

QR decomposition is an orthogonal matrix triangularization technique that reduces a full rank matrix into a simpler form. Consider a matrix $\mathbf{A}$ of size $(m \times n)$, then the QR decomposition is defined as

$$\mathbf{A} = \mathbf{Q} \begin{bmatrix} \mathbf{R} \\ \mathbf{0} \end{bmatrix}, \tag{4.1}$$

where $\mathbf{Q}$ is a $(m \times m)$ unitary matrix, $\mathbf{R}$ is a $(n \times n)$ upper triangular matrix and $\mathbf{0}$ is a null matrix. A unitary matrix is one that satisfies the following condition

$$\mathbf{I} = \mathbf{Q}^H \mathbf{Q}. \tag{4.2}$$

To apply QRD to the problem of channel estimation we recall the MIMO-OFDM system model

$$\mathbf{Y} = \mathbf{W}\mathbf{h} + \mathbf{V}. \tag{4.3}$$

As stated in Chapter 3, the LS estimation solution is found by minimizing the norm square of error function $\varepsilon = \mathbf{Y} - \mathbf{W}\hat{\mathbf{h}}$ to give the estimate

$$\hat{\mathbf{h}} = (\mathbf{W}^H \mathbf{W})^{-1} \mathbf{W}^H \mathbf{Y}. \tag{4.4}$$

The inversion of $\mathbf{W}^H\mathbf{W}$ of size $(LN_t \times LN_t)$ is high in complexity and will significantly increase when the size of $\mathbf{W}$ increases, which is dependent on the channel length or the number of transmit antennas. To avoid the matrix inversion we can directly apply QR decomposition to the error equation as follows

$$\mathbf{W}\hat{\mathbf{h}} = \mathbf{Y}$$
$$\mathbf{Q}\mathbf{R}\hat{\mathbf{h}} = \mathbf{Y} \tag{4.5}$$
$$\mathbf{R}\hat{\mathbf{h}} = \mathbf{Q}^H \mathbf{Y}$$

Note, $\mathbf{R}$ is an upper triangular matrix, hence $\hat{\mathbf{h}}$ can be solved through back-substitution. The QR solution is a numerically stable low complexity solution to

LS channel estimation of an MIMO-OFDM system. In summary, the solution is obtained through the following steps:

1. QR decompose $\mathbf{W}$ into $\mathbf{QR}$

2. Premultiple $\mathbf{Y}$ by $\mathbf{Q}^H$

3. Solve for $\hat{\mathbf{h}}$ by back-substitution

The QR decomposition can be calculated via Gram-Schmidt decomposition, Householder transformation, or Givens rotation. These methods can be separated into two categories: block-based and recursive-base. The classification of the QRD methods is shown in Figure 4.1. The block-based approach based on the Householder method and Gram-Schmidt method requires the entire matrix, $\mathbf{W}$, to be formed before the decomposition is performed. This implies that the received signal must wait for N samples to form $\mathbf{W}$ before the data is sent to the processor, where the QRD is calculated and the channel estimates are solved. The total time required to obtain the channel estimates is NT_s plus the processing time as shown in Figure 4.2. The second approach is the recursive method achieved through Givens rotation, which does not require the buffering of the data. The time required to obtain the channel estimates is just based on the processing time of the processor. In the Givens rotation method, orthogonal rotations are performed to annihilate the incoming elements individually. Givens rotation requires a larger number of floating point operations (FLOPs) as compared to the block-based methods. However, the rotations can be implemented in parallel using systolic arrays, which can reduce the overall execution time as compared to the block techniques.
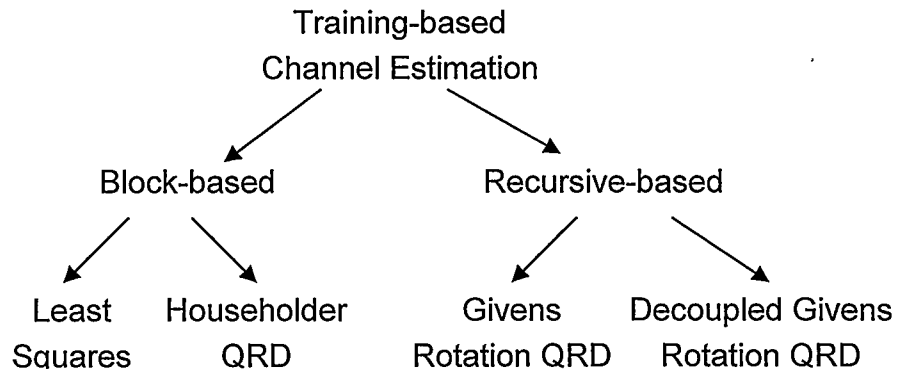
Figure 4.1: Classification of Training-based channel estimation algorithms
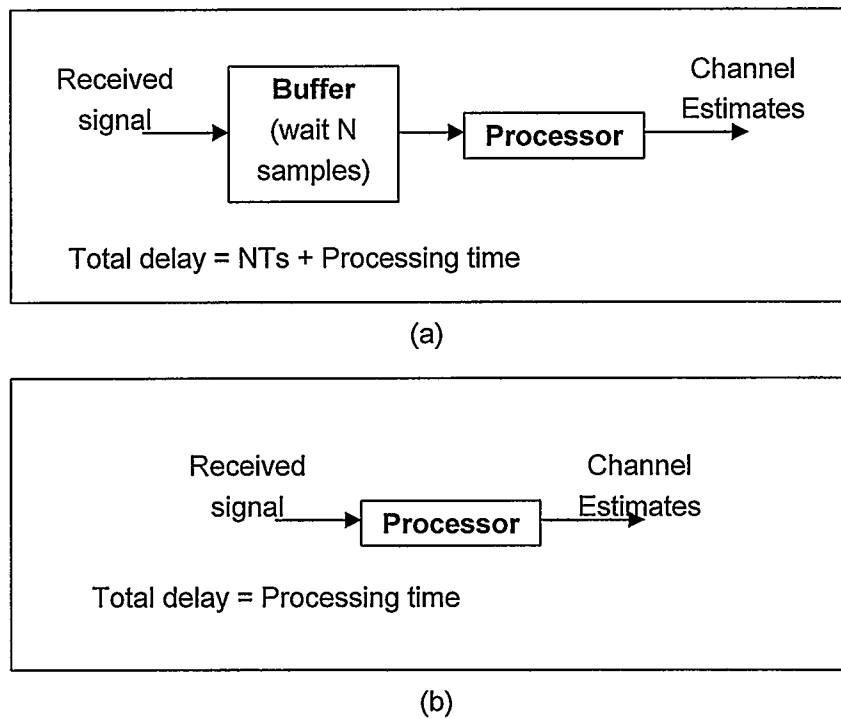
Figure 4.2: (a) Block estimation process. (b)Symbol-based estimation process

Next, we briefly describe the Householder method and Givens rotation method for QR decomposition. The Householder is chosen over the Gram-Schmidt because the Gram-Schmidt is not numerically stable.

4.1.1 Householder Method

In the Householder approach, a series of reflection matrix is applied to the matrix, $\mathbf{W}$, column by column to annihilate the lower triangular elements. The reflection transformations are orthonormal matrices that can be written as

$$\mathbf{H} = (\mathbf{I} + \beta \mathbf{v}\mathbf{v}^H) \tag{4.6}$$

where $\mathbf{v}$ is the Householder vector and $\beta = -2\|\mathbf{v}\|_2^2$. For a given matrix $\mathbf{W}$ of size $(m \times n)$, to annihilate the lower elements of the kth column the $\mathbf{H}_k$ is constructed as follows:

1. Let $\mathbf{v}$ equal the kth column of $\mathbf{W}$

2. Update $\mathbf{v}$ by $\mathbf{v} = \mathbf{x} + \|\mathbf{x}\|_2 e_1$, where $e_1 = [1, 0, \ldots ,0]^T$

3. Determine β by $\beta = -2\|\mathbf{v}\|_2^2$

4. $\mathbf{H}_k$ is calculated according to Equation (4.6).

The $\mathbf{H}_k$ (for k = 1,2, ... ,n) formed from the above steps are pre-multiplied by $\mathbf{W}$ sequentially as follows

$$\underbrace{\mathbf{H}_n \ldots \mathbf{H}_1}_{Q^H} \mathbf{W} = \begin{bmatrix} \mathbf{R} \\ \mathbf{0} \end{bmatrix}, \tag{4.7}$$

where, $\mathbf{R}$ is the upper triangular matrix and the sequence of rotation matrices form the complex transpose of the orthogonal matrix $\mathbf{Q}$.

4.1.2 Givens Rotations Method

In the Givens rotations (GR), the triangularization of the matrix is achieved by annihilating a single element at a time. For simplicity we will illustrate the algorithm with a (2 × 2) matrix $\mathbf{W} = \begin{bmatrix} w_{ii} & w_{ik} \\ w_{ki} & w_{kk} \end{bmatrix}$. To annihilate w_{ki}, the $\mathbf{W}$ matrix is premultiplied by a rotational matrix $\mathbf{J} = \begin{bmatrix} c^* & s^* \\ -s & c \end{bmatrix}$ in the following manner,

$$\underbrace{\begin{bmatrix} c^* & s^* \\ -s & c \end{bmatrix}}_{\mathbf{J}} \underbrace{\begin{bmatrix} w_{ii} & w_{ik} \\ w_{ki} & w_{kk} \end{bmatrix}}_{\mathbf{W}} = \underbrace{\begin{bmatrix} r_{ii} & r_{ik} \\ r_{ki} & r_{kk} \end{bmatrix}}_{\mathbf{R}}. \tag{4.8}$$

The objective is to choose c and s such that the r_{ki} element becomes 0. From Equation (4.8), the required condition is

$$-sw_{ii} + cw_{ki} = 0. \tag{4.9}$$

Moreover, c and s are constrained by

$$|c|^2 + |s|^2 = 1. \tag{4.10}$$

Therefore, substituting Equation (4.10) into (4.9) we get

$$c = \frac{w_{ii}}{\sqrt{|w_{ii}|^2 + |w_{ki}|^2}} \tag{4.11}$$

and

$$s = \frac{w_{ki}}{w_{ii}} c. \tag{4.12}$$

The non-zero terms of the **R** matrix are determined as follows

$$r_{ii} = c^* w_{ii} + s^* w_{ki}$$
$$r_{ik} = c^* w_{ik} + s^* w_{kk}$$
$$r_{kk} = -sa_{ik} + ca_{kk}.$$

(4.13)

To extend this approach to a general matrix of size $(m \times n)$, the rotational matrix in the general form for annihilation of the $(k,i)^{\text{th}}$ element is defined as

$$\mathbf{J}_{ki} = \begin{bmatrix} 1 & \cdots & 0 & \cdots & 0 & \cdots & 0 \\ \vdots & \ddots & \vdots & & \vdots & & \vdots \\ 0 & \cdots & c & \cdots & s^* & \cdots & 0 \\ \vdots & & \vdots & \ddots & \vdots & & \vdots \\ 0 & \cdots & -s & \cdots & c & \cdots & 0 \\ \vdots & & \vdots & & \vdots & \ddots & \vdots \\ 0 & \cdots & 0 & \cdots & 0 & \cdots & 1 \end{bmatrix} \begin{matrix} \\ \\ \leftarrow k^{th} \text{ row} \\ \\ \leftarrow i^{th} \text{ row} \\ \\ \end{matrix}$$

$$\uparrow \qquad \uparrow$$
$$k^{th} \text{ col.} \quad i^{th} \text{ col.}$$

where $\mathbf{J}_{ki}$, a $(m \times m)$ matrix, is used to pre-multiply the original matrix and sequentially annihilate the desired elements. The sequence of ration matrices is represented by

$$\underbrace{\mathbf{J}_{m,n-1}...\mathbf{J}_{m2}...\mathbf{J}_{32}\mathbf{J}_{m1}....\mathbf{J}_{21}}_{Q''} \mathbf{W} = \begin{bmatrix} \mathbf{R} \\ \mathbf{0} \end{bmatrix}$$

(4.14)

where **R** is an upper triangular matrix and **Q** is the complete rotation matrix.

4.1.3 Decoupled Givens Rotation QRD

The GR method for QRD has been deemed a good approach for hardware implementation due its highly parallel architecture. However, GR requires square root operations as shown in Equation (4.11), which require more processing time in hardware implementations. To reduce the complexity of Givens rotation, we investigated approaches to eliminate the square root operation and reduce the over FLOP count of the algorithm. In [48], a decoupled QRD method was developed for MIMO detection. The standard QRD is reformulated to avoid the square-root and division operations for MIMO detection. We will adapt this square-root and division free method to channel estimation. In the following section we will briefly describe the algorithm of the decoupled Givens rotation QR decomposition (DGR-QRD) described in [48]. Using equation (4.8), (4.11), and (4.12) the QRD of **W** in expanded form is defined as

$$
\mathbf{W} = \mathbf{QR}
$$

$$
= \begin{bmatrix} \dfrac{w_{ii}^{*}}{\sqrt{|w_{ii}|^2 + |w_{ki}|^2}} & \dfrac{-w_{ki}}{\sqrt{|w_{ii}|^2 + |w_{ki}|^2}} \\ \dfrac{w_{ki}^{*}}{\sqrt{|w_{ii}|^2 + |w_{ki}|^2}} & \dfrac{w_{ii}}{\sqrt{|w_{ii}|^2 + |w_{ki}|^2}} \end{bmatrix} \begin{bmatrix} \dfrac{|w_{ii}|^2 + |w_{ki}|^2}{\sqrt{|w_{ii}|^2 + |w_{ki}|^2}} & \dfrac{w_{ii}^{*}w_{ik} + w_{ki}^{*}w_{kk}}{\sqrt{|w_{ii}|^2 + |w_{ki}|^2}} \\ 0 & \dfrac{-w_{ki}w_{ik} + w_{ii}w_{kk}}{\sqrt{|w_{ii}|^2 + |w_{ki}|^2}} \end{bmatrix} \quad (4.15)
$$

The DGR-QRD is based on a new representation of the **R** matrix elements defined as

$$
r_{ij} = \frac{p_{ij}}{\sqrt{k_i}}. \quad (4.16)
$$

The division and the square root operations are avoided by computing and storing p_{ij} and k_i separately. Applying this idea the decomposition can be rewritten as

$$
\mathbf{W} = \underbrace{\begin{bmatrix} w_{ii}^* & -w_{ki} \\ w_{ki}^* & w_{ii} \end{bmatrix} \begin{bmatrix} \dfrac{1}{\sqrt{|w_{ii}|^2 + |w_{ki}|^2}} & 0 \\ 0 & \dfrac{1}{\sqrt{|w_{ii}|^2 + |w_{ki}|^2}} \end{bmatrix}}_{\mathbf{Q}} \times
$$

$$
\underbrace{\begin{bmatrix} \dfrac{1}{\sqrt{|w_{ii}|^2 + |w_{ki}|^2}} & 0 \\ 0 & \dfrac{1}{\sqrt{|w_{ii}|^2 + |w_{ki}|^2}} \end{bmatrix} \begin{bmatrix} |w_{ii}|^2 + |w_{ki}|^2 & w_{ii}^* w_{ik} + w_{ki}^* w_{kk} \\ 0 & -w_{ki} w_{ik} + w_{ii} w_{kk} \end{bmatrix}}_{\mathbf{R}} \tag{4.17}
$$

$$
= \underbrace{\begin{bmatrix} w_{ii}^* & -w_{ki} \\ w_{ki}^* & w_{ii} \end{bmatrix}}_{\Psi} \underbrace{\begin{bmatrix} \dfrac{1}{|w_{ii}|^2 + |w_{ki}|^2} & 0 \\ 0 & \dfrac{1}{|w_{ii}|^2 + |w_{ki}|^2} \end{bmatrix}}_{\mathbf{Z}^{-1}} \underbrace{\begin{bmatrix} |w_{ii}|^2 + |w_{ki}|^2 & w_{ii}^* w_{ik} + w_{ki}^* w_{kk} \\ 0 & -w_{ki} w_{ik} + w_{ii} w_{kk} \end{bmatrix}}_{\mathbf{P}}
$$

$$
= \Psi \mathbf{Z}^{-1} \mathbf{P}
$$

where Ψ is an orthogonal matrix, $\mathbf{Z}^{-1}$ is a diagonal matrix with elements $1/k_i$ and $\mathbf{P}$ is an upper triangular matrix.

The algorithm for the decoupled QR decomposition of a $(m \times n)$ complex matrix $\mathbf{W}$ is as follows:

1. Initialize the $\mathbf{P}$ matrix to equal $\mathbf{W}$ and $k_i = 1$ for $i = 1, \ldots, m$.

2. The p_{ki} element is annihilated by the following rotation matrix

$$
\begin{bmatrix} p_{ii}^* z_k & p_{ki}^* z_i \\ -p_{ki} & p_{ii} \end{bmatrix} \begin{bmatrix} p_{ii} \\ p_{ki} \end{bmatrix} = \begin{bmatrix} \bar{p}_{ii} \\ 0 \end{bmatrix} \tag{4.18}
$$

where $\bar{p}_{ii}$ is the updated element.

3. The denominator terms z_k and z_i are updated by

$$\bar{z}_k = p_{ii}^* z_k p_{ii} + p_{ki}^* z_k p_{ki} = \bar{p}_{ii}$$
$$\bar{z}_i = z_i z_k \left(p_{ii}^* z_k p_{ii} + p_{ki}^* z_k p_{ki} \right) = z_i z_k \bar{p}_{ii}. \tag{4.19}$$

4. From the above equation we can see that as the iterations increase the z and p values will increase exponentially which might eventually cause the system to become unstable. Scaling is performed on the new elements of p and z after every update to avoid overflow. The z values are limited to the range 0.25 to 4, thereby limiting the deviation of **P** matrix values from the original matrix **W**. As described in [48], scaling can be achieved with only binary shift operations which are low in complexity.

Applying the DGR-QRD, the channel estimate procedure becomes

$$\mathbf{W}\hat{\mathbf{h}} = \mathbf{Y}$$
$$\mathbf{\Psi}^H \mathbf{\Psi} \mathbf{Z}^{-1} \mathbf{P}\hat{\mathbf{h}} = \mathbf{\Psi}^H \mathbf{Y} \tag{4.20}$$
$$\mathbf{P}\hat{\mathbf{h}} = \mathbf{\Psi}^H \mathbf{Y}$$

where $\mathbf{\Psi}^H \mathbf{\Psi} = \mathbf{Z}$. Since **P** is an upper triangular matrix then $\hat{\mathbf{h}}$ can be solved by back-substitution.

4.1.4 Performance Analysis

Using the simulation parameters in Chapter 3, a MIMO-OFDM system was simulated to evaluate the performance of the proposed QR decomposition methods for LS channel estimation. The plot in Figure 4.3 suggests that the QRD

methods and LS channel estimation have the same performance in terms of the MSE of the estimate. This is expected because the QRD method essentially solves for the least square solution, but it achieves it through matrix decomposition. Whereas, in standard LS channel estimation, a pseudoinverse is used to solve for the channel unknowns. The use of QRD methods does not improve the performance in terms of lower channel estimation error. However, in the next section we show the benefit of QRD, which is the significant reduction of the complexity of the system.
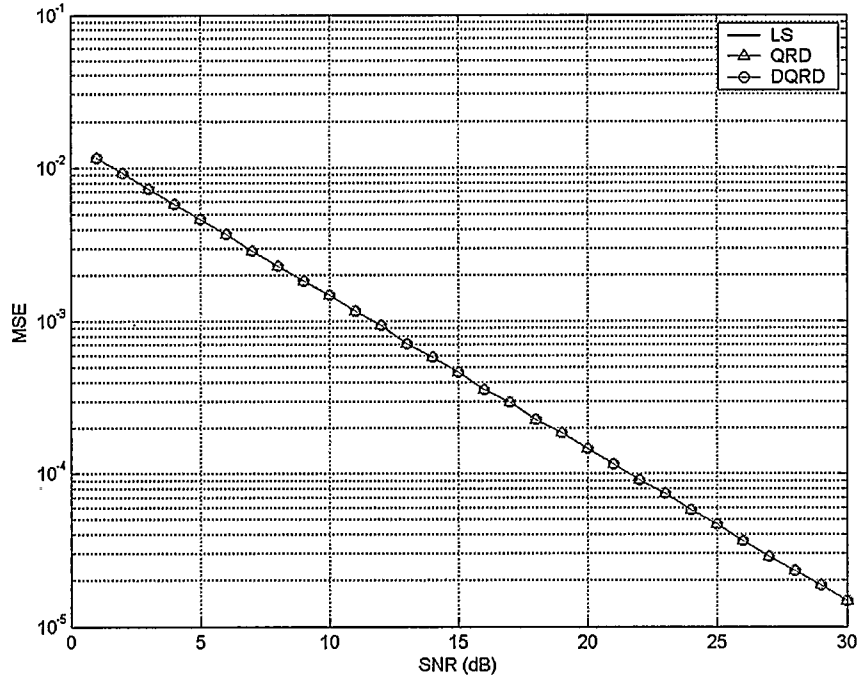
Figure 4.3: MSE curve for the various channel estimation algorithms

4.1.5 Complexity Analysis

The main advantage of using QR decomposition is to reduce the computational complexity of the LS channel estimation. In this section, we measure the computational complexity in terms of number of operations for each method. Our derivations are based on an M_t-by-M_r MIMO-OFDM system with N subcarriers and a channel length of L. The known matrix $\mathbf{W}$ has dimensions (N x LM_t). For simplicity in notation we denote LM_t with just M. For a consistent comparison, the complex operations are converted to real operation equivalents. Table 4-1 shows the real equivalent operations for the various complex operations. In addition, each type of real operations has different levels of complexity when implemented in hardware. We will set multiplications, additions, and subtractions to 1 FLOPs, divisions to 6 FLOPs, and square roots to 10 FLOPs. It should be emphasized that counting of the number operations is only an estimate of the computational complexity of the algorithms. A more exact measure would be to implement the algorithm in hardware and count the number of instructions and processing time required. However, in computer simulations, FLOP counts can give a good indication of the relative complexity of different algorithms.

Table 4-1: Complex to Real Operation Equivalents

Complex Operations	Number of Real Operations		
	Multiplication	Division	Addition/ Subtraction
Multiplication	4	2	0
Division	6	3	2
Addition/ Subtraction	0	0	2
Complex Magnitude	2	0	1

The operation counts were derived for the LS channel estimation, Householder QRD (H-QRD), Givens Rotation QRD (GR-QRD), and decoupled Givens Rotation QRD (DGR-QRD) channel estimation. Details of the LS channel estimation algorithm used in this comparison can be found in Appendix A. The complexity equations are derived by counting each type of operations in the various algorithms. The final equations for operation counts are presented in Table 4-2, Table 4-3, Table 4-4 and Table 4-5.

Table 4-2: LS Channel Estimation Operation Count

Operation	# of Complex Mult.	# of Complex Add/Sub	# of Complex Div.	# of Sq. Root
$\mathbf{A} = (\mathbf{W}^H\mathbf{W})$	NM^2	$NM^2 - M^2$	0	0
$\mathbf{A}^{-1}$	M^3	M^3	$3M^2/2 + M/2$	0
$\mathbf{B} = \mathbf{A}^{-1}\mathbf{W}^H$	NM^2	$NM^2 - NM$	0	0
$\hat{\mathbf{h}} = \mathbf{BY}$	NM	$NM - M$	0	0

Table 4-3: Householder QRD Channel Estimation Operation Count

Operation	# of Complex Mult.	# of Complex Add/Sub	# of Complex Div.	# of Complex Magnitude	# of Sq. Root
Determine $\|\mathbf{v}\|$	0	$NM/2 - M^2/4 - M/4$	0	$NM - M^2/2 + M/2$	M
Update $\mathbf{v}(1)$	M	M	M	M	M
Determine	0	0	M	0	0
Update $\mathbf{W}$	$NM^2 + 2NM - M^3/3 - M^2/2 + 5M/6$	$NM^2 + NM - M^3/3 - M^2/2 - M/6$	0	0	0
Update $\mathbf{Y}$	$2(NM - M^2/2 + M/2)$	$2NM - M^2$			
Back substitution	$M^2/2 - M/2$	$M^2/2 + M/2 - 1$	M		

Table 4-4: Givens Rotation QRD Channel Estimation Operation Count

Operation	# of Complex Mult.	# of Complex Add/Sub	# of Complex Div.	# of Sq. Root
Calculate rotation matrix	$5(NM - M^2/2 -M/2)$	$2(NM - M^2/2 -M/2)$	$2(NM - M^2/2 -M/2)$	$NM - M^2/2 -M/2$
Update R	$4(NM^2/2 - NM/2 - M^3/6 + M/6)$	$2(NM^2/2 - NM/2 - M^3/6 + M/6)$	0	0
Update Y	$4(NM - M^2/2 -M/2)$	$4(NM - M^2/2 -M/2)$	0	0
Back substitution	$M^2/2 - M/2$	$M^2/2 + M/2 - 1$	M	0

Table 4-5: Decoupled Givens Rotation QRD channel estimation operation count

Operation	# of Complex Mult.	# of Complex Add/Sub	# of Complex Div.	# of Sq. Root
Calculate rotation matrix	$2(NM - M^2/2 -M/2)$	0	0	0
Calculate z_i, z_j, p_{ii}, and p_{ji} values	$2(NM - M^2/2 -M/2)$	$2(NM - M^2/2 -M/2)$	0	0
Update P	$4(NM^2/2 - NM/2 - M^3/6 + M/6)$	$2(NM^2/2 - NM/2 - M^3/6 + M/6)$	0	0
Update Y	$4(NM - M^2/2 -M/2)$	$2(NM - M^2/2 -M/2)$	0	0
Back substitution	$M^2/2 - M/2$	$M^2/2 + M/2 - 1$	M	0

Using the system parameters for the MIMO-OFDM system specified in Chapter 3, we calculated the number of operations for a 2 transmit antenna system with a channel length of 5 for the various algorithms. In the following section, the complexity comparison in terms of FLOPs count is performed for the block-based methods and recursive-based methods separately. To accurately determine the complexity would require hardware implementation of the algorithms. However, FLOPs counts are legitimate for comparison of the relative complexity of the methods within the sub-categories. The intent of this analysis is to demonstrate that within the block-based schemes, the H-QRD method is lower in complexity than the LS method, hence a better alternative. Moreover, comparison of the recursive-based schemes demonstrates that the DGR-QRD has lower complexity than standard GR-QRD.

4.1.5.1 Block-Based Methods

First, we compare the block-based schemes which include the LS channel estimation scheme and the Householder QRD scheme. The results in Table 4-6 shows that the total number of operation for the LS method is much higher than the H-QRD method. For this simulation scenario using H-QRD achieves a complexity reduction by approximately 40%. This verifies that the H-QRD has significantly lower complexity than that of direct LS estimation via the pseudoinverse, hence a better option for channel estimation.

Table 4-6: Operation count of a 2 transmitter system with channel length of 5.

Algorithm	Complex Mult.	Complex Add./ Sub.	Complex Div.	Complex Magnitude	Square Root	**Number of FLOPS**
LS	14440	13690	155	0	0	**262450**
Householder QRD	8550	8192	30	605	20	**155999**

The impacts of varying antenna configurations and channel lengths on the algorithms were studied. First, retaining a constant channel length of 5, the operation counts were calculated for various number of transmitters. Figure 4.4 shows the results for one to four transmit antenna systems. As expected, when the number of antennas increases, both estimation techniques increase in complexity because the size of the unknown matrix $\mathbf{W}$ increases. The general trend of the H-QRD method is that it increases almost linearly with the number of transmit antennas of the system. The LS method increases exponentially at a considerably higher rate than the H-QRD methods. Overall, the H-QRD is lower in complexity and it is especially preferable for higher number of transmit antennas since it does not explode in complexity as the LS solution.

In Figure 4.5, the operation counts for channel estimation for a two transmit antenna system with varying channel lengths are shown. Increasing the channel length increases the number of unknown parameters, thereby will increase the complexity of the channel estimation. Again, it shows that the LS increases exponentially as the channel length increases and has much higher complexity than the H-QRD for long channel lengths.
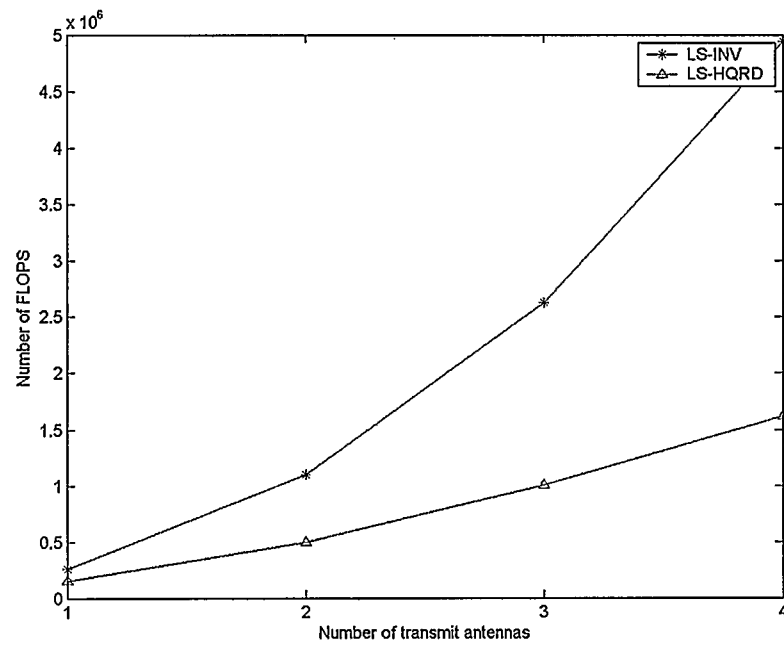
Figure 4.4 : FLOP counts for LS and H-QRD for various antennas configurations
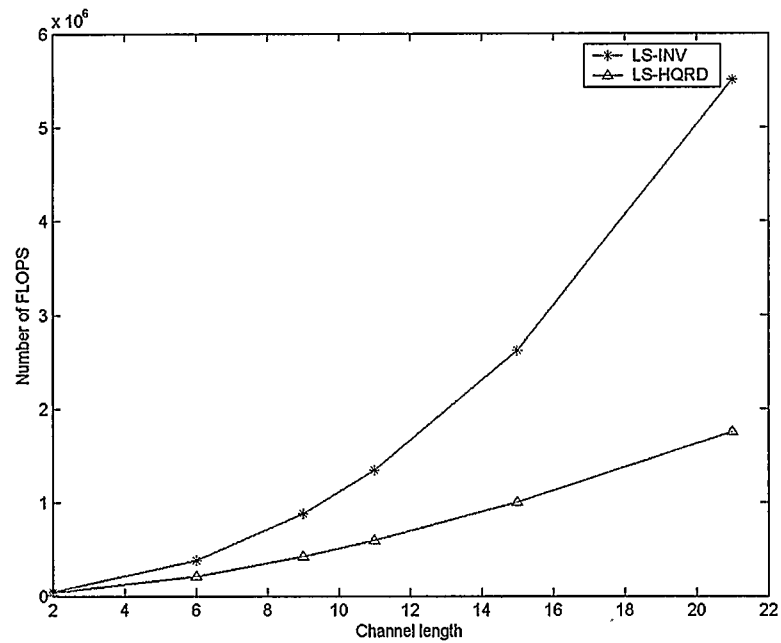
Figure 4.5 : FLOP counts for LS and H-QRD for various channel lengths

4.1.5.2 Recursive-based Methods

Now, we compare the complexity of the recursive methods: standard GR-QRD and DGR-QRD. The DGR-QRD was proposed to reduce the complexity of the standard GR-QRD by reducing the number of complex divisions and eliminating the square root operations. From Table 4-1, we see that the complex division corresponds to 11 real operations which have almost twice as much as a complex multiplication. Therefore, it is beneficial to minimize the number of complex division operations. The FLOP count of the GR-QRD and DGR-QRD is shown in Table 4-7. From Table 4-7, it can be observed that the DGR-QRD slightly reduces the number of complex multiplications and additions/ subtractions. The bulk of the reduction results from reducing the 1180 complex divisions to 10 and eliminating of all the square root operations. The overall number of FLOP count is reduced by about 15%.

Table 4-7: Operation count of a two transmit antenna system with channel length of 5.

Algorithm	Complex Multiplication	Complex Addition/ Subtraction	Complex Division	Square Root	**Number of FLOPS**
GR-QRD	16170	8994	1180	585	**313823**
Decoupled GR-QRD	15585	7824	10	0	**265268**

Next, we investigate the complexity of the GR-QRD and DGR-QRD algorithms for various lengths of the channel. The result in terms of number of FLOPs is shown in Figure 4.6. When the channel length increases, there are more unknowns to be determined; hence the complexity is expected to increase. The two schemes increase with similar trends.

Finally, the complexity of the block and recursive techniques is compared and the results are shown in Figure 4.7. It clearly shows all the QRD techniques have fewer number of FLOPs than the LS method.
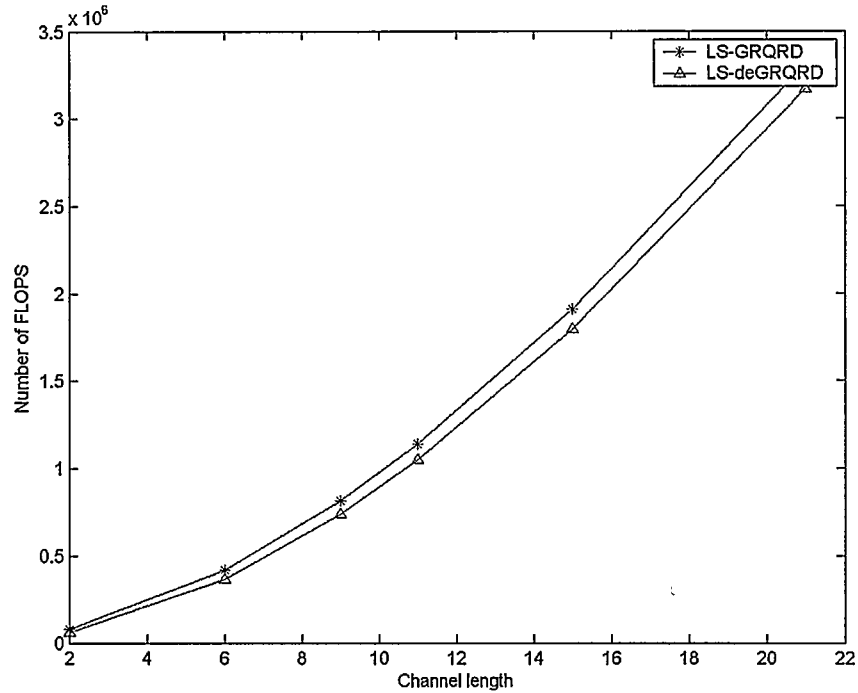
Figure 4.6: FLOP counts for GR-QRD and DGR-QRD for various channel lengths
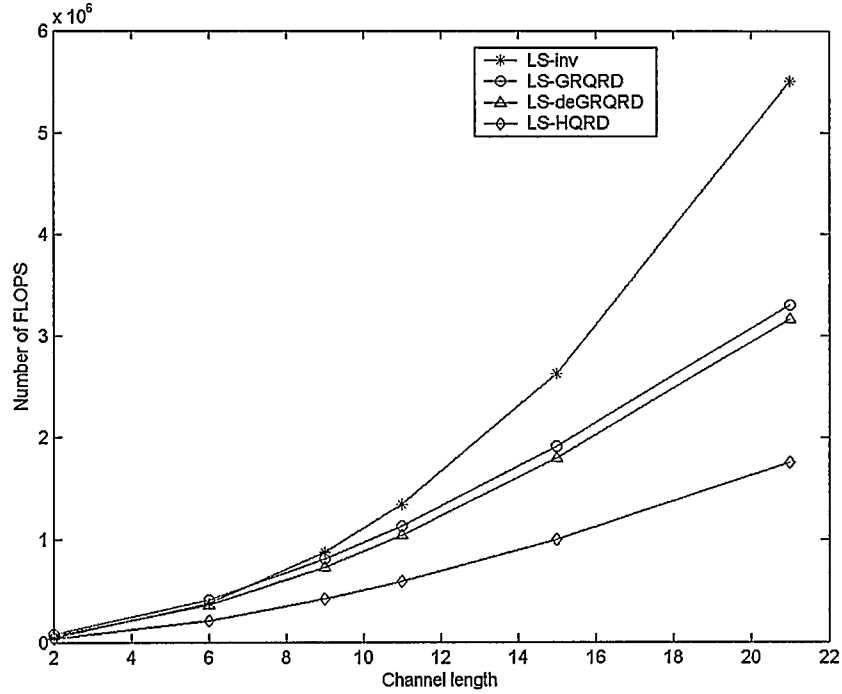
Figure 4.7: FLOP counts for LS, H-QRD, GR-QRD and DGR-QRD for various channel lengths

4.2 QR Decomposition MMSE Channel Estimation

It was mentioned in Chapter 3 that through the use of prior knowledge about the channel the MMSE estimator outperforms the LS solution at the cost of higher complexity. There are several factors that contribute to the high complexity of MMSE estimation. Usually in practice the covariance matrix of the channel is unknown; therefore, it needs to be calculated at the receiver. The covariance matrix can be approximated by performing a time average of the instantaneous covariance matrix of the channel determined at the receiver. The determination of the instantaneous covariance is high in complexity, and the convergence time of the average covariance matrix results in high latency. In addition, the noise variance of the AWGN has to be calculated. Even if the

channel covariance and the noise level is known, the computation of the MMSE solution is higher in complexity than the LS solution due to the added inverse operation of the channel covariance matrix (refer to Equation 3.31). If the channel has a large number of taps it will significantly increase the complexity of the algorithm due to the large inversion. The computational complexity can be reduced by considering the characteristics of the channel delay profile. For example, the channel length can be shortened by limiting to only the significant paths. However, it might impact the accuracy of the estimates. The tradeoff between computational complexity and estimation accuracy must be considered when choosing the number of significant channel taps. Alternatively, in hopes of retaining estimation accuracy we explore methods of reducing the computational complexity of the MMSE by simplification of the solution by QRD.

In this section, we will assume the channel covariance is known and the complexity of its calculation is not taken into account. Given the channel covariance matrix, the MMSE solution can be determined by the following equation

$$\hat{\mathbf{h}} = (\sigma_V^2\, \mathbf{C}_h^{-1} + \mathbf{W}^H\mathbf{W})^{-1}\mathbf{W}^H\mathbf{Y}. \tag{4.21}$$

The added complexity of the MMSE estimation over the LS method is largely due to the inversion of the channel covariance matrix and the inversion of the $(\sigma_V^2\, \mathbf{C}_h^{-1} + \mathbf{W}^H\mathbf{W})$ term. The system construction and channel environment affect the structure of the channel covariance matrix. The fundamental assumption in MIMO-OFDM systems is that the transmit and receive antennas are sufficiently separated such that the multiple channels are independent. In addition, the multipath components of each channel are assumed to be independent and

uncorrelated. Under these assumptions the covariance matrix of the channel is a diagonal matrix of the following form

$$
\begin{aligned}
C_{\mathbf{h}} &= E\{\mathbf{h}\mathbf{h}^H\} \\
&= \begin{bmatrix}
\sigma_1^2 & 0 & \cdots & 0 \\
0 & \sigma_2^2 & & \vdots \\
\vdots & & \ddots & 0 \\
0 & \cdots & 0 & \sigma_{LN_t}^2
\end{bmatrix} \\
&= diag\left(\sigma_l^2\right), \qquad\qquad l = 1,...,LN_t.
\end{aligned}
$$

(4.22)

Since $C_{\mathbf{h}}$ is diagonal, the inversion of $C_{\mathbf{h}}$ is simply the inversion of the diagonal elements. This will amount to a total of LN_t division operations for the inversion of $C_{\mathbf{h}}$, which is significantly lower than the complexity of a full matrix inversion. Having accounted for the $C_{\mathbf{h}}^{-1}$ operation the MMSE solution, there still exists the $(\sigma_v^2 \, diag\left(\dfrac{1}{\sigma_l^2}\right) + \mathbf{W}^H\mathbf{W})^{-1}$ operation which poses high computational complexity. We will propose the use of QRD to eliminate the inversion in the MMSE solution.

4.2.1 QR Decomposition for MMSE Channel Estimation

The obvious approach would be to manipulate the MMSE solution into a form that we can directly apply QRD. The MMSE equation is rewritten as

$$
(\sigma_v^2 \, C_{\mathbf{h}}^{-1} + \mathbf{W}^H\mathbf{W})\,\hat{\mathbf{h}} = \mathbf{W}^H\mathbf{Y}.
$$

(4.23)

Let $\mathbf{A} = \sigma_v^2 \, C_{\mathbf{h}}^{-1} + \mathbf{W}^H\mathbf{W}$ and $\mathbf{B} = \mathbf{W}^H\mathbf{Y}$, we get

$$
\mathbf{A}\,\hat{\mathbf{h}} = \mathbf{B}.
$$

(4.24)

We can apply QRD to $\mathbf{A}$, ($\mathbf{A} = \mathbf{Q'R'}$), substituting into Equation (4.24) to get

$$\mathbf{R'\hat{h}} = \mathbf{Q'}^H \mathbf{B},\qquad\qquad(4.25)$$

and the channel estimates can be obtained by back substitution. However, the direct implementation of the QRD in place of the inverse actually has higher complexity due to the addition computations to form the $\mathbf{A}$ and $\mathbf{B}$ matrices. The QRD LS estimation described in Section 4.1 has significantly lower complexity because the QRD is directly operates on the known matrix $\mathbf{W}$ as oppose of the $\mathbf{W}^H\mathbf{W}$. In order to lower the complexity of the MMSE solution using QRD we need to restructure the MMSE solution to eliminate the $\mathbf{W}^H\mathbf{W}$ operation. First we will define the following

$$\bar{\mathbf{W}} = \begin{bmatrix} \mathbf{W} \\ \sigma_v \, diag\left(\dfrac{1}{\sigma_l}\right) \end{bmatrix}\qquad\qquad(4.26)$$

and

$$\bar{\mathbf{Y}} = \begin{bmatrix} \mathbf{Y} \\ \mathbf{0} \end{bmatrix}\qquad\qquad(4.27)$$

which are the extended form of the known matrix, $\mathbf{W}$, and received vector, $\mathbf{Y}$, respectively. Now, we show that the LS solution of the $\bar{\mathbf{W}}$ and $\bar{\mathbf{Y}}$ is equivalent to the MMSE solution shown in Equation (4.21).

$$\hat{\mathbf{h}} = (\overline{\mathbf{W}}^H \overline{\mathbf{W}})^{-1} \overline{\mathbf{W}}^H \overline{\mathbf{Y}}$$

$$= \left(\begin{bmatrix} \mathbf{W}^H & \sigma_V diag\left(\dfrac{1}{\sigma_I}\right) \end{bmatrix} \begin{bmatrix} \mathbf{W} \\ \sigma_V diag\left(\dfrac{1}{\sigma_I}\right) \end{bmatrix} \right)^{-1} \begin{bmatrix} \mathbf{W}^H & \sigma_V diag\left(\dfrac{1}{\sigma_I}\right) \end{bmatrix} \begin{bmatrix} \mathbf{Y} \\ \mathbf{0} \end{bmatrix} \qquad (4.28)$$

$$= \left(\mathbf{W}^H \mathbf{W} + \sigma_V^2 diag\left(\dfrac{1}{\sigma_I^2}\right) \right)^{-1} \mathbf{W}^H \mathbf{Y}$$

Applying QRD to $\overline{\mathbf{W}}$ to get,

$$\overline{\mathbf{W}} = \overline{\mathbf{Q}}\,\overline{\mathbf{R}} \qquad (4.29)$$

then the QRD solution of the MMSE channel estimates in terms of the extended matrices is

$$\overline{\mathbf{R}}\hat{\mathbf{h}} = \overline{\mathbf{Q}}^H \overline{\mathbf{Y}} \qquad (4.30)$$

hence, the channel estimates can be solved for by back substitution.

It was discovered that the channel estimates can be extracted from the partitioned forms of the extended matrix $\overline{\mathbf{W}}$ without further back substitution. The extended matrices are defined in the following partitioned form:

$$\overline{\mathbf{W}} = \begin{bmatrix} \mathbf{W} \\ \sigma_V diag\left(\dfrac{1}{\sigma_I}\right) \end{bmatrix}, \quad \overline{\mathbf{Q}} = \begin{bmatrix} \mathbf{q}_{11} & \mathbf{q}_{12} \\ \mathbf{q}_{21} & \mathbf{q}_{22} \end{bmatrix}, \text{ and } \overline{\mathbf{R}} = \begin{bmatrix} \mathbf{R}^* \\ \mathbf{0} \end{bmatrix}. \text{ Then equation (4.30) can be}$$

represented in the partition as follows

$$\begin{bmatrix} \mathbf{R}^* \\ \mathbf{0} \end{bmatrix} \hat{\mathbf{h}} = \begin{bmatrix} \mathbf{q}_{11}^H & \mathbf{q}_{21}^H \\ \mathbf{q}_{12}^H & \mathbf{q}_{22}^H \end{bmatrix} \begin{bmatrix} \mathbf{Y} \\ \mathbf{0} \end{bmatrix}. \qquad (4.31)$$

From Equation (4.31) we can see that

$$\mathbf{R}^* \hat{\mathbf{h}} = \mathbf{q}_{11}^H \mathbf{Y}$$
$$\hat{\mathbf{h}} = \left(\mathbf{R}^*\right)^{-1} \mathbf{q}_{11}^H \mathbf{Y} \qquad (4.32)$$

The QR decomposition of $\overline{\mathbf{W}}$ in partition form is

$$\begin{bmatrix} \mathbf{W} \\ \sigma_V diag\left(\dfrac{1}{\sigma_I}\right) \end{bmatrix} = \begin{bmatrix} \mathbf{q}_{11} & \mathbf{q}_{12} \\ \mathbf{q}_{21} & \mathbf{q}_{22} \end{bmatrix}\begin{bmatrix} \mathbf{R}^* \\ 0 \end{bmatrix} \qquad (4.33)$$

From Equation (4.33) we can extract this relationship

$$\sigma_V diag\left(\frac{1}{\sigma_I}\right) = \mathbf{q}_{21}\mathbf{R}^*$$

$$\sigma_V diag\left(\frac{1}{\sigma_I}\right)\left(\mathbf{R}^*\right)^{-1} = \mathbf{q}_{21} \qquad (4.34)$$

$$\left(\mathbf{R}^*\right)^{-1} = \frac{1}{\sigma_V} diag\left(\sigma_I\right)\mathbf{q}_{21}$$

Substituting Equation (4.34) into (4.32) we get

$$\hat{\mathbf{h}} = \frac{1}{\sigma_V} diag\left(\sigma_I\right)\mathbf{q}_{21}\mathbf{q}_{11}^{H}\mathbf{Y} \qquad (4.35)$$

The derivation above shows that after QRD of the extended matrices, the channel estimation can be extracted from the orthogonal matrix $\overline{\mathbf{Q}}$. This eliminates the back substitution process which reduces processing time and hardware. The drawback of solving for the channel estimates using the above method is that it has higher computational cost. In the previous QRD methods, the $\mathbf{Q}$ matrix is not explicitly calculated or stored as it is not required to solve for the unknown. To calculate $\mathbf{Q}$ will require approximately $4(N^2M - NM^2 + M^3/2)$ FLOPs using the Householder method [46].

4.2.2 Performance Analysis

The proposed implementation of the QRD-MMSE was tested through simulation using the same system parameter as before. As expected, the QRD implementation gives the same results as the standard MMSE solution. The benefit of QRD-MMSE is in terms of the complexity reduction through QRD. In the next section complexity comparison will be performed between the standard MMSE and QRD-MMSE solution.

4.2.3 Complexity Comparison

The complexity in terms of number of operations of the MMSE channel estimation and the H-QRD-MMSE channel estimation was derived. The results are listed in Table 4-8 and Table 4-9.

Table 4-8: FLOP counts for MMSE channel estimation

Operation	# of Complex Mult.	# of Complex Add/Sub	# of Complex Div.	# of Sq. Root
$\mathbf{A} = \sigma_v^2 \, \mathbf{C}_h^{-1}$	M	0	M	0
$\mathbf{B} = \mathbf{W}^H \mathbf{W}$	NM^2	$NM^2 - M^2$	0	0
$\mathbf{A} + \mathbf{B}$	0	M	0	0
$\mathbf{C} = (\mathbf{A} + \mathbf{B})^{-1}$	M^3	M^3	$3M^2/2 + M/2$	0
$\mathbf{D} = \mathbf{C}^{-1} \mathbf{W}^H$	NM^2	$NM^2 - NM$	0	0
$\hat{\mathbf{h}} = \mathbf{D} \mathbf{Y}$	NM	$NM - M$	0	0

Table 4-9: FLOP counts for QRD-MMSE channel estimation

Operation	# of Complex Mult.	# of Complex Add/Sub	# of Complex Div.	# of complex magnitude	# of Sq. Root
Form $\mathbf{W}$	0	0		M	$M+1$
QRD of $\mathbf{W}$ by Householder	$N^2M + 3NM + 3N - M^2 + 4M + 3$	$N^2M + 7NM/2 + N + M$	$2M$	NM	M
Back substitution	$M^2/2 - M/2$	$M^2/2 + M/2 - 1$	M	0	0

The FLOP counts were calculated for the MMSE channel estimation and QRD-MMSE implementation of the MMSE solution. The results of a two transmit antenna system with channel length of 5 is shown in Table 4-10. QRD-MMSE requires about half the complexity of the standard MMSE method. Additionally, the effect of the channel length on the complexity of the methods is in shown in Figure 4.8. We observe that the complexity of the MMSE method increases exponentially as the number of channel increase due to the added complexity of a large matrix inversion. However, the QRD method increases in a more linear manner. This demonstrates that the proposed QRD-MMSE method is lower in complexity and is more robust to varying channel length.

Table 4-10: Operation count of a two transmit antenna system with channel length of 5

Algorithm	Complex Multipli-cation	Complex Addition/ Subtraction	Complex Division	Complex Magnitude	Square Root	Number of FLOPS
MMSE	14450	13700	165	0	0	**262890**
QRD-MMSE	9155	8715	30	660	31	**166980**
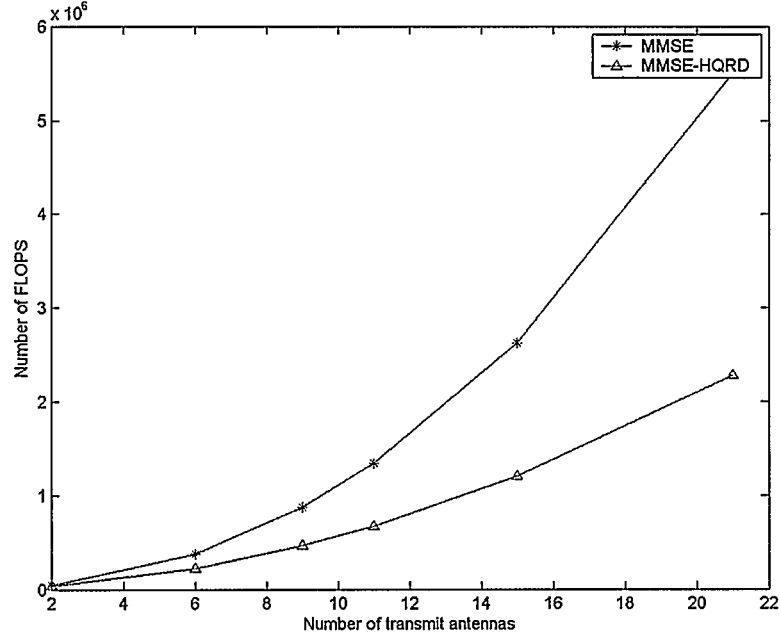
Figure 4.8: Operation count for various channel lengths for a 2 transmitter system

4.3 Summary

In this chapter, we have addressed the complexity issues of the standard LS and MMSE channel estimation schemes. For LS channel estimation, the pseudoinverse calculation is undesirable due to high computational complexity. We suggested the use of QRD to avoid the matrix inversion. The results showed the Householder implementation of the QRD has almost half the complexity of the standard LS solution. Moreover, the recursive Givens rotation method also showed lower complexity than the LS method, especially in long channel length situations. The decoupled Givens rotation method was applied to further reduce the complexity of the recursive Givens rotation approach. The MMSE channel estimation has better performance but with higher complexity. We proposed a QRD-MMSE method that significantly reduces the standard MMSE.

CHAPTER FIVE

ADAPTIVE CHANNEL ESTIMATION

In the previous chapters, low-complexity channel estimation techniques were developed for time-invariant channel. In a time-invariant channel, channel estimation is performed at the beginning of the frame and the estimates are used in the remainder of the frame for signal detection or equalization. In a time varying environment such an approach is not sufficient since the channel changes within the frame. In this chapter, low-complexity adaptive techniques are investigated for estimation of time varying channels. First, the time varying channel will be described and a system model is developed in Section 5.1. In Section 5.2, the comb-type pilot arrangement will be discussed for time varying channels. In Section 5.3, we will present various adaptive techniques for channel estimation in a time varying environment. Finally, performance analysis is performed on the various algorithms.

OFDM has been adopted in many current standards, such as IEEE 802.11a and HIPERLAN/2, due to its ability of high data rate transmission and robustness to frequency selective fading. In IEEE 802.11a, the OFDM frame is structured such that block-type pilots are placed at the beginning of the frame for channel estimation. This is suitable for a WLAN, where the transmitters and receivers are assumed to be mostly stationary. Under such an assumption the channel can be viewed as time invariant, therefore block-typed pilot arrangement is sufficient. However, when the transmitter or receiver units are mobile, the channel becomes time varying due to large Doppler shifts as discussed in Chapter

2. Depending on the Doppler shifts, the channel can vary significantly within the frame. Therefore, in mobile OFDM systems an alternate method of comb-typed pilot arrangement is required to estimate the channel over the frame duration.

5.1 Time Varying System Model

The frequency response of a frequency selective Rayleigh fading channel can be model as

$$H[n,k] = \sum_{l=0}^{L-1} h[n,l] e^{-\frac{j2\pi kl}{K}}, \tag{5.1}$$

as described in Section 2.4.1. In our previous discussions it was assumed that the channel is invariant; therefore, the channel stays constant for all n with in the duration of the frame. In a time varying channel, the CIR changes for different values of n which complicates the channel estimation. The rapid changing of the channel parameters can induce ICI. Consider the received signal of the MIMO-OFDM system under a time-varying channel for the jth received antenna,

$$y_t^{(j)}(n) = \sum_{i=1}^{M_t} \sum_{l=0}^{L_{ji}-1} h^{(j,i)}(n,l)\, s_t^{(i)}(n-l) + v_t^{(j)}(n), \qquad n = 0,1,\ldots,N-1 \tag{5.2}$$

This is similar to the received signal presented in Equation 2.11, except that in Equation 5.2, the channel is now also a function of time n. Note that the time domain transmitted signal $s_t^{(i)}(n\text{-}1)$ can be represented as a summation of the frequency components as described by Equation 2.6. Substituting the equivalent representation of $s_t^{(i)}(n\text{-}1)$ into equation (5.2) we get

$$y_t^{(j)}(n) = \frac{1}{\sqrt{N}} \sum_{i=1}^{M_t} \sum_{l=0}^{L_{ji}-1} h^{(j,i)}(n,l) \sum_{k=0}^{N-1} S_t^{(i)}(k) e^{j2\pi(n-l)k/N} + v_t^{(j)}(n),$$

$$= \frac{1}{\sqrt{N}} \sum_{i=1}^{M_t} \sum_{k=0}^{N-1} S_t^{(i)}(k) e^{j2\pi nk/N} \sum_{l=0}^{L_{ji}-1} h^{(j,i)}(n,l) e^{-j2\pi lk/N} + v_t^{(j)}(n)$$

$$(5.3).$$

It can be observed that the above equation contains the Fourier transform of the CIR. Therefore substituting equation (5.1) into $y_t^{(i)}(n)$ we get

$$y_t^{(j)}(n) = \frac{1}{\sqrt{N}} \sum_{i=1}^{M_t} \sum_{k=0}^{N-1} S_t^{(i)} H^{(j,i)}(n,k) e^{j2\pi nk/N} + v_t^{(j)}(n) \qquad (5.4)$$

The time domain received signal, $y_t^{(i)}(n)$, is demodulated by FFT transformation and the frequency domain received signal can be defined as

$$Y_t^{(j)}(k) = \frac{1}{\sqrt{N}} \sum_{n=0}^{N-1} \left(\frac{1}{\sqrt{N}} \sum_{i=1}^{M_t} \sum_{m=0}^{N-1} S_t^{(i)}(m) H^{(j,i)}(n,m) e^{j2\pi nm/N} + v_t^{(j)}(n) \right) e^{-j2\pi nk/N}$$

$$= \frac{1}{N} \sum_{i=1}^{M_t} \left(\sum_{m=0}^{N-1} S_t^{(i)}(m) \sum_{n=0}^{N-1} H^{(j,i)}(n,m) e^{-j2\pi(k-m)n/N} \right) + \frac{1}{\sqrt{N}} \sum_{n=0}^{N-1} v_t^{(j)}(n) e^{-j2\pi nk/N} \qquad (5.5$$

$$= \frac{1}{N} \sum_{i=1}^{M_t} \left(S_t^{(i)}(k) \sum_{n=0}^{N-1} H^{(j,i)}(n,k) + \underbrace{\sum_{\substack{m=0 \\ m \neq k}}^{N-1} S_t^{(i)}(m) \sum_{n=o}^{N-1} H^{(j,i)}(n,m) e^{-j2\pi(k-m)n/N}}_{\text{ICI}} \right) + V_t^{(j)}(i$$

The first term is the desired received signal at subcarrier k, and the second term is the ICI from the other subcarriers caused by the time-varying channel. Note in the time invariant case, the $H^{(j,i)}(k)$ is not a function of n. Hence, as expected the second term becomes zero, therefore no ICI is observed.

The time-varying characteristic of the channel is determined by the Doppler spread of the system, which depends on the relative motion of the

transmitter and receiver. The normalized Doppler frequency is $f_d T_B$, where f_d is the Doppler shift as described in Equation (2.5) and T_B is the duration of the OFDM block. From [20], we know that the power spectrum of a Rayleigh fading process with Doppler is

$$S_l(f) = \begin{cases} \dfrac{\sigma_l^2}{\pi \sqrt{f_d^2 - f^2}}, & |f| < f_d \\ 0, & \text{otherwise} \end{cases} \tag{5.6}$$

The correlation of the CIR can be characterized as

$$E\left\{h_l(n_1)h_l^*(n_2)\right\} = \sigma_l^2 J_0\left(2\pi f_d \left|n_1 - n_2\right| T_s\right) \tag{5.7}$$

where $T_s = T_B/N$ and $J(.)$ is the 0th order Bessel function of the first kind

$$J_0(x) = \sum_{k=0}^{\infty} \frac{(-1)^k}{2^{2k}(k!)^2} x^{2k}. \tag{5.8}$$

The Jake's model is a well-known method of simulating a time-correlated Rayleigh fading channel. The time varying channels in our simulations are created according to the Jake's model found in [49].

In general, a channel with a normalized Doppler frequency less than 0.01 can be considered constant. We calculated the normalized Doppler frequencies for one OFDM block at various velocities and the results are summarized in Table 5-1. A OFDM block contains 64 subcarriers and has a block duration of 4 μsec, adhering to the IEEE 802.11a standard. At realistic velocities, the normalized Doppler frequency is significantly lower than 0.01 for one OFDM block. It requires a speed of 500 km/h for the normalized Doppler frequency to be close to 0.01, which then causes the channel to be time varying within an OFDM block.

For practical purposes an OFDM system operating under IEEE 802.11a standards can be treated as time-invariant within one OFDM block. Since the channel is stationary for the duration of one block, then the ICI within the OFDM block is negligible.

Table 5-1: Normalized Doppler frequency for one OFDM block

Velocity (km/h)	F_dT
5	9.9047×10^{-5}
30	5.7778×10^{-4}
100	1.9259×10^{-3}
500	9.6296×10^{-3}

From Table 5-1, we concluded that the channel can be assumed to be time-invariant within an OFDM block. Now, we must consider the time variation with an OFDM frame, which contains a certain number of OFDM blocks. The general structure of an OFDM frame is diagrammed in Figure 5.1. The frame is partitioned into two parts, the preamble and the data domain. In the preamble, time and frequency synchronization, and channel estimation is performed. Once, the channel estimates have been determined it is used in the data domain to detect the transmitted signals. The maximum length of the data domain is restricted to 4096 bytes, but the actual number of symbols depends on the modulation scheme used. The maximum number of symbols is calculated as follows:

$$\frac{4096 \times 8}{number\ of\ bits\ per\ symbol \times number\ of\ subcarriers} \tag{5.9}$$

For example, an OFDM system using 16-QAM can have a maximum of approximately 196 symbols in the data domain of one frame. Under maximum load conditions, the normalized Doppler frequencies of such a system are shown in Table 5-2. Evidently, we can see that even at very slow traveling speeds the $f_d T$ is higher than 0.01, therefore the channel cannot be considered to be time invariant for the duration of the frame. Figure 5.2 shows the variations of the channel over one OFDM frame. Under low mobility systems, such as 5 km/h, the change in the channel between the beginning and the end of the frame is very slight. When the mobile is moving at 30 km/h, the channel variations become significant. As the speed of the mobile increases the variations are more rapid as demonstrated in Figure 5.2. This implies that for higher velocities the existing channel estimation approach in IEEE 802.11a is not sufficient. Channel estimation has to be performed throughout the OFDM frame in order to track the channel variations over the frame.
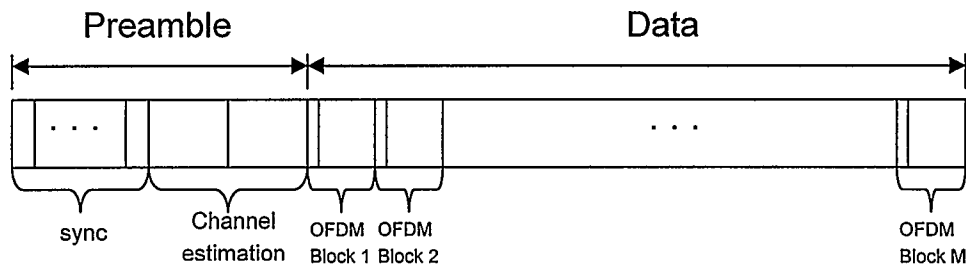
Figure 5.1: Structure of an OFDM frame

Table 5-2: Normalized Doppler frequency for one OFDM frame

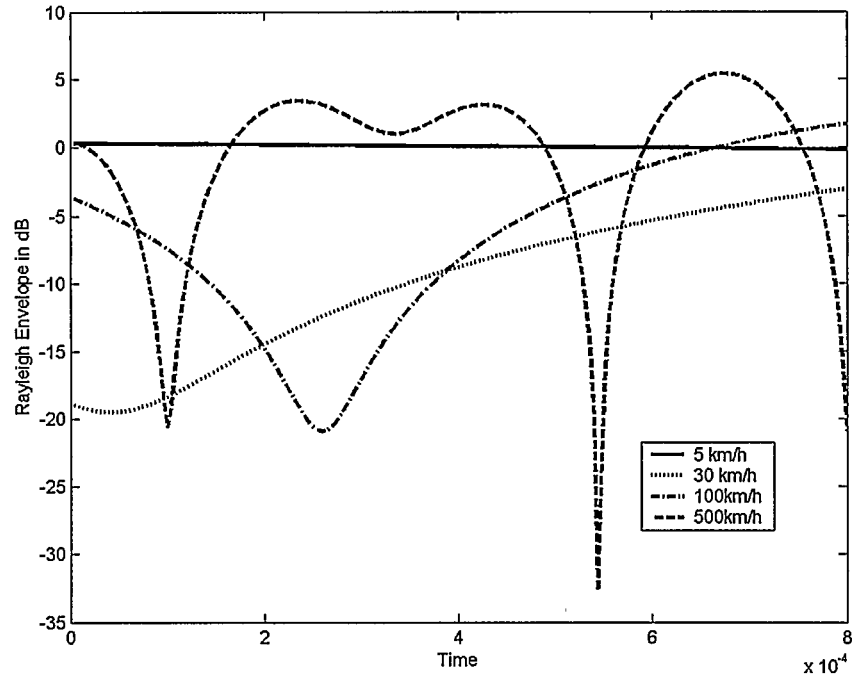| Velocity (km/h)	F_dT
5	0.01941
30	0.1132
100	0.3774
500	1.8874

Figure 5.2: Channel variation of a Rayleigh fading channel at different velocities

Now that we have established that in a mobile OFDM system, it is reasonable to assume that the channel is constant within one OFDM block, but will vary within one OFDM frame contenting X number of OFDM blocks. Next, we focus on estimating the channel as it changes over the OFDM frame using the comb type pilot arrangement.

5.2 Comb-Type Pilot Arrangement

The basic idea of the comb-type arrangement is that fewer pilots are used per channel estimation but most frequently. As shown in Figure 3.1(a), selected subcarriers are reserved for pilots and channel estimation is calculated at each time interval. How often the channel estimation is performed will depend on the severity of the channel variations. Since only a few of the subcarriers contain pilot signals, only the channel response at those frequencies can be determined. Interpolation is required to estimation the channel response of the remaining frequencies. There are various methods for performing the interpolation, namely linear interpolation, second order interpolation, low pass interpolation, spline cubic interpolation, and time domain interpolation. The performance of the various approaches was tested in [34]. In general, low pass interpolation achieved the best performance and linear interpolation had the worst performance. In Section 3.3.2, it was determined that for MIMO-OFDM systems it is more convenient to estimate the CIR and then perform Fourier transform to obtain the CFR, which is equivalent to time domain interpolation. Hence, time domain interpolation is chose for our analysis. Recall the MIMO-OFDM system model,

$$\mathbf{Y} = \mathcal{X}\boldsymbol{\Phi}\mathbf{h} + \mathbf{V} \tag{5.10}$$

In the comb-type arrangement, Np pilots are placed in the transmitted symbol. To ensure that the LS problem is full rank, the minimal number of pilots required is $N_t L$. The location of the pilots affects the performance of the channel estimates. It was proven in [15] that equi-spaced pilots resulted in the lowest channel estimation errors. Therefore, the pilots are uniformly inserted into the signal

$$\begin{aligned} \mathcal{X}(k) &= \mathcal{X}(mL + l) \\ &= \begin{cases} x_p(m), & l = 0 \\ data & l = 1, \ldots, L-1 \end{cases} \end{aligned} \tag{5.11}$$

where $L = N / N_p$ and $x_p(m)$ is the pilot value at the mth location. Using the received signal vector, $\mathbf{Y}_p$, at the pilot locations, the channel can be estimated by the following

$$\hat{\mathbf{h}} = (\boldsymbol{\Phi}_p^H \mathcal{X}_p^H \mathcal{X}_p \boldsymbol{\Phi}_p)^{-1} \boldsymbol{\Phi}_p^H \mathcal{X}_p^H \mathbf{Y}_p. \tag{5.12}$$

where $\boldsymbol{\Phi}_p$ with the Fourier transform matrix at the pilot locations. The CFR can be obtained by taking the FFT of the estimated CIR in Equation (5.12). The impact of number of pilots used in the estimation was studied. A 2-by-2 MIMO-OFDM system where each individual channel consisted of 6 delay paths was considered. The mobile is assumed to be traveling at 100 km/hr and the SNR is set to 30 dB. The pilots were uniformly spread over the OFDM block. The results of the performance of using different number of pilots are shown in Figure 5.3. First of all, the block LS estimation was included to illustrate that in a time varying channel, estimating at the beginning of the frame is insufficient. It can be observed in Figure 5.3 that the MSE for block estimation increases significantly

over the course of the frame. Also, as reference, the MSE curve using all 52 subcarriers for pilots was calculated. This, as expected, maintains the lowest MSE throughout the frame duration. According to linear algebra, the minimum required number of pilots must equal the number of unknowns to be solved. In this simulation, with 2 transmit antennas and 6 delay paths, the minimum number of pilots required is 12. From Figure 5.3, we can see that the performance of minimum of 12 pilot subcarriers is quite poor; however, it is able to maintain the same level of performance over the entire frame as the channel varies. Increasing to 24 pilots improves the MSE of the estimates substantially.
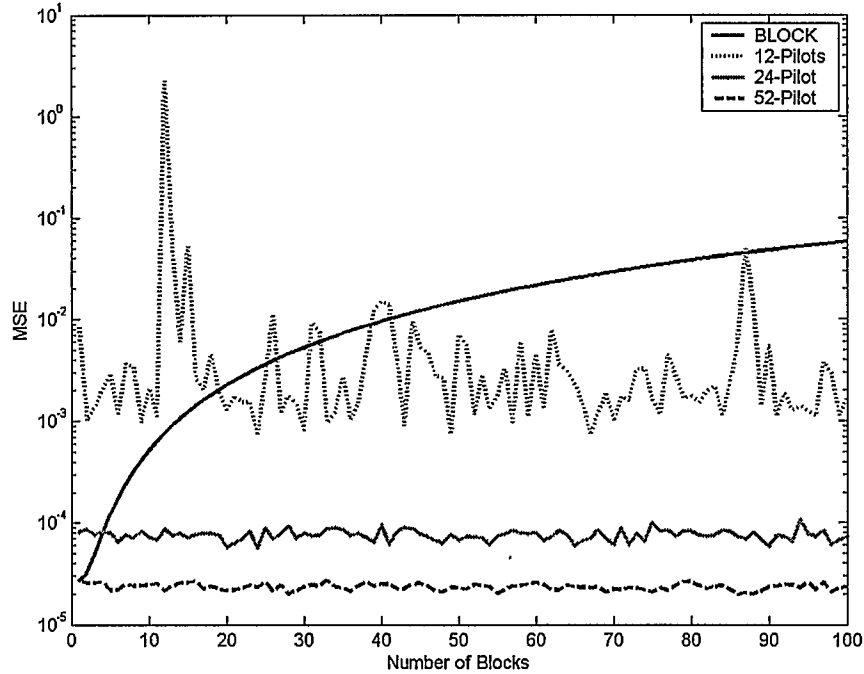

Figure 5.3: MSE curve for time varying channel for various number of pilots

In addition, our simulation confirmed that the placement of the pilots in fact affects the MSE of the estimate. In Figure 5.4, we have the MSE curve for using 24 and 36 pilot subcarriers. The 24 pilots were evenly spread throughout the subcarriers, with the following placement pattern: {1,3,5,7,9,11,13,15,17,19,21, 23,25,27,29,31,33,35,37,41,43,45,47}. In the case of 36 pilots, they were place on the first 36 subcarriers. Even though 36 pilot subcarriers were used, the performance of the 24 pilots was better due to the pilot placement pattern. Several important conclusions can be drawn from our analysis. First, using the minimum number of pilots does not give good performance. Seconely, twice the minimum number of pilots significantly improves the performance. However, we have to take into account the bandwidth efficiency of the system. For example, if 24 pilots are required to provide reasonable performance, then almost half the available bandwidth (52 subcarriers) is used to transmit pilots. Moreover, when using comb-type estimation the placement pattern of the subcarriers affects the overall MSE of the channel estimates. Due to the inefficiencies of the comb-type pilot arrangement approach to channel estimation in a time varying channel, we need to look for alternative methods to improve the performance with the minimum number of pilots. In the following section, we proposed the use of adaptive techniques to estimate the time varying channel with only the minimum required number of pilots.
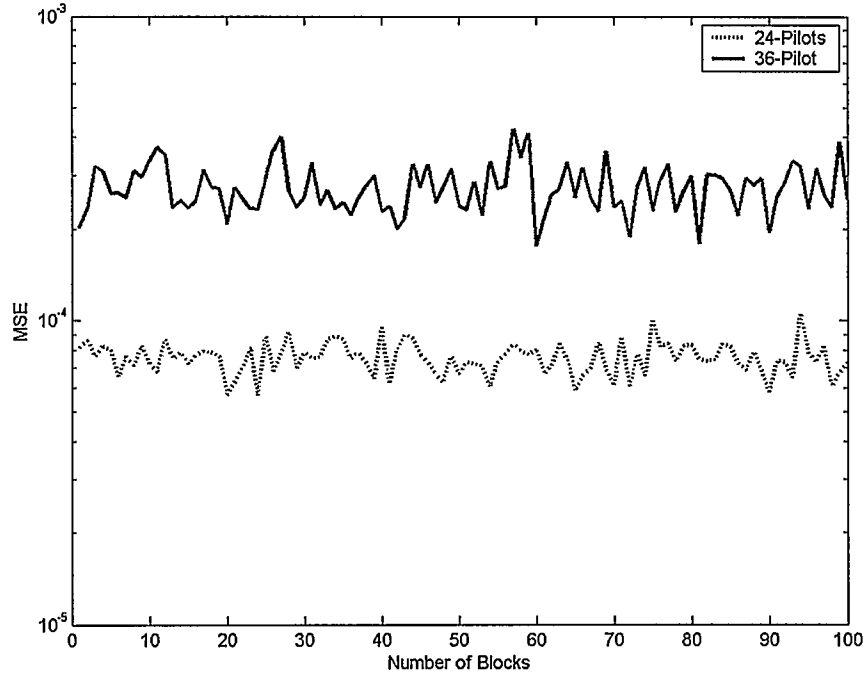
Figure 5.4: MSE curve for 24 pilots and 36 pilots.

5.3 Adaptive Filtering

When the channel varies from block to block adaptive filtering techniques are suitable for tracking the channel variations. In adaptive filtering problems, recursive algorithms are used to find the filter coefficients that produces the minimum error between the desired value and received value. Since the channel can be modeled as a tap-delay line filter, the channel estimation problem can be formulated as that of an adaptive filtering problem. Figure 5.5 illustrates the process of adaptive filtering to estimate the channel taps. The pilot symbols, x(n), are passed into the transversal filter and an estimate of the received signal, $\hat{y}(n)$, is outputted. The error between the actual received signal and the estimated received signal are fed into the adaptive weight control mechanism

where some recursive algorithm is used to update the channel weights. Commonly used recursive algorithms are least mean square (LMS) and recursive least squares (RLS). The LMS algorithm is a statistical approach to solving the wiener filter problem. The objective of the algorithm is to find the optimal weight vector that gives the minimum mean-squared error [47]. The LMS algorithm uses the steepest decent method to iteratively search the quadratic surface of the MSE curve for the minimum point. RLS follows the fundamental idea of LS estimation that was developed in Chapter 3; however, instead of calculating the estimate at each iteration, the previous value of the estimate is used to determine the current estimate. The RLS algorithm performs a time averaging instead of statistical averaging as in the LMS algorithm. In general, the LMS is known to have low complexity, but it suffers from slow convergence as compared to the RLS approaches. Due to the fast convergence of the RLS, we will concentrate on the implementation and analysis of the RLS for MIMO-OFDM.
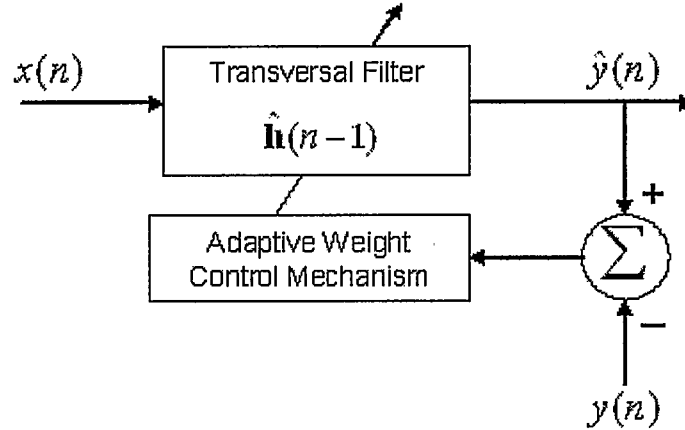

Figure 5.5: Block diagram of the adaptive filtering process.

5.3.1 Recursive Least Squares for MIMO-OFDM

The application of adaptive filtering for channel estimation in MIMO-OFDM is more complex due to the multiple channels. The tap-delay line channel model of a MIMO system was shown in Figure 2.11. To adaptively adjust the estimates of each multipath channel requires the use of multichannel adaptive filtering techniques. In multichannel filtering the error between the received signal and the sum of each channel output is used to adjust the channel estimates. In [50], a fast multichannel QR decomposition least squares adaptive algorithm was introduced to solve for the CIR. In the case of MIMO-OFDM, we have established that it is more convenient to process the received signal in the frequency domain. The received signal in the frequency domain can be represented as a multiplication of the channel frequency response and the transmitted signal. In the following section, we investigate the use of adaptive filtering in the frequency domain to estimate the channel impulse response.

5.3.1.1 RLS Algorithm in the Frequency Domain

In the frequency domain, the objective of adaptive filtering is to use the values of the previous subcarriers to estimate the current subcarrier. In the recursive approach, the kth inputs and outputs, and the previous value of the channel $h(k\text{-}1)$ are used to estimated $h(k)$. To better illustrate this idea, recall the system model of the frequency domain received signals represented in Equation (3.25). The received signal of a single subcarrier is given as

$$\mathbf{Y}(k) = \mathbf{W}(k)\mathbf{h} + \mathbf{V}(k) \qquad (5.13)$$

where

$$\mathbf{Y}(k) = \begin{bmatrix} Y^{(1)}(k) & Y^{(2)}(k) & \cdots & Y^{(M_r)}(k) \end{bmatrix}$$

$$\mathbf{W}(k) = \begin{bmatrix} W_1^{(1)}(k) & W_2^{(1)}(k) & \cdots & W_L^{(1)}(k) & \cdots & W_1^{(M_r)}(k) & W_2^{(M_r)}(k) & \cdots & W_L^{(M_r)}(k) \end{bmatrix}$$

$$\hbar = \begin{bmatrix} \mathbf{h}^{(1,1)} & \mathbf{h}^{(1,2)} & \cdots & \mathbf{h}^{(1,M_r)} \\ \mathbf{h}^{(2,1)} & \mathbf{h}^{(2,2)} & & \\ \vdots & & \ddots & \\ \mathbf{h}^{(M_t,1)} & & & \mathbf{h}^{(M_t,M_r)} \end{bmatrix}$$

With the above equation for the kth subcarrier, the LS solution for the estimated CIR matrix, $\hat{\hbar}$, is obtained by minimizing the cost function

$$J(\hbar) = \left(\mathbf{Y}(k) - \mathbf{W}(k)\hbar \right)^H \left(\mathbf{Y}(k) - \mathbf{W}(k)\hbar \right) \tag{5.14}$$

Taking the gradient of cost function and equating it to zero we get

$$\hat{\hbar} = \left(\mathbf{W}^H(k)\mathbf{W}(k) \right)^{-1} \mathbf{W}^H(k)\mathbf{Y}(k). \tag{5.15}$$

In a time variant channel, the channel changes over time, and it is not practical to calculate the LS estimate at every block. Therefore, RLS algorithms are used where the LS solution is not explicitly calculated. A prescribed initial condition is assumed and the information in the new data samples is used to update the old estimates [47]. RLS uses the technique of least square filtering with a cost function defined as the sum of weighted error squares,

$$\mathcal{J}(k) = \sum_{k=1}^{n} \lambda^{n-k} \left(\mathbf{Y}(k) - \mathbf{W}(k)\hbar \right)^H \left(\mathbf{Y}(k) - \mathbf{W}(k)\hbar \right) \tag{5.16}$$

where, $\hbar$ is the CIR matrix to be estimated, λ is the exponential weight factor or forgetting factor and n is the variable length of the observation data. The forgetting factor provides time-weighting of the input data so that more emphasis

is placed on more recent data points. The value of λ is a positive constant close to, but less than unity. With the known (pilot) vector, $\mathbf{W}(k)$, and the received signal, $\mathbf{Y}(k)$, where $k = 1, 2,..., Np$, the exponentially weighted RLS algorithm described in [47] can be used to adaptively track the CIR matrix. The algorithm is summarized in Table 5-3. The inverse correlation matrix, $\mathbf{P}(k)$, is of size $(LM_t \times LM_t)$ and the Kalman gain vector, $\mathbf{G}(k)$, is of size $(LM_t \times 1)$.

The RLS method has good performance, but it has the problem of numerical instability. This motivates the application of stable orthogonal linear transformations to the original RLS problem. In [47], it states that the QRD is a numerically stable method of solving the LS estimation. And in Chapter 4, we have shown that the QRD LS lower in complexity. In the following section, QRD will be applied to solve the RLS problem.

Table 5-3: Summary of RLS algorithm for MIMO-OFDM channel estimation

Initialization:

$\mathbf{P}(0) = \delta^{-1}\mathbf{I}$, where δ is a small positive constant (i.e. 0.001)

$\hat{h}(0) = \mathbf{0}_{M_r \times LM_t}$

For each pilot vector $\mathbf{W}(k), k = 1, 2,..., N_P$, compute

$$\mathbf{G}(k) = \frac{\lambda^{-1}\mathbf{W}(k)\mathbf{P}(k-1)}{1 + \lambda^{-1}\mathbf{W}(k)\mathbf{P}(k-1)\mathbf{W}^H(k)}$$

$e(k) = \mathbf{Y}(k) - \mathbf{W}(k)\hat{h}(k-1)$

$\hat{h}(k) = \hat{h}(k) + \mathbf{G}^H(k)e(k)$

$\mathbf{P}(k-1) = \lambda^{-1}\mathbf{P}(k-1) - \lambda^{-1}\mathbf{G}^H(k)\mathbf{W}(k)\mathbf{P}(k-1)$

5.3.1.2 QR Decomposition Recursive Least Squares

In the QR decomposition recursive least squares (QRD-RLS) algorithm, triangular transformation using Givens rotations is used to recursively solve the LS problem. The adaptive filtering performed directly to the data matrix as oppose to the RLS method, which works on the time averaged correlation matrix of the input data. The numerical dynamic range of the QRD-RLS method is half the range of the RLS problem, thereby making the QRD-RLS more numerically stable [47]. Another benefit of the QRD-RLS, is the ability to efficiently implement the algorithm in parallel using systolic array structures.

To develop the QRD-RLS algorithm for channel estimation in MIMO-OFDM systems the RLS cost function described in Equation (5.16) needs to be rewritten in matrix-vector notation. Assuming a prewindowing of N_p samples of the input data, the data matrix at time n is defined as

$$
\mathcal{W}(n) = \begin{bmatrix} W_1^{(1)}(n-N_p+1) & W_2^{(1)}(n-N_p+1) & \cdots & W_L^{(1)}(n-N_p+1) \\ W_1^{(1)}(n-N_p+2) & W_2^{(1)}(n-N_p+2) & & \vdots \\ \vdots & & \ddots & \vdots \\ W_1^{(1)}(n) & \cdots & \cdots & W_L^{(1)}(n) \end{bmatrix}
$$

$$
\begin{matrix} \cdots & W_1^{(M_t)}(n-N_p+1) & W_2^{(M_t)}(n-N_p+1) & \cdots & W_L^{(M_t)}(n-N_p+1) \\ \cdots & W_1^{(M_t)}(n-N_p+2) & W_2^{(M_t)}(n-N_p+2) & & \vdots \\ \cdots & \vdots & & \ddots & \vdots \\ \cdots & W_1^{(M_t)}(n) & \cdots & \cdots & W_L^{(M_t)}(n) \end{matrix}
$$

$$(5.17)$$

and the weighting factor matrix is

$$
\Lambda(n) = \begin{bmatrix} \sqrt{\lambda^{n-N_p}} & 0 & \cdots & 0 \\ 0 & \sqrt{\lambda^{n-N_p+1}} & \cdots & 0 \\ \vdots & \vdots & \ddots & \vdots \\ 0 & 0 & \cdots & 1 \end{bmatrix}.
$$

$$(5.18)$$

The cumulative squared error can be written in matrix form as

$$\mathcal{J}(n) = \left\| \Lambda(n)\mathcal{Y}(n) - \Lambda(n)\mathcal{W}(n)\hbar(n) \right\|^2 . \tag{5.19}$$

Now, we apply QRD to $\Lambda(N_p)\mathcal{W}(N_p)$ to get

$$\mathbf{Q}^H(n)\Lambda(n)\mathcal{W}(n) = \begin{bmatrix} \mathbf{R}(n) \\ \mathbf{0} \end{bmatrix} . \tag{5.20}$$

where $\mathbf{Q}^H(n)$ is the complex transpose of the orthogonal matrix of size N_p x N_p, and $\mathbf{R}(n)$ is a M_tL x M_tL upper triangular matrix. The same orthogonal matrix is applied to $\Lambda(n)\mathcal{Y}(n)$ to give

$$\mathbf{Q}^H(n)\Lambda(n)\mathcal{Y}(n) = \begin{bmatrix} \mathbf{z}(n) \\ \Delta(n) \end{bmatrix} . \tag{5.21}$$

where $\mathbf{z}(n)$ is a M_tL x M_r matrix and $\Delta(n)$ is $(N_p\text{-}M_tL)$ x M_r matrix. Since $\mathbf{Q}$ is orthogonal, it can premultiply each vector within the norm without altering the value of the norm. Substituting in Equations (5.20) and (5.21) into the cost function in Equation (5.19) we get

$$\begin{aligned} \mathcal{J}(n) &= \left\| \mathbf{Q}(n)\Lambda(n)\mathcal{Y}(n) - \mathbf{Q}(n)\Lambda(n)\mathcal{W}(n)\hbar(n) \right\|^2 \\ &= \left\| \begin{matrix} \mathbf{z}(n) - \mathbf{R}(n)\hbar(n) \\ \Delta(n) \end{matrix} \right\|^2 \end{aligned} . \tag{5.22}$$

Minimization of the top partition in the above function gives

$$\mathbf{R}(n)\hat{\hbar}(n) = \mathbf{z}(n) . \tag{5.23}$$

In recursive algorithms the previous values are assumed to be known and the new input data are used to solve for the current values. Assume that $\mathbf{R}(n\text{-}1)$ and $\mathbf{z}(n\text{-}1)$ are known, then the current values can be obtained by

$$\mathbf{T}(n)\begin{bmatrix} \sqrt{\lambda}\mathbf{R}(n-1) \\ \mathbf{W}(n) \end{bmatrix} = \begin{bmatrix} \mathbf{R}(n) \\ \mathbf{0}^T \end{bmatrix}. \qquad (5.24)$$

where $\mathbf{T}(n)$ is an orthogonal matrix that zeros the new data vector. Similarly, $\mathbf{z}(n)$ is updated as

$$\mathbf{T}(n)\begin{bmatrix} \sqrt{\lambda}\mathbf{z}(n-1) \\ \mathbf{Y}(n) \end{bmatrix} = \begin{bmatrix} \mathbf{z}(n) \\ \delta(n) \end{bmatrix}. \qquad (5.25)$$

where $\mathbf{Y}(n)$ is the received signal vector from all the received antennas, and $\delta(n)$ is the last row on the right hand side matrix. With the current values of $\mathbf{R}(n)$ and $\mathbf{z}(n)$ the new channel estimates can be easily obtained by back substitution since $\mathbf{R}(n)$ is an upper triangular. In Figure 5.6, a systolic implementation of the QRD-RLS algorithm using parallel processing cells is shown. At each sampling time, the pilot signal vector and the received signal vector is passed into the first row of processing units. Each cell processes the data and relays the necessary information to adjacent cells according to a common clock of the systolic array. The systolic arrays are well-suited for implementing the QRD-RLS algorithm under real-time and high data bandwidth requirements.
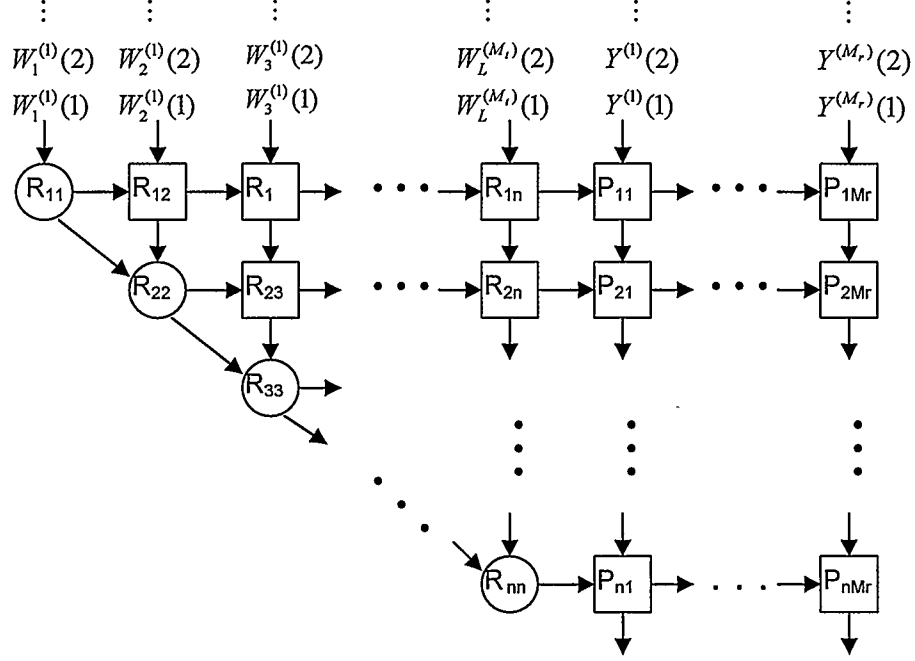
Figure 5.6: A systolic implementation of QRD-RLS for MIMO-OFDM

5.3.1.3 Inverse QR Decomposition Recursive Least Squares

The QRD-RLS algorithm is computationally efficient and numerically stable, nonetheless, the back substitution procedure to obtain the channel estimates adds time delays to the algorithm. In [51], a better alternative was developed to eliminate the need for back-substitution by updating the inverse of $R(n)$. In the following section the inverse QR decomposition recursive least squares (IQRD-RLS) algorithm will be adapted to a MIMO-OFDM system. From Equation (5.23), we see that the channel is given as

$$\hat{h}(n) = R^{-1}(n)z(n) .$$
(5.26)

Assuming that $\mathbf{R}^{-1}(n-1)$ is known, the $\mathbf{R}^{-1}(n)$ needs to be updated recursively. To determine the orthogonal updating matrix $\mathbf{D}(n)$, we must first define a intermediate matrix

$$\mathbf{a}(n) = \frac{\mathbf{R}^{-H}(n-1)\hbar(n)}{\sqrt{\lambda}}. \tag{5.27}$$

The orthogonal matrix $\mathbf{D}(n)$ is different from the $\mathbf{T}(n)$ of the QRD-RLS algorithm in that it is not obtained in a straightforward manner through the zeroing of the new data vector by a sequence of Givens rotations. The $\mathbf{D}(n)$ is obtained by performing Given rotations to zero the n elements of the augmented $\mathbf{a}(n)$ matrix as follows

$$\mathbf{D}(n)\begin{bmatrix} \mathbf{a}(n) \\ \mathbf{1}^T \end{bmatrix} = \begin{bmatrix} \mathbf{0} \\ \mathbf{b}(n) \end{bmatrix}. \tag{5.28}$$

where $\mathbf{1} = [1, 1, \ldots, 1]$ and $\mathbf{b}(n)$ is the resulting vector of the series of Givens rotations. It turns out that the $\mathbf{D}(n)$ obtained in the above equation also satisfies the following equation

$$\mathbf{D}(n)\begin{bmatrix} \lambda^{-1/2}\mathbf{R}^{-H}(n-1) \\ \mathbf{0}^T \end{bmatrix} = \begin{bmatrix} \mathbf{R}^{-H}(n) \\ \mathbf{u}^H(n) \end{bmatrix}. \tag{5.29}$$

Therefore, using $\mathbf{D}(n)$, the $\mathbf{R}^{-1}(n)$ matrix can be recursively updated. With the updated $\mathbf{R}^{-1}(n)$ matrix, the channel estimates can be obtained by simply multiplications as shown in Equation (5.26).

5.4 Simulation Results

In the previous section, three different algorithms, RLS, QRD-RLS, and IQRD-RLS, were presented for recursively estimating the channel for a MIMO-OFDM system. These three methods use different approaches to solve the

recursive LS problem. In our first analysis, we study the convergence time and final MSE value of the three methods. Figure 5.7 shows the MSE curves of the three algorithms applied to estimate the time varying channel of a MIMO-OFDM system with. All three algorithms have similar performance in that they all converge to the same MSE value. However, the QRD-RLS and IQRD-RLS implementation converges faster than the RLS method. In addition, the QRD method can be implemented in a highly parallel systolic array structure which makes it desirable for real-time implementations.
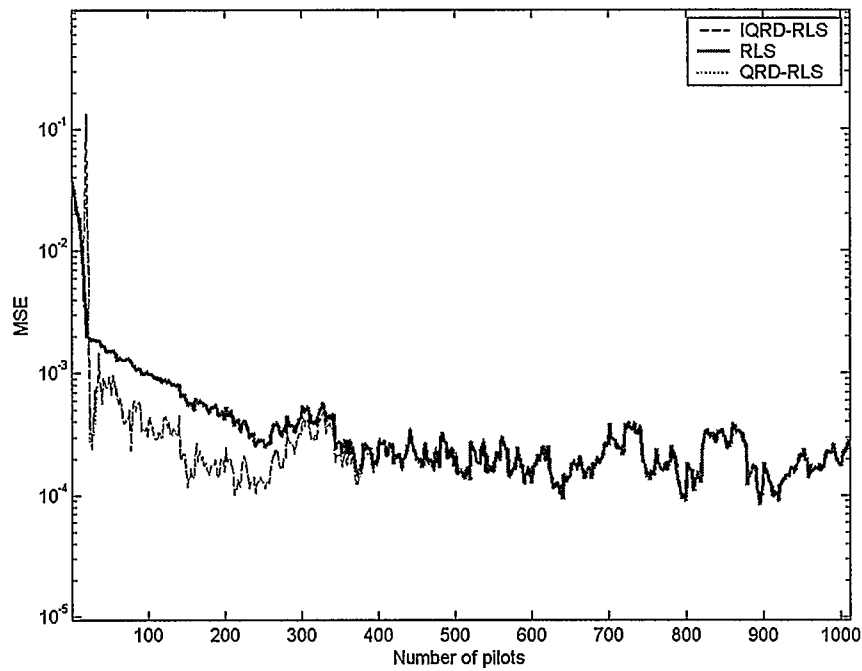

Figure 5.7: MSE curve of recursive adaptive algorithms

Next, the recursive algorithms are compared with block-based LS methods. Figure 5.8 illustrates the structural difference between of the recursive methods and the straightforward block LS estimation using the pilots. The method of block LS estimation using the pilots subcarriers is diagramed in Figure 5.8(a) over two consecutive OFDM blocks. The transmitted pilot symbols are collected and buffered until the end of the nth block, and then all the pilot information is used to calculate the channel estimate $\hat{h}(n)$. The estimation is performed at the end of every block to get the most accurate estimate of the channel. The second method of recursive channel estimation is illustrated in Figure 5.8(b). Basically, at each pilot subcarrier an updated channel estimate is obtained using the previous channel estimates and the current pilot information. As the diagram shows, a new estimate is obtained at each pilot subcarrier. It should be noted that it is valid to use the last estimate of the previous block as initial conditions of the current block, since the channel does not change drastically between adjacent blocks.
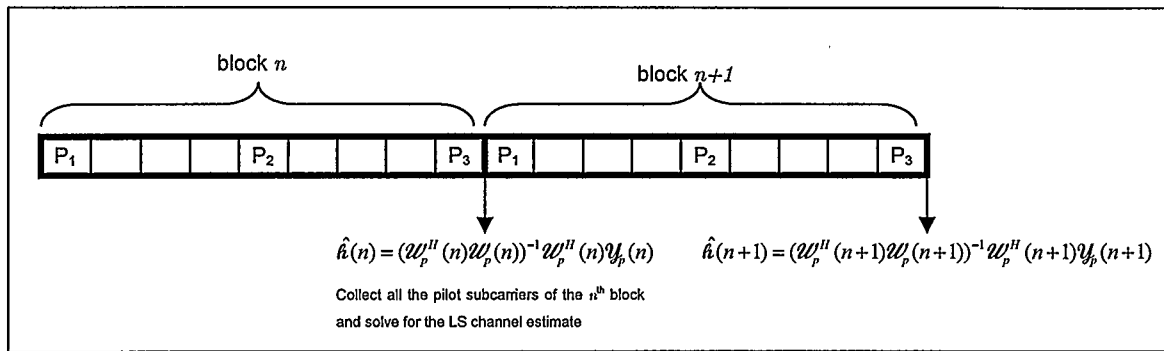
(a)
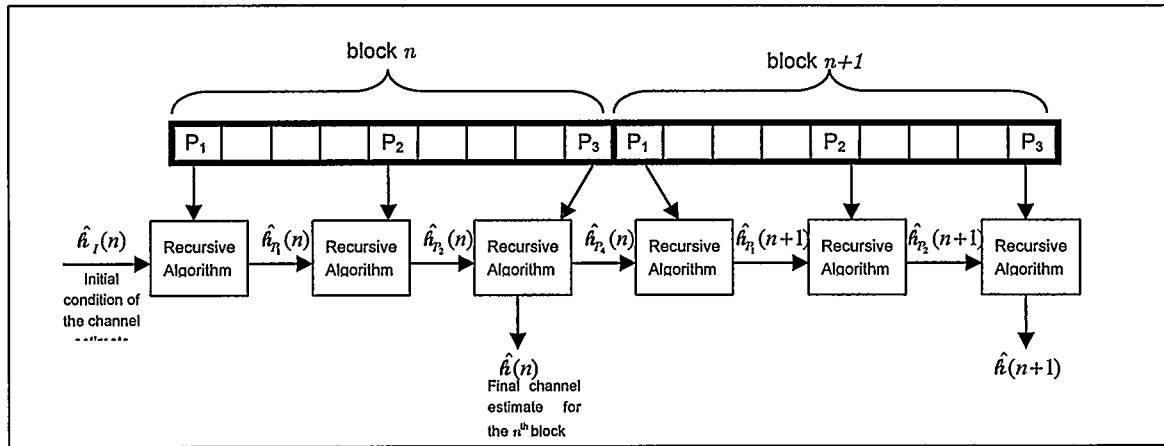
(b)

Figure 5.8: Block-type vs Adaptive

Using the same simulation parameters as those given in Section 3.3.1 a time-variant MIMO-OFDM system was simulated. The time varying nature of the channel due to the Doppler Effect was simulated using the Jake's model as described previously in this chapter. The performance of the recursive algorithm, measured in terms of MSE of the estimated channel, is shown in Figure 5.9. The system has 2 transmit antennas, and each channel consists of 10 delay taps. The mobile unit is assumed to be traveling at a speed of 100 km/h and the received SNR is 30 dB. The block LS solution was calculated using the minimum number of pilots (20 subcarriers), twice the minimum (40 subcarriers), and all the

subcarriers as pilots (52 subcarriers) as benchmarks. The RLS, QRD-RLS, and IQRD-RLS adaptive algorithms were implemented using only the minimum of 20 pilots. All three algorithms converge to a MSE that is lower than the LS solution of using 20 and 40 subcarriers. The adaptive algorithms are able to achieve a better performance than the block LS solutions using fewer pilot symbols. The improvement in performance of the recursive techniques comes at the cost of increased complexity, since the channel estimate is updated at each pilot subcarrier. However, the QRD-RLS and IQRD-RLS algorithms have been proved to be very efficient for real-time implementations, thereby making the estimation in recursive manner feasible.

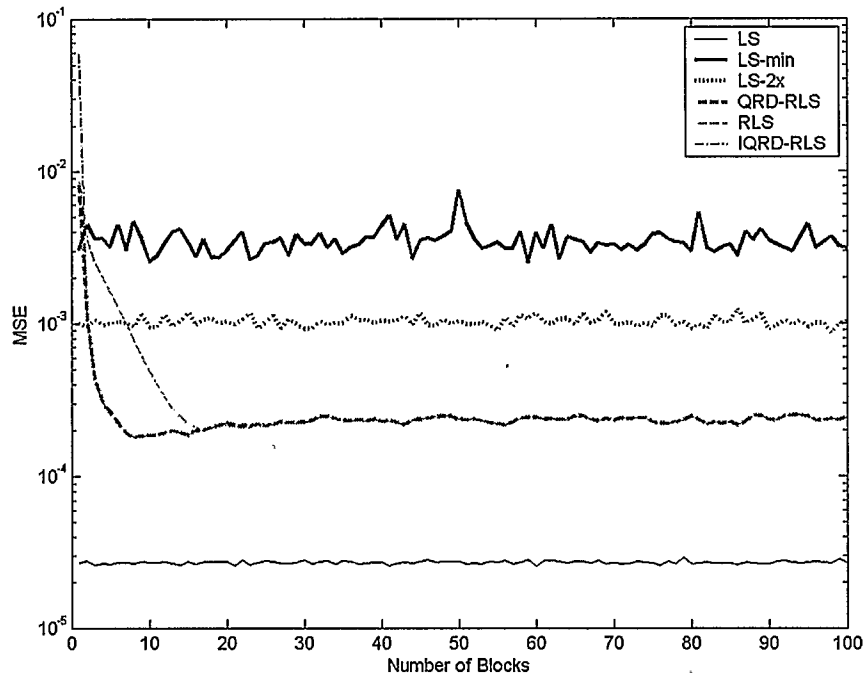Figure 5.9: Velocity = 100km/hr at SNR 30 dB

The performance of the recursive algorithm for various mobile speeds is shown in Figure 5.10. As expected for slower changing channels, such as the 5 km/hr case, the performance is better. Conversely, in the extremely fast changing channel of 500 km/hr. the performance degrades.
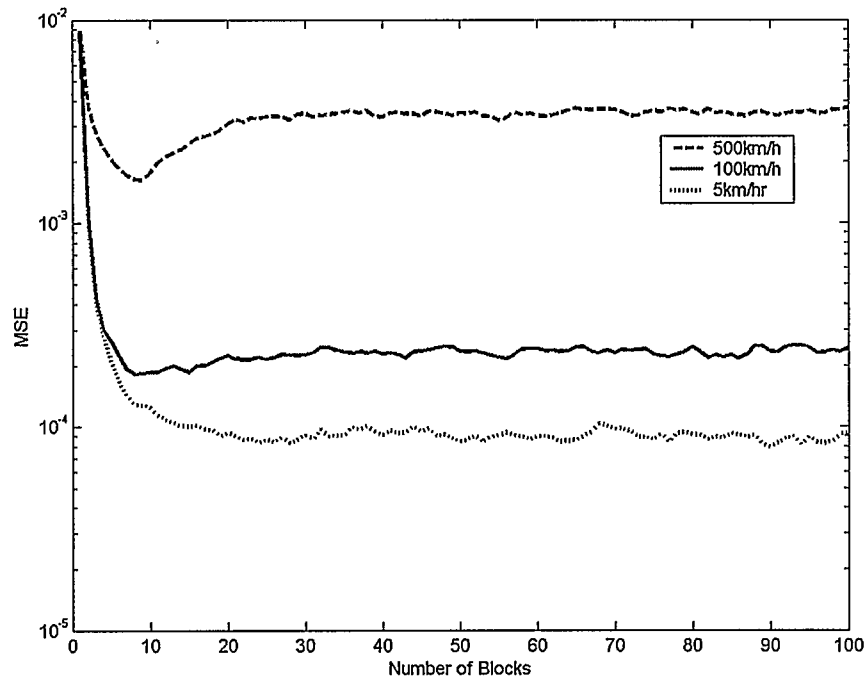
Figure 5.10: MSE curve of the recursive algorithms for various mobile speeds.

5.5 Summary

In this chapter we discussed channel estimation of a time-varying channel for MIMO-OFDM systems. The channel and system model described show that channel estimation needs to be performed adaptively in order to capture the variations in the channel. We implemented three recursive algorithms, RLS, QRD-RLS, and IQRD-RLS, to adaptively track a time-varying channel. The results showed that the adaptive algorithms adequately estimated the channel. Additionally, the QRD-RLS and IQRD-RLS can be implemented efficiently using the systolic array architecture. Furthermore, the IQRD-RLS is preferable since it tracks the inverse correlation matrix therefore would not require back substitution to solve for the channel matrix.

CHAPTER SIX

CONCLUSION AND FUTURE WORKS

6.1 Thesis Summary and Conclusions

MIMO-OFDM has the potential to significantly increase the capacity and reliability of a system due to the added spatial degree of freedom from the multiple independent paths. Moreover, the use of OFDM techniques makes the system robust to frequency selective channels. The promising prospects of MIMO-OFDM are hindered by the complicated receiver processing due to the additional unknown parameters. In particular, channel estimation is extremely complicated for MIMO-OFDM systems. In this thesis, the problem of channel estimation of a frequency selective channel for MIMO-OFDM systems was studied. The main objective was to develop low complexity channel estimation techniques suitable for real-time implementations.

In Chapter 3, it was established that for MIMO-OFDM systems training-based channel estimation is preferable over blind estimation due to its simplicity. The two main approaches in training-based estimation are the least squares (LS) method and minimum mean square error (MMSE) method. Our analysis confirmed that the MMSE outperforms the LS estimation at the expense of increased complexity. In addition, our simulation results showed that at high SNR, the performance of the MMSE estimator approaches the performance of the LS estimator. Therefore, the LS method is preferable for high SNR circumstances since it has the same performance as the MMSE estimator but with much lower complexity.

The LS and MMSE estimation technique is relatively low in complexity compared to blind estimation methods. However, the LS and MMSE still involves complex matrix inversions, which are not well-suited for real-time hardware implementations. In Chapter 4, we applied QR decomposition (QRD) to eliminate the matrix inversion to simplify the overall channel estimation complexity. Our simulations showed that the Householder implementation of the QRD has the same performance as the standard LS method in terms of MSE. The complexity analysis suggested the QRD-LS reduce the number of FLOPS by 40%. Also, we studied the performance of the recursive Givens rotation (GR) method for QR decomposition. The results indicated the GR algorithm is higher in FLOP counts than the Householder algorithm, but the efficient hardware implementation of the GR method using highly parallel systolic arrays can reduce the overall execution time over the Householder technique. In order to reduce the complexity of the GR algorithm, a decoupled GR (DGR) method was adopted. Complexity analysis showed that the elimination of the square root operation and minimization of divisions of the DGR algorithm reduces the overall complexity compared to the GR algorithm.

QR decomposition was applied to the MMSE solution in the second part of Chapter 4. Direct implementation of the QRD to the MMSE solution does not reduce the computational complexity. Mathematical manipulations were proposed to modify the MMSE solution into the LS form, where the QRD can be directly applied. Complexity analysis showed that the proposed QRD implementation of the MMSE solution is significantly lower in complexity (by 36%) as compared to the standard MMSE solution.

In Chapter 5, adaptive channel estimation was investigated for time-varying channels. Recursive implementation of the low-complexity QRD estimation techniques presented in Chapter 4 was applied to MIMO-OFDM systems. The results indicated that adaptive channel estimation outperforms block-based channel estimation with the use of fewer pilot tones. Furthermore, the inverse QRD recursive LS (IQRD-RLS) algorithm was implemented to reduce the complexity. Simulation results suggested that the recursive QRD methods have faster convergence than the RLS methods.

Channel estimation is highly complicated in MIMO-OFDM systems. In this thesis, we have proposed the use of QRD to reduce the complexity of the LS and MMSE estimator for time-invariant channels. Complexity analysis showed the use of QRD significantly reduces the LS and MMSE estimators. In addition, the efficient implementation of the GR QRD will further reduce the execution time. Lastly, the recursive QRD is implemented and demonstrated better results for estimating time-varying channels.

6.2 Future Works

Due to the limited time frame of this research, there are still some important issues that have not been dealt with. The following is a list of suggested future works that can be investigated:

- Complexity analysis of the proposed algorithm through hardware implementation. It was mentioned in this thesis that FLOP count only provides a relative comparison of the complexity of the algorithms. It will require real-time hardware implementation to accurately determine the exact processing time of the channel estimation algorithms.

- Investigation of channel estimation in fast-varying channels where the channel changes within an OFDM block. In this thesis, we have limited the time-varying channel to change within an OFDM frame, but not within an OFDM block. When the channel changes within an OFDM block, ICI occurs. The effects of ICI on channel estimation can be studied.

- Study the effect of frequency offsets on channel estimations. In our analysis, we have assumed perfect frequency synchronization; therefore, the negative effect of ICI has not been analyzed.

APPENDIX A

STANDARD LEAST SQUARES ALGORITHM

This appendix presents the standard LS algorithm and computes the complexity of the algorithm. Given a general system model,

$$Y = Wh + V \qquad\qquad \text{(A.1)}$$

where Y is N x 1, W is N x M, h is M x 1 and V is N x 1. The LS solution is given as

$$\hat{h} = \left(W^H W\right)^{-1} W^H Y. \qquad\qquad \text{(A.2)}$$

To obtain the LS solution specified in Equation (A.2), the $W^H W$ term has to be inverted. The LU decomposition is a common method of implementing the matrix inverse operation. To invert the square matrix $W^H W$, the LU decomposition is applied such that $W^H W = L*U$, where L is lower triangular with unit diagonal elements and U is an upper triangular matrix. The inverse of $W^H W$ can be obtained by the multiplication of the inverse of L and U as follows $\left(W^H W\right)^{-1} = U^{-1} L^{-1}$. Once the $\left(W^H W\right)^{-1}$ is determined, then the LS estimate of $\hat{\theta}$ can be obtained according to Equation (A.2).

A.1 LU Decomposition Algorithm

In this section, the LU decomposition algorithm is presented. Let $\mathbf{A}$ be a $(M \times M)$ matrix defined as follows:

$$\mathbf{A} = \begin{bmatrix} a_{11} & a_{12} & \cdots & a_{1M} \\ a_{21} & a_{22} & & \vdots \\ \vdots & & \ddots & \vdots \\ a_{M1} & \cdots & \cdots & a_{MM} \end{bmatrix}.$$

To LU decompose $\mathbf{A}$, perform the following algorithm on $\mathbf{A}$ to get a modified $\tilde{\mathbf{A}}$:

Let $\tilde{\mathbf{A}} = \mathbf{A}$

for $k = 1: M - 1$

    for $r = k + 1: M$

$$\tilde{a}_{r,k} = \frac{a_{r,k}}{a_{k,k}} \qquad\qquad \text{(Step a.1)}$$

        for $s = k + 1: M$

$$\tilde{a}_{r,s} = a_{r,s} - \tilde{a}_{r,k}\, a_{k,s} \qquad\qquad \text{(Step a.2)}$$

        end

    end

end

After performing the above algorithm, the modified $\tilde{\mathbf{A}}$ is defined as follows:

$$\tilde{\mathbf{A}} = \begin{bmatrix} \tilde{a}_{11} & \tilde{a}_{12} & \cdots & \tilde{a}_{1M} \\ \tilde{a}_{21} & \tilde{a}_{22} & & \vdots \\ \vdots & & \ddots & \vdots \\ \tilde{a}_{M1} & \cdots & \cdots & \tilde{a}_{MM} \end{bmatrix}.$$

From $\tilde{\mathbf{A}}$ the $\mathbf{U}$ and $\mathbf{L}$ matrix can be extracted. The $\mathbf{U}$ matrix is equal to the upper triangular elements of $\tilde{\mathbf{A}}$,

$$\mathbf{U} = \begin{bmatrix} \tilde{a}_{11} & \tilde{a}_{12} & \cdots & \tilde{a}_{1M} \\ 0 & \tilde{a}_{22} & & \vdots \\ \vdots & \ddots & \ddots & \vdots \\ 0 & \cdots & 0 & \tilde{a}_{MM} \end{bmatrix}.$$

and the $\mathbf{L}$ matrix is composed of the remaining lower triangular elements of $\tilde{\mathbf{A}}$ and unit diagonal elements,

$$\mathbf{L} = \begin{bmatrix} 1 & 0 & \cdots & 0 \\ \tilde{a}_{21} & 1 & \ddots & \vdots \\ \vdots & \ddots & \ddots & 0 \\ \tilde{a}_{M1} & \cdots & \tilde{a}_{M\,M-1} & 1 \end{bmatrix}.$$

The multiplication of the $\mathbf{L}$ and $\mathbf{U}$ matrix will give the original $\mathbf{A}$ matrix,

$$\begin{bmatrix} a_{11} & a_{12} & \cdots & a_{1M} \\ a_{21} & a_{22} & & \vdots \\ \vdots & & \ddots & \vdots \\ a_{M1} & \cdots & \cdots & a_{MM} \end{bmatrix} = \underbrace{\begin{bmatrix} 1 & 0 & \cdots & 0 \\ \tilde{a}_{21} & 1 & \ddots & \vdots \\ \vdots & \ddots & \ddots & 0 \\ \tilde{a}_{M1} & \cdots & \tilde{a}_{M\,M-1} & 1 \end{bmatrix}}_{\mathbf{L}} \underbrace{\begin{bmatrix} \tilde{a}_{11} & \tilde{a}_{12} & \cdots & \tilde{a}_{1M} \\ 0 & \tilde{a}_{22} & & \vdots \\ \vdots & \ddots & \ddots & \vdots \\ 0 & \cdots & 0 & \tilde{a}_{MM} \end{bmatrix}}_{\mathbf{U}}.$$

$\underbrace{}_{\mathbf{A}}$

Now that the **L** and **U** matrices have been determined, the inverse of **L** and **U** has to be calculated. The sample algorithm for calculating the inverse of the upper triangular matrix **U** is given as follows:

$$\text{Initialize } \mathbf{U}^{-1} = inv\_\mathbf{U} = \begin{bmatrix} \dfrac{1}{\tilde{a}_{11}} & 0 & \cdots & 0 \\ 0 & \dfrac{1}{\tilde{a}_{22}} & \ddots & \vdots \\ \vdots & \ddots & \ddots & 0 \\ 0 & \cdots & 0 & \dfrac{1}{\tilde{a}_{MM}} \end{bmatrix} \qquad \text{(Step b.1)}$$

The upper elements are inverted as follows:

for $k = 2$ to M

    for $r = k - 1 : -1 : 1$

        sum $= 0$

        for $m = r + 1 : k$

            sum $=$ sum $+ \; inv\_u_{mk} u_{rm}$ (Step b.2)

        end

        $inv\_u_{j,k} = -\dfrac{\text{sum}}{u_{jj}}$ (Step b.3)

    end

end

The triangular matrix inversion algorithm can be similarly applied to invert the L matrix. Then we can obtain $\mathbf{A}^{-1} = \mathbf{U}^{-1}\mathbf{L}^{-1}$.

In summary, the complete process for calculating the inverse of an $(M \times M)$ matrix $\mathbf{A}$ can be summarized by the following steps:

1. Decompose $\mathbf{A}$ into $\mathbf{L}$ and $\mathbf{U}$ matrices

2. Invert $\mathbf{L}$ and $\mathbf{U}$

3. Multiple $\mathbf{U}^{-1}$ and $\mathbf{L}^{-1}$ to get $\mathbf{A}^{-1}$

REFERENCES

[1] G. L. Stuber, J. R. Barry, S. W. Mclaughlin, Y. Li, M. A. Ingram, and T. G. Pratt, "Broadband MIMO-OFDM wireless communications," *Proceedings of IEEE*, vol. 92, no. 2, pp. 271-294, Feb. 2004.

[2] G. J. Foschini and M. J. Gans, "On limits of wireless communications in a fading environment when using multiple antennas," *Wireless Personal Communications*, vol. 6, pp. 311-335, Mar. 1998.

[3] E. Telatar, "Layered space-time architecture for wireless communication in a fading environment when using multielement antennas," *Bell Labs Technical Journal*, pp. 41-59, Autumn 1996.

[4] G. Raleigh and J. M. Cioffi, "Spatio-temporal coding for wireless communications," *IEEE Transactions on Communications*, vol. 46, no. 3, pp. 357-366, Mar. 1998.

[5] H. Bolcskei, D. Gesbert, and A. J. Paulraj, "On the capacity of OFDM-based spatial multiplexing systems," *IEEE Transactions on Communications*, vol. 50, no. 2, pp. 225-234, Feb. 2002.

[6] G. J. Foschini, "Layered space-time architecture for wireless communication in a fading environment when using multi-element antennas," *Bell Labs Technical Journal*, vol. 1, no. 2, pp 41-59, Autumn 1996.

[7] ETSI, "Radio Broadcasting Systems: Digital Audio Broadcasting (DAB) to Mobile, Portable, and Fixed Receivers," ETS 300-401 ed. 2, May 1997.

[8] ETSI, "Digital Video Broadcasting: Framing Structure, Channel Coding, and Modulation for Digital Terrestrial Television," ETS 300-744, Aug. 1997.

[9] ETSI, "Broadband Radio Access Networks (BRAN); HIPERLAN Type 2 Technical Specification Part I-Physical Layer," DTS/BRAN030003-1, Oct. 1999.

[10] IEEE 802.11, "IEEE Standard for Wireless LAN Medium Access Control (MAC) and Physical Layer (PHY) Specifications," Nov. 1997.

[11] IEEE 802.16a, "IEEE Standard for Local and Metropolitan Area Networks, Part 16: Air interference for fixed broadband wireless access systems-

Amendment 2: Medium Access Control Modifications and Additional Physical Layer Specifications for 2-11 GHz," Apr. 2003.

[12] G. J. Foschini, G. D. Golden, P. W. Wolnianshy and R. A. Valenzuela, " Simplified processing for high spectral efficiency wireless communication employing multi-element arrays," *IEEE Journal of Selected Areas in Communications*, vol. 17, no. 11, pp. 1841-1852, Nov. 1999.

[13] W. Choi, K. Cheong, and J. Cioffi, "Iterative soft interference cancellation for multiple antenna systems," in *Proceedings of Wireless Communications and Networking Conference*, vol. 1, pp. 304-309, Sept. 2000.

[14] D. So and R. Cheng, "Detection techniques for V-BLAST in frequency selective fading channels," in *Proceedings of Wireless Communications and Networking Conference*, vol. 1, pp. 487-491, Mar. 2002.

[15] C. H. Aldana, E. de Carvalho, and J. M. Cioffi, "Channel estimation of multicarrier multiple input single output systems using the EM algorithm," *IEEE Transactions on Signal Processing*, vol. 51, no.12, pp.3280-3292, Dec. 2003

[16] Y. G. Li, N. Seshadri, and S. Ariyavisitakul, "Channel Estimation for OFDM systems with transmitter diversity in mobile wireless channels," *IEEE Journal on Selected Areas in Communications*, vol. 17, no. 3, pp. 461-471, Mar. 1999.

[17] H. Minn, D. I. Kin, and V. K. Bhargava, "A reduced complexity channel estimation for OFDM systems with transmit diversity in mobile wireless channels," *IEEE Transactions on Communications*, vol. 50, no. 5, pp. 799-807, May 2002.

[18] I. Barhumi, G. Leus, and M. Moonen, "Optimal Training Design for MIMO OFDM Systems in Mobile Wireless Channels," *IEEE Transactions on Signal Processing*, vol. 51, no. 6, pp. 1615-1624, June 2000.

[19] S. Coleri, M. Ergen, A. Puri, and A. Bahai, "A study of channel estimation in OFDM systems," in *Proceedings of Vehicular Technology Conference 2002*, vol. 2, pp. 894-898, Sept. 2002.

[20] T.S. Rappaport, *Wireless Communications Principles and Practices Second Edition*. New Jersey: Prentice-Hall, 2002.

[21] P.M. Shankar, *Introduction to Wireless Systems*. New York: John Wiley and Sons, 2002.

[22] H. Dam, M. Berg, S. Andersson, R. Bormann, M. Frerich, and T. Henβ, "Performance evaluation of adaptive antenna base stations in a commercial GSM network," in *Proceedings of Vehicular Technology Conference (VTC)*, Piscataway, USA, 1999, pp. 47-51.

[23] K. Sheikh, D. Gesbert, D. Gore, and A. J. Paulraj, "Smart antennas for broadband wireless access networks," *IEEE Communications Magazine*, vol. 37, no. 11, pp. 100-105, Nov. 1999.

[24] R.T. Derryberry, S.D. Gray, D.M. Ionescu, F. Mandyam, and B. Raghothaman, "Transmit diversity in 3G CDMA systems," *IEEE Communications Magazine*, vol. 40, no. 4, pp. 68-75, April 2002.

[25] D. Tse, and P. Viswanath, *Fundamentals of Wireless Communication*, New York: Cambridge University Press, 2005.

[26] S. M. Alamouti, "A simple transmit diversity technique for wireless communications," *IEEE Journal of Selected Areas in Communications,* vol. 16, no.8, pp. 1451-1458, October 1998.

[27] V. Tarokh, H. Jafarkhani, and A. R. Calderbank, "Space-time block coding for wireless communications: Performance results," *IEEE Journal of Selected Areas in Communications,* vol. 17, no.3, pp. 451-460, March 1999.

[28] R. V. Nee and R. Prasad, *OFDM for Wireless Multimedia Communications,* Massachusetts: Artech House, 2000.

[29] A. T. Tomisato and T. Matsumoto, "A MIMO turbo equalizer for frequency-selective channels with unknown interference," *IEEE Transactions on Vehicular Technology,* vol. 52, no. 3, pp. 476-482, May 2003.

[30] K. J. Kim and J. Yue, "Joint channel estimation and data detection algorithms for MIMO-OFDM," in conference record of the *IEEE 36th Asilomar Conference* 2002, vol. 2, pp. 1857-1861, Nov. 2002.

[31] W. King and B. Champagne, "Generalized blind subspace channel estimation," in *Proceedings of IEEE 58th Vehicular Technology Conference,* vol. 2, pp. 1209-1213, Oct. 2003.

[32] S. M. Kay, *Fundamentals of Statistical Signal Processing: Estimation Theory,* Prentice-Hall, Inc., 1993

[33] B. Han, X. Gao, X. You and M. Weckerle, "Joint channel estimation and symbol detection for SFBC-OFDM systems via the EM algorithm," in *Proceedings of IEEE International Conference 2004*, vol. 6, pp. 3148-3152, Jun. 2004.

[34] S. Coleri, M. Ergen, A. Puri, and A. Bahai, " Channel estimation techniques based on pilot arrangement in OFDM systems," IEEE Transactions on Broadcasting, vol. 48, no. 3, pp. 223-229, Sept. 2002.

[35] J.-J. van de Beek, O. Edfors, M. Sandell, S.K. Wilson, and P.O. Borjesson, "On channel estimation in OFDM system," in *Proceedings of IEEE Vehicular Technology Conference 1995*, vol. 2, pp. 815-819, Sept. 1995.

[36] O. Edfors, M. Sandell, J.-J. van de Beek, S. K. Wilson, and P. O. Borjesson, "Analysis of DFT-based channel estimation for OFDM," *Wireless Personal Communications*, vol. 12, no. 1, pp. 55-70, Jan. 2000.

[37] O. Edfors, M. Sandell, J.-J. van de Beek, S. K. Wilson, and P. O. Borjesson, "OFDM channel estimation by singular value decomposition," *IEEE Transactions on Communications*, vol. 46, no. 7, pp. 931-939, July 1998.

[38] Y. G. Li, L. J. Cimini, Jr., and N. R. Sollenberger, "Robust channel estimation for OFDM systems with rapid dispersive fading channels," *IEEE Transactions on Communications*, vol. 46, no. 7, pp. 902-915, July 1998.

[39] Y. G. Li, "Simplified channel estimation for OFDM systems with multiple transmit antennas," *IEEE Transactions on Wireless Communications*, vol. 1, no. 1, pp. 67-75, Jan. 2002.

[40] Y. G. Li, "Pilot-symbol-aided channel estimation for OFDM in wireless systems," *IEEE Transactions on Vehicular Technology*, vol. 49, no. 4, pp. 1207-1215, July 2000.

[41] V. K. Jones and G. G. Raleigh, "Channel estimation for wireless OFDM systems," in *Proceedings of IEEE Global Telecommunications Conference 1998*, vol. 2, pp. 980-985, Nov. 1998.

[42] W. G. Jeon, K. H. Paik, and Y. S. Cho, "An efficient channel estimation technique for OFDM systems with transmitter diversity," *in Proceedings of IEEE International Symposium on Personal Indoor and Mobile Radio Communications 2000*, vol. 2, pp. 1246-1250. Sept. 2000

[43] Y. Zhao, W. Li, and W.Wu, "An efficient channel estimation method for OFDM systems with multiple transmit antennas," in *Proceedings of IEEE*

International Conferences on Info-Tech and Info-Net 2001, vol. 2, pp. 335-339, Oct. 2001.

[44] W. G. Jeon, K. H. Paik, and Y.S. Cho, "Two-dimensional MMSE channel estimation for OFDM systems with transmitter diversity," in *Proceedings of IEEE Vehicular Technology Conference 2001*, vol. 3, pp. 1682-1685, Oct. 2001.

[45] Part 11: Wireless LAN Medium Access Control (MAC) and Physical Layer (PHY) Specifications: High-speed Physical Layer in 5 GHz Band, IEEE Std 802.11a-1999(R2003)

[46] G. H. Golub and C. F. Van Loan, *Matrix Computations Third Edition*, MaryLand: John Hopkins University Press, 1996

[47] S. Haykin, *Adaptive Filter Theory Fourth Edition*, New Jersey: Prentice Hall, 2002

[48] L. M. Davis, "Scaled and decoupled Chloesky and QR decomposition with application to spherical MIMO detection," in *Proceedings of Wireless Communications and Networking Conference 2003*, vol. 1, pp. 326-331, March 2003.

[49] P. Dent, G.E. Bottomley, and T. Croft, "Jakes fading model revisited," *IEEE Electronics Letters*, vol. 29, issue 13, pp. 1162-1163, June 1993.

[50] A. A. Rontogiannis and S. Theodoridis, "Multichannel fast QRD-LS Adaptive Filtering: New Technique and Algorithms," *IEEE Transactions on Signal Processing*, vol. 46, no. 11, pp. 2862-2876, Nov. 1998.

[51] S. T. Alexander and A. L. Ghirnikar, "A method for recursive least squares filtering based upon an inverse QR decomposition," *IEEE Transactions on Signal Processing*, vol. 41, no. 1, pp. 20-30, Jan. 1993.